SORPTION EQUILIBRIA AND KINETICS OF SEQUENTIAL SORPTION IN ZEOLITE MOLECULAR SIEVES

BY

HENRY MENG, B.Sc.

A Thesis
Submitted to the School of Graduate Studies
in Partial Fulfillment of the Requirements
for the Degree
Doctor of Philosophy

McMaster University

SORPTION EQUILIBRIA AND KINETICS OF SEQUENTIAL SORPTION IN ZEOLITE MOLECULAR SIEVES

Doctor of Philosophy (1984) McMaster University

(Chemical Engineering) Hamilton, Ontario

TITLE: Sorption Equilibria and Kinetics of Sequential Sorption in Zeolite Molecular Sieves

AUTHOR: Henry Meng, B.Sc. (McMaster University)

SUPERVISOR: Professor R.B. Anderson

Number of Pages: X, 180

ABSTRACT

The counter-diffusion of a series of low molecular weight, permanent gas sorbate pairs on synthetic zeolites of various pore-geometries and -dimensions, was investigated in a semi-automatic flow system. Results of the binary diffusion studies were compared to the single component kinetics of the same species to determine the effect of the adsorbate/desorbate interactions as well as the relationship between the zeolitic pore dimension and molecular size and the respective contributions to the binary diffusion rates.

Equilibrium studies of the individual sorbate molecules were carried out in a conventional BET volumetric apparatus. The experimental isotherms were correlated to a two-dimensional analog of a three-dimensional virial equation with good results.

Existing diffusion models applicable to the binary sorption system were investigated. Also, a novel kinetic model for diffusion in zeolites based on the principle of random walk has been developed. Qualitatively, the model produces many of the pertinent features observed in the experimental studies.

ACKNOWLEGEMENT

The author is deeply grateful to his supervisor, Professor R.B. Anderson for his constant encouragement and unremitting guidance throughout this work.

I am especially in debted to Dr. and Mrs. Anderson for giving me care and moral support in times of personal difficulties.

Thanks are also due to Dr. G.R. Purdy of the Metallurgical Engineering Department and to Dr. L.W. Shemilt of the Chemical Engineering Department for their valuable suggestions during the course of this work. The author would like to extend his thanks to Mr. Alan Melnyk, Dr. Kevin Smith, Dr. C.B. Lee, Dr. Jacques Monnier and Mr. Ted Calverley for their helpful discussions in solving technical problems as well as for providing friendship.

The financial assistance from the National Science and Engineering Research Council and from the McMaster University is sincerely appreciated.

Henry Meng

(August, 1984)

TABLE OF CONTENTS

LIST OF TABLES

LIST OF FIGURES

CHAPTER I

MOLECULAR SIEVES

1.1 INTRODUCTION

Zeolites are crystalline aluminosilicates with a framework structure enclosing cavities occupied by large cations and water molecules. Both have considerable freedom of movement, thus permitting cation exchange and reversible dehydration.

Natural occurring zeolite minerals are found in basaltic rocks of volcanic origin as well as in ocean and lake sediments. The earliest mention of zeolite as a distinct new class of mineral was in 1756 with the discovery of stilbite. Since then, about 37 different natural species have been found, the most recent one being merlinoite, discovered in 1976. Table 1.1 lists the names of all natural zeolite minerals in a chronological order.

In 1840, Damour [16] observed that zeolite minerals can undergo reversible dehydration without causing any apparent structural change. The sorption property of the dehydrated zeolites was further investigated by Grandjean in 1909 [23]; air, ammonia, hydrogen, carbon disulfide were rapidly adsorbed. Additional sorption experiments involving chabazite were conducted by Weigel and Steinhoff in 1925 [55]; water vapour, methanol, ethanol and formic acid were sorbed but acetone, ether and benzene were excluded. Based on these observations, McBain deduced the pore opening of chabazite to be about 5 A. This is a first description of the phenomenon of selective sorption at a molecular scale by these zeolite minerals and he introduced the name "molecular sieve". The molecular sieving properties of

TABLE 1.1 Dates of discovery of Natural Zeolites [4]

Zeolite	Date	Zeolite	Date
Stilbite	1756	Mordenite	1864
Natrolite	1758	Clinoptilolite	1890
Chabazite	1772	Offretite	1890
Harmotome	1775	Erionite	1890
Analcime	1784	Kihoeite	1893
Laumontite	1785	Gonnardite	1896
Thomsonite	1801	Dachiardite	1905
Scolecite	1801	Stellerite	1909
Heulandite	1801	Ferrierite	1918
Gmelinite	1807	Viseite	1942
Mesolite	1813	Yugawaralite	1952
Gismondine	1816	Wairakite	1955
Brewsterite	1822	Bikitaite	1957
Epistilbite	1823	Paulingite	1960
Phillipsite	1824	Garronite	1962
Levynite	1825	Mazzite	1972
Herschelite	1825	Barrerite	1974
Edingtonite	1825	Merlinoite	1976
Faujasite	1842		

zeolites were rigorously investigated by Barrer and co-workers in the 40s; among his many contributions is a first definitive experiment on separation of hydrocarbon mixtures involving zeolite mineral chabazite, normal paraffins such as propane, n-butane, n-pentane and n-heptane were separated from branched chain molecules of isobutane and isooctane. The increased size of branched paraffins prevented them from entering the pores and thus effecting the separation.[3]

Prior to 1950, zeolites were mostly used as dessicants. In 1956, Reed and Breck [11] of Union Carbide corporation successfully manufactured the synthetic zeolite A, other synthetic zeolites soon followed, some of them do not appear to have counterparts in nature. These new synthetic zeolites, with precisely known crystal structure, uniform chemical compositions and high purity, exhibit high thermal stability as well as activity/selectivity for certain reactions, were soon employed as catalysts. One example that illustrates the exploitation of both selective sorption and catalytic properties is the preferential hydrogenation of n-olefins in mixtures containing branched chain olefins. Synthetic zeolites containing transition metal ions have also been found to be active for oxidation of H_2, CO, C_2H_4 and NH_3. [37]

Today, one finds zeolites an integral component in many industrial processes. Among them; as a catalysts in many hydrocarbon conversion processes including the famous Mobil methanol to gasoline process using a shape selective zeolite ZSM5. [53, 2,38] Other industrial applications include the drying of refrigerant, air, industrial and natural gases, and the separations of air components, hydrogen isotopes, as well as the separations of 2,6- and 2,7-dimethynaphthalenes with NaY,[25] and p-xylene

in mixtures containing xylenes and ethybenzenes on faujasite.[32] Further important examples are the recoveries of radioactive ions from radioactive waste solution, of carbon dioxide and sulfur compounds from natural gas.

1.2 STRUCTURE OF TYPE A ZEOLITE

The structure of all zeolites consist of a three dimensional framework of SiO_4 and AlO_4 tetrahedra, usually in simple arrangement of a polyhedron. Each polyhedron itself is a three-dimensional array of silica-alumina tetrahedra in a definite geometric form. For type A zeolite,[12] the basic sodalite group has the tetrahedra arranged at corners of a truncated octehedron and these octahedra are linked in a cubic array by joining them in cubes on the square face, Fig. 1.1a. The pocket or cavity thus formed is called the α-cage with a free diameter of 11.4 A that is entered through six circular apertures formed by a nearly circular ring of eight oxygen atoms with a free diameter of 4.2 A. These pockets and the connecting passageways give rise to a system of unduloid-like channels with a maximum and minimum diameters of 11.4 and 4.2 A, respectively. The truncated octahedra themselves enclose a second set of pockets, each having a free diameter of 6.6 A (β-cages). The smaller cavities are connected to the larger α-cages through a distorted six-membered oxygen ring of 2.2 A free diameter. The narrow aperture size of the β-cages rendered it inaccessible to most molecules with the possible exception of He and H_2.

The unit cell of zeolite A contains 24 tetrahedra. Its ideal chemical formula is

$$Na_{12}((AlO_2)_{12}\cdot(SiO_2)_{12}).27H_2O$$

Since the oxidation number of Al is +3 and that of the Si is +4, one

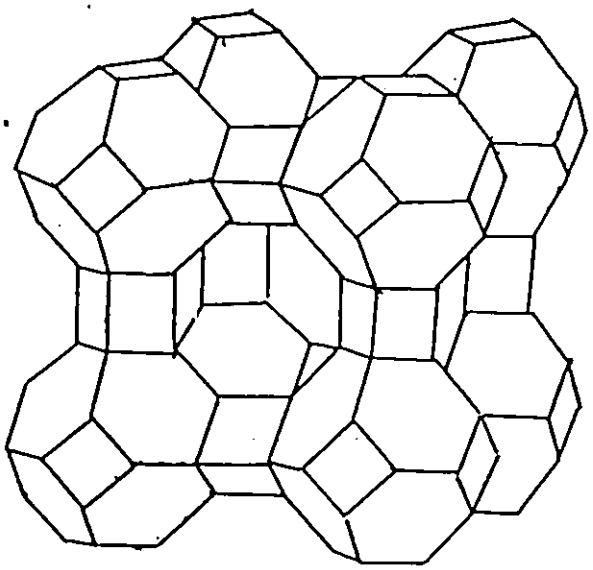

FIG 1.1 (a) FRAMEWORK OF ZEOLITE A

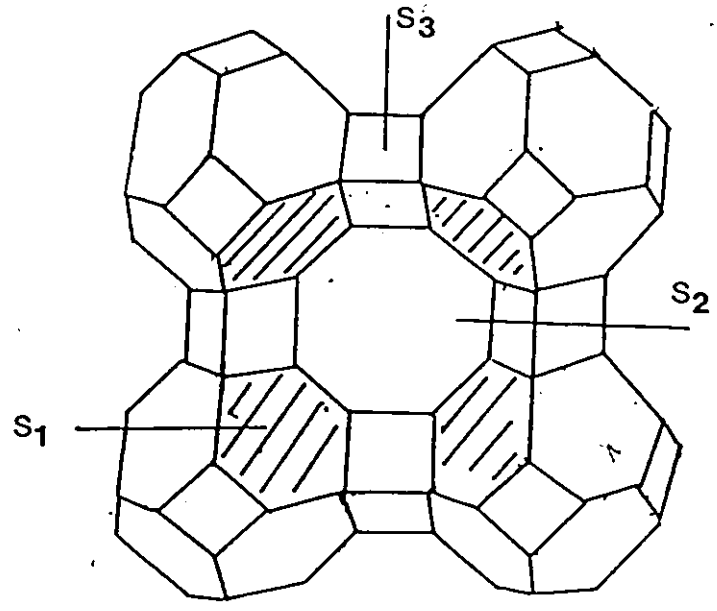

FIG 1.1 (b) CATIONIC SITES

monovalent cation per Al atom must be included in the unit cell to maintain electrical neutrality. Normally, zeolite A is synthesized in sodium form. However, since the cations in zeolite are quite mobile and can easily be ion-exchanged, other cationic forms are prepared in this way. The ion-exchange property provides another way in regulating the aperture size through controls of the size and number of cations involved.

In zeolite A, there are three kinds of cationic sites available to the twelve sodium cations, Fig. 1.1b. The first is near the center of the six-membered oxygen ring (type I site). The second is near the center of the eight-membered oxygen ring (type II site). The third is in the central cavity, near the center of the four-membered oxygen ring (type III site). The distribution of sodium ions per unit cell is eight, three and one in type I, II, and III sites, respectively. The cations of type II in particular reduce the free diameter of the window aperture so that only molecules with critical diameter less than 4.0 A can pass through, thus, the sodium form of zeolite A is designated as 4A. If the sodium cations are exchanged with calcium cations, since one calcium ion replaces two sodium ions, the number of cations present is reduced and if two-thirds of the sodium cations are exchanged, the unit cell then contains only eight cations, all of which can be accomodated into the type I sites, thus, removing the cationic obstruction at the window aperture, making the effective size to about 5.0 A. This calcium form zeolite A is designated as molecular sieve type 5A.

1.3 STRUCTURE OF MORDENITE

The chemical formula for an ideal unit cell of mordenite is

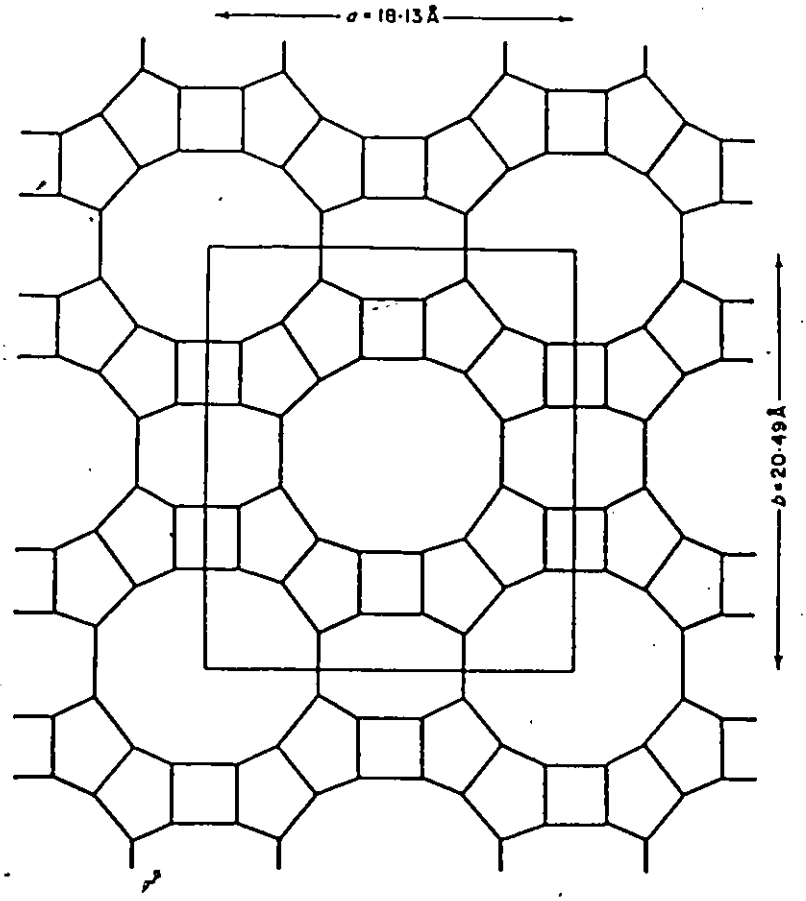

FIG 1.2 FRAMEWORK STRUCTURE OF MORDENITE in cross-section normal to the wide channels, Al or Si atoms are at each corner and Oxygen near the midpoint of each edge, the cations are not shown

$$Na_8\{(AlO_2)_8.(SiO_2)_{40}\}.24H_2O$$

Mordenite with ratio of Si:Al=5:1 is one of the most siliceous zeolite. Its crystal structure [36] consists of five membered rings. Each Si and Al tetrahedron is associated with at least one such ring. These rings are interconnected to form a chain and each chain in turn is cross-linked to other identical chains to form the basic crystal structure of mordenite.

The high silicon content of mordenite together with the presence of the five-membered rings resulted in a high thermal and acid stability as compared to other zeolites. The pore structure consists of elliptical non-interconnected channels parallel to the c-axis, Fig 1.2. In fact, mordenites are made up of two-channel systems; the major channels are circumscribed by twelve-membered oxygen rings with the dimensions of 7.0x6.7 A. There are side pockets open off to the major channels with a free diameter of 3.9 A, but these pockets are inaccessible to practically all molecules because they are connected to the distorted 8-membered oxygen rings which with a free diameter of 2.8 A provide a severe steric limitation. Furthermore, in the sodium form of mordenite, the small pore channel is further blocked by the sodium cation located near the 8-membered ring. Thus, they effectively isolate the main channel system and close off the minor pores to even the smallest molecules, e.g. He. There are four sodium cations located in this position per unit cell. The positions of the remaining four sodium cations are less certain but they are most probably located in the main channel system.

The sodium mordenite can be treated with aqueous ammonium solution and the subsequent removal of ammonia resulted in the formation of hydrogen-mordenite. Although H-mordenite does not have sodium cations

blocking the minor channels, but the small pores remain inaccessible to most molecules perhaps with the exception of He and H_2 because of the narrow opening of the distorted 8-membered rings. Therefore, even in H-mordenite, the main pore system remains isolated and mordenites are regarded as having an one-dimensional channel system as compared to the three-dimensional zeolite A.

After extensive study of the sorption behavior of both natural and synthetic mordenite, Barrer [5] estimated the effective free pore diameter to be only 4.0 A. Meier [36], however, calculated a minimum free diameter of 6.6 A for the main channel based on the crystal structure. He proposed the existence of stacking faults which could effectively reduce the pore size to Barrer's dimension. Sand [46] has shown that stacking faults in mordenite do not exist, he attributed the small pore characteristics to the presence of amorphous material in the pores and in some cases, to the locations of the exchangeable cations.

It is generally regarded that diffusion in mordenite is one-dimensional in the non-interconnecting main channel. Diffusion in Na-mordenite is probably inhibited to some degree by the presence of large cations but in H-mordenite, such cationic hindrance effect should be reduced significantly.

1.4 SORPTION PROPERTIES OF ZEOLITES

Industrial applications of zeolites in both sorption and catalysis rely heavily on the nature of their crystallographic structure. Unlike other microporous sorbents such as activated carbon, zeolites do not have pore size distribution. Its pore system is very well defined and the pore size depends on the structure of a particular anionic framework involved as well

as the nature of exchangeable cation. The average diameter of the common zeolites varies from 3 to 10 A. When dehydrated, the high internal surface area and void spaces left will sorb gas, vapour and liquid. However, molecules that are significantly larger than the pore diameter are completely excluded and depending on the relative sizes of pores and sorbate molecules, smaller molecules will either be sorbed rapidly or slowly. Moreover, since the zeolite framework is capable of slight deformation, molecules that are marginally larger than the pore diameter can be admitted under moderate operating conditions, e.g. at an elevated pressure. Thus, the zeolitic framework structures provide the fundamental basis for their sorption and molecular sieving properties, and are responsible for processes such as the separation of normal- and iso-paraffins as well as shape selective catalytic cracking.

In addition to the steric considerations of pore geometry and molecular size, other factors can influence sorptive and diffusional properties; the size and location of cations in the zeolites may place additional diffusion limitations by partly blocking the conducting channels. In zeolite A, the free diameter of the anionic openings is about 5 A, the presence of sodium cation reduces it to 4 A as mentioned earlier. If the sodium ions are exchanged with potassium, the increased ionic size further restricts the openings to about 3 A. Moreover, the presence of cation also enhances the zeolitic electrostatic field and the adsorption of molecules capable of strong interaction with it is favored, e.g. for molecules with π-bonds and/or unbonded electrons, and those with permanent dipole moments such as carbon monoxide and ammonia, the strongest interaction is for molecules with quadrupole moments like nitrogen and carbon dioxide.

The interaction between the cation and the sorbate also are intimately related to the polarizing power of the cations (charge/size ratio) which determines the strength of local electrostatic field. The polarizing ability increases as the cation size decreases because of the higher concentration of positive charge. Hence, zeolite 4A with the cation radius of sodium of 0.95 A has a stronger polarizing power than 3A with the radius of potassium ion of 1.33 A. This property tends to decrease molecular diffusivity through enhanced electronic interaction with the cations; polar molecules and those with π-bonds or unbonded electrons although having a higher affinity have lower diffusivities than molecules of comparable size not having these electronic properties.

CHAPTER II

THE THEORY AND METHODS OF MEASUREMENT OF MASS TRANSPORT IN ZEOLITES, PREVIOUS WORK AND SCOPE OF PRESENT STUDY

2.1 INTRODUCTION

Mass transport mechanisms in porous solid medium are generally categorized into three groups; bulk gas phase, Knudsen, and surface or activated diffusion. The criterion that distinguishes bulk phase and Knudsen diffusion depends largely on the mean free path of the diffusing molecules; if the mean free path is much smaller than the pore size, molecular collision predominates and bulk gas mechanism prevails; for molecule A diffusing into molecule B, the diffusion coefficient is given as [21]

$$D_{A,B} = \frac{1.0 \times 10^{-3} \cdot T^{1.75} \cdot (1/M_A + 1/M_B)}{P\{(\sum_A \nu_i)^{1/3} + (\sum_B \nu_i)^{1/3}\}^2} \qquad (2.1)$$

where T is temperature in K, M_A and M_B are molecular weights, P is pressure in atmosphere, and ν_i, special diffusion volumes for each element which can be summed to give the diffusion volume for the molecule, $\Sigma_A \nu_i$ or $\Sigma_B \nu_i$. Knudsen diffusion occurs when the mean free path becomes larger than the conducting channel size and molecules thus collide with pore wall more frequently than with each other. The Knudsen diffusivity is characterized by

$$D_k = 9700\, r \sqrt{T/M} \qquad (2.2)$$

where r is the radius of pore in cm. Eqns 2.1 and 2.2 are the results of rigorous development of the kinetic theory.

Zeolitic diffusion is unique in that the intraparticle diffusion takes place in an extremely well defined regular pore system that has the dimensions or pore diameter on a molecular scale. From equilibrium isotherm

studies, the state of molecules in a zeolite has been found to resemble closely those of liquid state. However, the diffusion coefficients are often several orders of magnitude lower. Thus, interpretations of intraparticle zeolitic diffusion based on bulk phase or Knudsen diffusion theory are invalid. Industrial uses of zeolites are often in a pelleted form, which has, in addition to intraparticle pore system, void spaces between the adjacent constituent crystals forming macropores; diffusion in these interparticle voids has been interpreted as Knudsen diffusion and in certain cases as bulk phase diffusion depending on the method of sample preparation.

The low intraparticle diffusivity in zeolites coupled with its high activation energy are more in line with the surface diffusion mechanisms which also exhibits low diffusivity and an activation energy in the range of half to two-thirds of heat of sorption. In addition, the nature and size of the diffusing molecules can have a strong influence on the diffusivity; of two similar sized molecules, the one that interacts less strongly with cations and/or local electrostatic field has the higher mobility. On a purely steric consideration, increasing molecular size increases the interaction with the anionic framework. This lowers the diffusivity as well as increases the activation energy. As the molecular size approaches pore dimensions, such effect can become increasingly pronounced and the activation energy may exceeds heat of sorption.

In general, zeolitic diffusion rate increases with increasing temperature reflecting the nature of an activated mechanism. The rate limiting step often occurs at the narrow connecting passageway between two adjacent cavities where a sufficient energy is required before a molecule can diffuse through. The diffusivity follows a typical Arrhenius temperature

dependence

$$D = D_0 \, EXP(-E/RT) \qquad (2.3)$$

The increased diffusion rate at higher temperatures is the result of more and more molecules (following Bolzmann distribution) gaining sufficient kinetic energy for overcoming the activation barrier.

2.2 METHODS OF STUDYING THE MOBILITY OF SORBED MOLECULES

Information regarding mass transport in zeolites can be obtained by several techniques. We can classify them into two groups;

(i) Diffusion coefficients inferred by examining properties related to sorbate to sorbate content or mobility. These include

(a) sorbate mobility inferred from jump time by nuclear magnetic resonance method (NMR),

(b) change with time, as the content of sorbate changes, in the intensity of specific absorption characteristics of sorbate-solid interaction, and

(c) moment analysis of the spread of chromatographic response peak.

(ii) Direct measurement of mass transport into and out of porous solid and the analysis of transient uptake curves. These include

(d) the change with time of volume of gas or vapour around sorbent, keeping pressure constant,

(e) the change with time of pressure of gas or vapour around sorbent, keeping volume constant,

(f) the change with time in the weight of sorbent bathed in a constant pressure of sorbate vapour.

In addition, intracrystalline diffusion coefficients can be evaluated

through sorption studies in flow system; sorbate can either be introduced via pulse injection into a carrier gas or with a step change in concentration.

The NMR technique involves the determination of correlation time for molecular motion and the diffusivity is then calculated using an assumed jump distance. Thompson and Resing [54] measured the relaxation time of SF_6 on 13X zeolites and interpreted it in terms of molecular diffusivities. However, such values depend on the assumption that an average distance a molecules travels in one diffusion step is one molecular diameter, 6A. Karge and Klose [27] studied the desorption of pyridine by following its characteristic infrared absorption bands. The diffusivity was evaluated through monitoring the changes in the intensity of the absorption bands with the content of pyridines.

In the chromatographic method, moment analysis in the spread of chromatographic response peaks gives information on micropore diffusivity. However, results sometimes differ from other techniques because of complications from effects such as external mass transfer resistance and axial dispersion. [51,43,31]

Methods (d), (e) and (f) involve equipment and procedures typical of the conventional volumetric and gravimetric equilibrium sorption studies. Limitations are set by the rates at which pressure, volume and weight changes can be accurately recorded. Diffusivities are invariably calculated by matching sorption rate curves to simple Fick's law models. Extensive kinetics studies have been obtained through equipment of these types. [18,56] One drawback of these methods is that owing to the closed system nature, heat transfer can become a serious problem causing kinetic data

to be collected under non-isothermal condition. Large temperature rise in sample beds and substantial thermal effect on rate curves have been reported. [29,18] Under these conditions, the experimentalist would have to resort to the much complex non-isothermal kinetic models. [44]

The flow method is essentially a constant pressure technique. At zero time, activated zeolite crystals are exposed to a constant stream of gas mixture; sorbate plus carrier gas at a pre-set concentration. The rate data are collected by monitoring the changes in the effluent concentration with time at a fixed position usually using a thermal conductivity cell. An apparent advantage of this technique is that owing to the high thermal conductive carrier gas (helium), heat transfer is less of a problem and sorption occurs at a more isothermal condition than the static methods. Chan and Anderson [14] successfully predicted the entire sorption spectra in a study of temperature-programmed desorption of encapsulated N_2, Ar and CO_2 in 3A zeolites. Another salient feature is its adaptability to multicomponent sorption studies; simply by replacing the thermal conductivity cell with a gas chromatography, one can monitor multisorption rates by analyzing the effluent gas composition change with time.

2.3 PAST WORK

In the industrial applications of zeolites such as selective sorption, diffusion of molecular species into and out of the fine microporous structure is often the rate determining step. In processes of catalytic nature, simultaneous migration of reactant and product in opposite directions within the zeolite must take place. This type of diffusion is defined as counter-diffusion in contrast to the co-diffusion case where two or more

distinct species are travelling in the same direction. Accordingly, the design of industrial units requires information on diffusion and/or counter diffusion rates. Although single component diffusion has been extensively investigated, little information is available on the more important case of the counter diffusion in zeolites. This is partly due to the complex nature of the zeolitic diffusion itself and partly due to the difficulties in adopting conventional single component sorption apparatus, for example, volumetric and gravimetric equipments in studies of multicomponent system.

Satterfield and Katzer [50] studied the liquid-phase counter diffusion of cumene in NaY zeolite into benzene and 1-methyl-naphathlene into cumene. They found the desorptive diffusivities decreased by three orders of magnitude over the reported values for the pure component sorption rates in NaY. In addition, the binary diffusivities depended heavily on cation size and the rate varied in the order:

$$NaY < CaY < SK\text{-}500 < CeY < HY$$

Satterfield and Cheng [47] investigated a series of pairs of liquid hydrocarbons in counter diffusion and found their rates to be strongly affected by the critical molecular diameter and were generally one to three orders of magnitude lower than that for unidirectional diffusion into the initially evacuated zeolite. In yet another study, Satterfield and Katzer [48] found the desorptive counter diffusion rate of cumene in H-mordenite into benzene decreased by two orders of magnitude. They attributed the cause to the slow formation in the H-mordenite pores during the saturation step of radical ions and diisopropylbenzene molecules causing blockages of the pores. Riekert [41] in a study with synthetic mordenite and type T zeolites, found the exchange rates of carbon dioxide against ethane and vice-versa to

be an order of magnitude lower than the pure component rates in both cases. In another study of counter diffusion of carbon dioxide and sulfur dioxide in Na-mordenite, Ma and Roux [35] discovered the single component rates to be two orders of magnitude higher.

In a related study of co-diffusion of butane and isobutane as well as butene and isobutene on CaX zeolite, Ma and Lee [34] found the binary diffusion rates of both components to be an order of magnitude lower than the pure component case. Habgood [24] also investigated the co-diffusion of methane and nitrogen on 4A. He found the diffusion rate of nitrogen in the binary mixture was slightly higher than the single component rate whereas the methane diffusivity essentially remained unchanged. He developed a model which uses chemical potential gradient as the fundamental driving force of diffusion and with it successfully correlated the experimental data including the maxima in the nitrogen uptake curve. [42]

Moore and Katzer [39] studied the counter diffusion of liquid hydrocarbons in type Y zeolites. They found that both the molecular type and size had a strong effect upon the counter diffusion rates. The correlation in the binary case paralleled the single component case, but the binary diffusivities were in general an order of magnitude lower. In the same paper, they also reported that the adsorptive counter diffusion rates were higher than the desorptive counter diffusion rates. In a study of temperature-programmed desorption of argon in 3A zeolite, Chan [14] found by injecting pulses of H_2O into the carrier gas, the desorption rate of argon doubled.

2.4 SCOPE OF THE PRESENT THESIS

In the present study, the counter diffusion of a series of low molecular weights, permanent gas sorbate pairs on synthetic zeolites of various pore-geometries and -dimensions, were investigated. Results of the binary diffusion studies were compared to the single component kinetics of the same species to determine the effect of the adsorbate-desorbate interaction, as well as the relationship between the zeolitic pore dimension and molecular size and their respective contributions to the binary diffusion rates. Equilibrium studies of the individual sorbate gas were also performed and the experimental isotherms were correlated to a two-dimensional analog of a three-dimensional virial equation with good results. Existing diffusion models applicable to the binary sorption systems were investigated. Also, a novel kinetic model for diffusion in zeolites based on the principle of random walk has been developed.

In Chapter I, some general information about the historical background, structural and sorption properties of zeolites is given. Chapter II describes the theory of diffusion and the methods of measurement of mass transport. Previous work in counter diffusion studies is also summarized. The experimental systems, as well as factors that may influence sorption rates such as the zeolite particle size distribution, are given in Chapter III. Results of the equilibrium and kinetic studies are presented and discussed in Chapter IV. Chapter V describes the results of the various diffusion models simulation studies. Finally, the conclusions are given in Chapter VI.

CHAPTER III

EXPERIMENTAL

3.1 SAMPLE PREPARATION

All of the samples used in the sorption experiments were synthetic zeolite powders. Zeolite 4A was provided by Linde Division of Union Carbide corporation, Lot No. (450339). Na-mordenite and H-mordenite were obtained from Norton company, Lot No. (BG-11) and (BG-10), respectively. Information regarding the chemical composition, crystallographic data and structural properties of the respective zeolites are given in Tables 3.1 and 3.1. In the sample preparation, approximately 1 g of the zeolite powder was sprinkled onto a thin layer of glasswool. The glasswool was then rolled into a cylindrical form and subsequently inserted into a sorption sample tube. Using the glasswool as a solid diluent has the advantages of; facilitating mass and heat transfer, maximizing void space thus avoiding the formation of macropores that are ofteh encountered with the powder aggregates, and minimizing pressure drop in the sample bed. After loading, the sample tube was connected to a vacuum system equipped with a mercury diffusion pump backed by a conventional rotary oil pump for degassing. Sample evacuation was done at 450 ^{o}C for 24 hours under a vacuum of 10^{-5} Torr indicated by a McLeod gauge. The heating temperature was slowly increased from the room temperature by driving the potentiometer knob of a proportional controller at a constant rate.

A single batch of powder was used repeatedly in a given set of sorption experiments involving single and/or binary sorbate gases, e.g., CO_2-C_2H_4 and zeolite 4A. The used samples were reactivated under the same vacuum but at a lower temperature of 350^{o}C for 15 hours. The sorption capacity of the used

TABLE 3.1 PHYSICAL PROPERTIES OF ZEOLITE A [12]

Chemical Composition	
Typical Oxide Formula:	$Na_2O \cdot Al_2O_3 \cdot 2\ SiO_2 \cdot 4.5\ H_2O$
Typical Unit Cell Contents:	$Na_{12}[(AlO_2)_{12}(SiO_2)_{12}] \cdot 27\ H_2O$, pseudo cell and 8X for true cell
Variations:	Si/Al = ~0.7 to 1.2; occlusion of $NaAlO_2$ in β-cages
Crystallographic Data	
Symmetry:	Cubic
Space Group:	Pm3m (Fm3c for true cell)
Unit Cell Constants:	a = 12.32 A, pseudo cell a = 24.64 A for true cell
Density:	1.99 g/cc
Unit Cell Volume:	1870 A^3 pseudo cell
Structural Properties	
Framework:	Cubic array of β-cages linked by D4R units
SBU: D4R	Void volume: 0.47 cc/cc
Cage type: α, β (one each)	Framework density: 1.27 g/cc
Channel System:	Three-dimensional, ∥ to [100]; 4.2 A and ∥ to [111]; 2.2 A minimum diameter
Hydrated–	
Free Apertures:	2.2 A into β-cage and 4.2 A into α-cage
Cation Locations:	8 S_I on 6-rings, 4 cations with H_2O in the 8-rings
Dehydrated–	
Free Apertures:	4.2 A
Cation Locations:	8 S_I in 6-rings, 3 S_{II} in 8-rings, 1 S_{III} at the 4-ring
Effect of Dehydration:	None on framework, 4 cations move to S_{II}
Location of H_2O Molecules:	Dodecahedral arrangement in α-cage 4 molecules in β- cage.
Largest Molecule Adsorbed:	C_2H_4 at RT, O_2 at -183°C
Kinetic Diameter, σ, A:	3.9 and 3.6

TABLE 3.2 PHYSICAL PROPERTIES OF ZEOLITE MORDENITE [12]

Chemical Composition			
Typical Oxide Formula:	$Na_2O \cdot Al_2O_3 \cdot 10\ SiO_2 \cdot 6\ H_2O$		
Typical Unit Cell Contents:	$Na_8[(AlO_2)_8(SiO_2)_{40}] \cdot 24\ H_2O$		
Variations:	Si/Al = 4.17–5.0; Na, Ca > K		
Crystallographic Data			
Symmetry:	Orthorhombic	Density:	2.13 g/cc
Space Group:	Cmcm	Unit Cell Volume:	2794 A^3
Unit Cell Constants:	a = 18.13		
	b = 20.49		
	c = 7.52		
Structural Properties			
Framework:	Complex chains of 5-rings crosslinked by 4-rings		
	Chains consist of 5-rings of SiO_4 tetrahedra and single AlO_4 tetrahedra		
SBU:	Unit 5-1	Void volume:	0.28 cc/cc
		Framework density;	1.70 g/cc
Channel System:	Main system ∥ to c; channels with 2.8 A restrictions ∥ to b		
Hydrated–			
Free Apertures:	12-rings ⊥ to c-axis, 6.7 x 7.0 A		
	8-rings, 2.9 x 5.7 A, ⊥ to b		
Cation Locations:	Four Na^+ in the restrictions with minimum dimension of 2.8 A in channels ⊥ to b		
Dehydrated–			
Free Apertures:	Probably no change		
Cation Locations:	Unknown		
Effect of Dehydration:	Very stable		
Location of H_2O Molecules:	Unknown		
Largest Molecule Adsorbed:	C_6H_6		
Kinetic Diameter, σ, A:	6.2		

Table 3.3 Physical constants of sorbate gases

Gas	C_2H_4	C_2H_6	CO_2	He
B.P.(^oC)	-103.7	-88.6	-78.5	-268.8
Crit.Temp (^oC)	9.7	32.1	31.1	-267.8
Quadrupole (A^3)	0.48	0.27	0.64	-
Polarizability (A^3)	3.5	3.9	1.9	-
Ion. Pot. (volts)	12.2	12.8	14.4	24.59
Length (A)	2.5	2.6	2.6	0.93
Width (A)	2.2	2.5	1.8	0.93

samples was periodically checked. Adsorbate gases used were carbon dioxide, ethane and ethylene. The mixtures contained 5% of one of these gas and the balance was helium. Some of the physical constants of the sorbate gases pertinent to this study are listed in Table 3.3. Sorption data were calculated based on per gram of the dry weight.

3.2 FLOW SYSTEM

The kinetic sorption experiments were carried out in a flow system. Fig. 3.1 shows the schematic of the apparatus. Before each sorption run, the system was throughly flushed with helium via the sorption-tube bypass until a steady base line on the recorder chart was established. The depth of the powder sample was about 1 cm, and hence, readsorption was considered to be negligible. Flow rates of the gas mixtures were adjusted to vary between 40 to 80 cc/min; too high a flow rate resulted in unsteady responses whereas lower flow rates gave small responses. No significant flow rate changes were observed in blank runs through the sample-tube bypass and sample bed with helium thus indicating negligible pressure drop. A thermostat was used to regulate the sorption bath temperature between 10-80 ^{o}C. A chromel-alumel thermocouple as well as a mercury thermometer monitors the bath temperature which was maintained to within 0.1^{o}C for periods up to several days.

At the onset of a particular counter diffusion sorption experiment, gas mixture A, at 40 psig, from the regulator, passes through a flow controller (Matheson, model 8249), cold trap, reference side of the thermal conductivity cell (TCC), sorption tube, a second cold trap, detector side of the TCC, automatic sampling valve and finally to a soap film flowmeter. The flow controller can maintain a pre-set flow rate to within 0.1% regardless

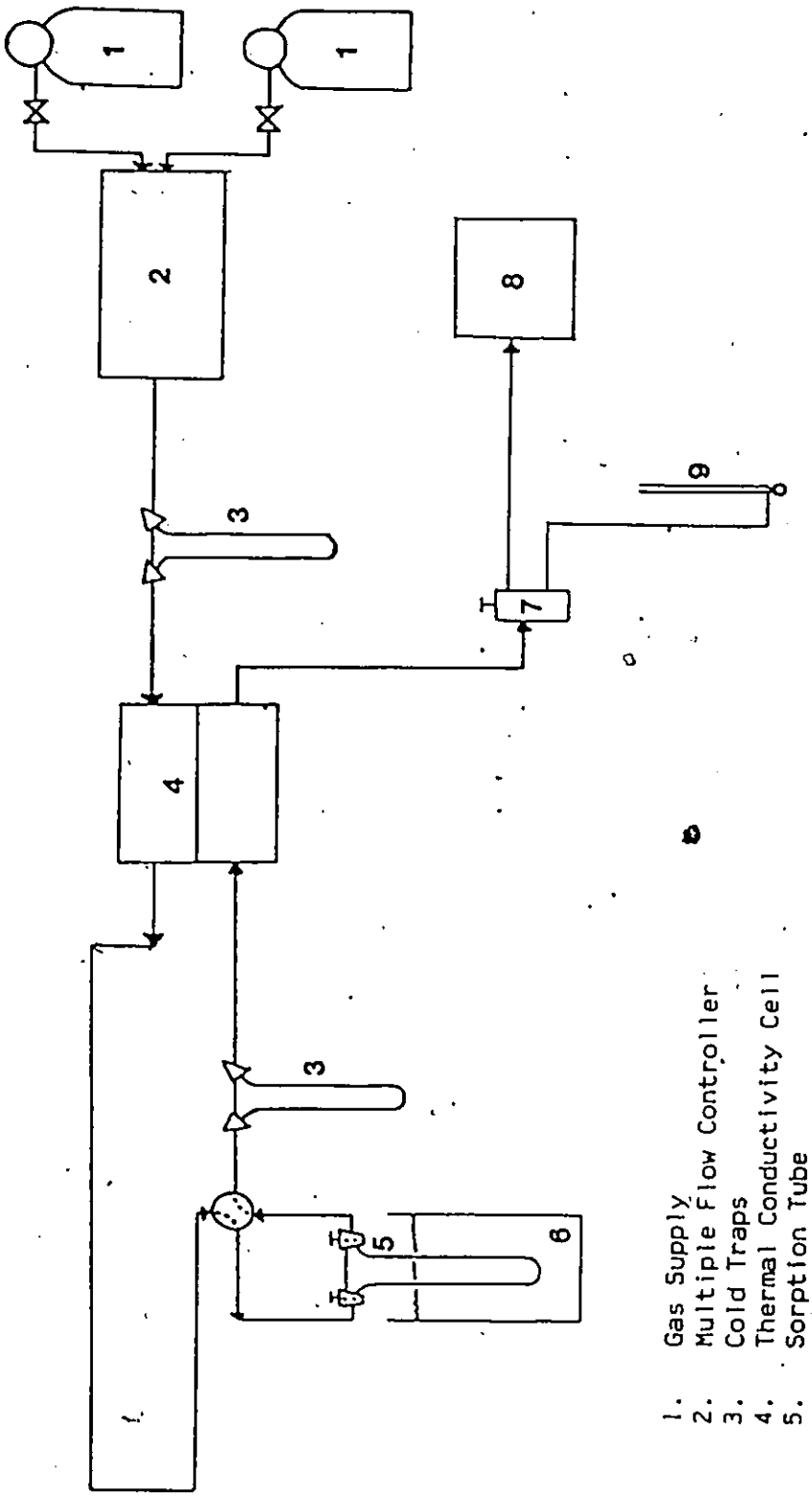

1. Gas Supply
2. Multiple Flow Controller
3. Cold Traps
4. Thermal Conductivity Cell
5. Sorption Tube
6. Bath
7. Automatic Injection Valve
8. Gas Chromatography
9. Bubble Flowmeter

FIG 3.1 SCHEMATIC OF FLOW SYSTEM

of upstream or downstream disturbances. Moreover, with a proper set up, it may be employed as a mixer to obtain sorbate concentration ranging from 0-100%. The TCC (Gow-Mac model 10-952) with tungsten filaments monitors the effluent gas concentration continuously. Signal responses were registered on a recorder (Linear Instrument, model 291/MM). Two dry-ice acetone cold traps ($-78^{o}C$) remove water and other condensables.

With the completion of mixture A adsorption, signaled by the returning of the recorder pen to the base line, the system was purged. Gas mixture B was then introduced into the system and it followed the same flow path as gas A as mentioned previously. However, the instantaneous composition of the effluent gas was now analyzed by a gas chromatography (Varian, model 920) through pulse injections using an automatic sampling valve. An integrator (Hewlett Packard 3390A) records the time history of the chromatographic responses, which was calibrated with injections of known concentration before and after each run. Identical experimental procedures were followed in desorption of a single sorbate, except gas B was pure helium.

The gas chromatographic responses of a typical counter diffusion experiment is shown in Fig. 3.2. In this experiment, we initially saturated the zeolite 4A with CO_2 and then passed 5% ethylene in helium over the saturated zeolite. CO_2 has a shorter chromatographic retention time and is therefore the first of two peaks. The entire run took about 150 mins. At the early stage, CO_2 desorbed rapidly and its concentration decreased monotonically with increasing time. The uptake of ethylene was very fast, in fact, during the first 10 minutes, the adsorption rate of ethylene was so rapid that there has been a complete removal of ethylene from the gas phase. In the second stage, CO_2 continued to desorb but the adsorption of ethylene

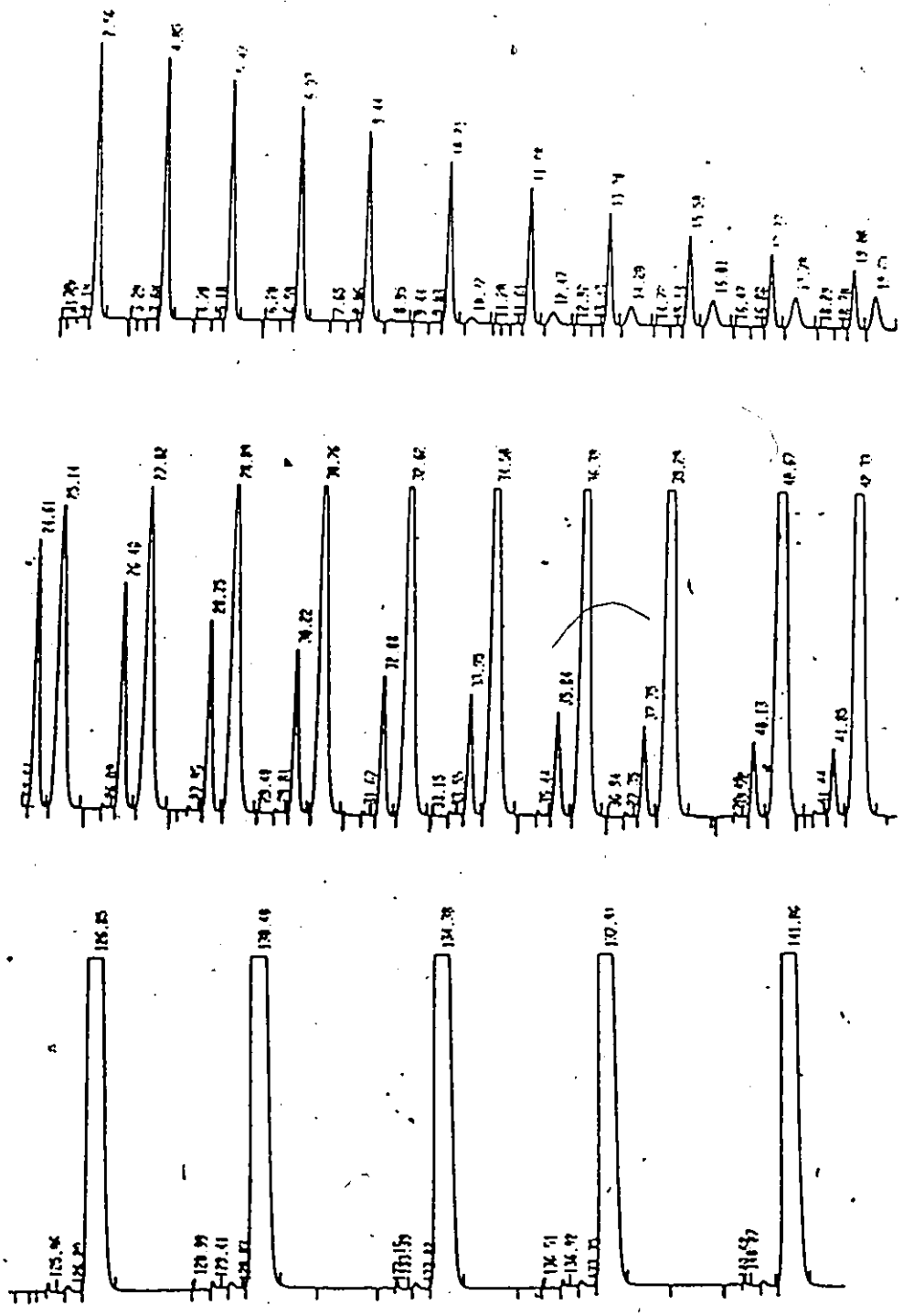

FIG 3.2 Gas Chromatographic Responses of binary diffusion of Ethylene and Carbon Dioxide

can be seen to be approaching equilibrium. In the last stage, the adsorption of ethylene has already reached equilibrium indicated by the constancy of successive peak counts. Finally, the desorption of CO_2 also reached the completion shown by the disappearance of the CO_2 peaks.

3.3 VOLUMETRIC APPARATUS

The equilibrium data of the various sorbate gases on zeolites were gathered from a conventional BET volumetric sorption apparatus. The schematic of this constant volume, variable pressure system is shown in Fig. 3.3. The system consists of two parallel series of calibrated bulbs (B1, B2), each contains five bulbs with calibrated volumes of

4.566, 9.065, 14:188, 21.762, 32.427

and

4.655, 16.259, 22.679, 50.305, 123.492

in cm^3 for B1 and B2, respectively. Capillary tubing connects the bulbs to the sorption sample tube, vacuum and gas storage systems. A mercury manometer determines the system pressure. The temperature of the gas bulbs was maintained at 32^oC by circulating thermostatted water through the jacket. The sorption sample tube was immersed in a Dewar flask equipped with a mercury thermometer and the temperature was maintained by circulating thermostatted water through a copper coil.

The void space (Vv), the volume in the capillary tubing to the right of S1 in Fig. 3.3 was determined to be 11.565 cm^3 at the room temperature. (Appendix A-1.1) The space to the left of S1 and including the void volume in the sample tube is known as the dead space. The Dead Space Factor (DSF) relates the gas in the the dead space in CC(STP) to pressure and was

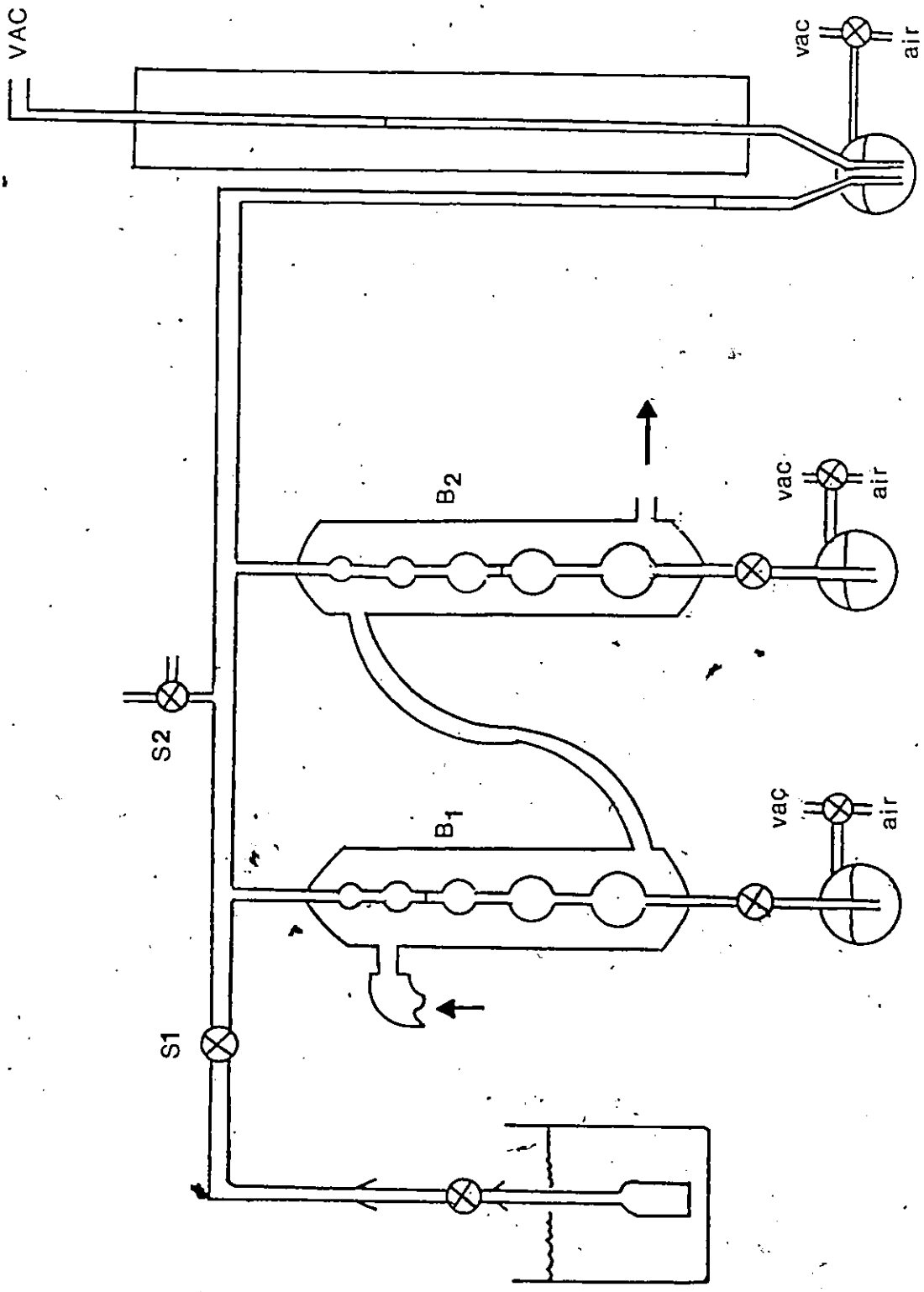

FIG 3.3 ADSORPTION APPARATUS

determined with helium at several temperatures between -78^{o} and $80^{o}C$. (Appendix A-1.2)

Before each equilibrium experiment, the entire sorption system was evacuated via S2 to a pressure of 10^{-5} Torr indicated by the Mcleod gauge. With S1 closed, sorbate gas was then introduced from the storage bulb. (Not shown in the schematic) The amount introduced (Vi) could be calculated by knowing Vv, room temperature, total volume in the bulbs and pressure. Adsorption was initiated by opening the S1 valve. Since the total amount of the gas remains constant, the pressure of the system rapidly decreases as adsorption proceeds. Equilibrium was considered to be reached when the system pressure remains constant for two or more hours, and this final pressure setting is regarded as the equilibrium pressure. The amount adsorbed Q may be calculated by

$$Q = [\ Vi - (\ Vv + Vb + Vds\ )\ ] / W \qquad 3.1$$

in CC(STP)/g, where W is the dry weight of zeolite. After the completion of the first equilibrium point, the system pressure can be adjusted to a new setting by either increasing or decreasing the bulb volume through raising or lowering the mercury level in the bulbs. Similar experimental procedure and method of calculation apply to the subsequent equilibrium points. With a proper combination of bulb volume and pressure settings, the entire equilibrium isotherm can be generated.

3.4 PARTICLE SIZE MEASUREMENT

The successful analysis of the sorption rate data depends on a correct choice of particle geometry for the rate equation. Barrer [4] demonstrated this by comparing Fick's law solution for cubes and spheres having a same

volume to surface ratio; the diffusion rate of the spheres was shown to exceed that of the cubes because of the absence of corners and edges. The particle shape effect, however, is relatively insignificant when compared to the effect of "diffusion length". This is because particles of different sizes adsorb at different rates depending on their diffusion length. Thus, the measurement of particle size distribution is important. Eagan [17] demonstrated this by comparing the diffusion rate curves of cubes having a measured log-normal size distribution to that of a single cube having its edge length equal to the weight average length of the measured distribution. A difference of as large as 20% in calculated diffusivities was reported.

In this study, the shape and particle size distribution of the zeolites were determined with a Philip EM 300 transmission electron microscope. In the sample preparation, approximately .1 g of the zeolite 4A powder was dispersed in 100 mls of aqueous solution of methanol. The suspension was rigorously stirred first with a magnetic stirrer for 30 minutes and then agitated with a sonic disperser (Fisher Sonic Dismembrator, model 300) for another 15 minutes. A few drops of a solution containing polystyrene latex spheres were added to the suspension as a reference standard (diameter 2.02 microns) for later electron microscope inspection. Using a syringe, a tiny drop of this finely dispersed suspension was placed on top of a copper grid (mesh 200, dia. 3 mm) which was pre-coated with collodion film for support. When dried, the grid was further coated with evaporated carbon to improve electrical conductivity. For zeolite mordenite, instead of methanol, a better dispersion of particles was achieved by using a 20% aqueous ammonia solution.

Typical micrographs taken from the transmission electron microscope are

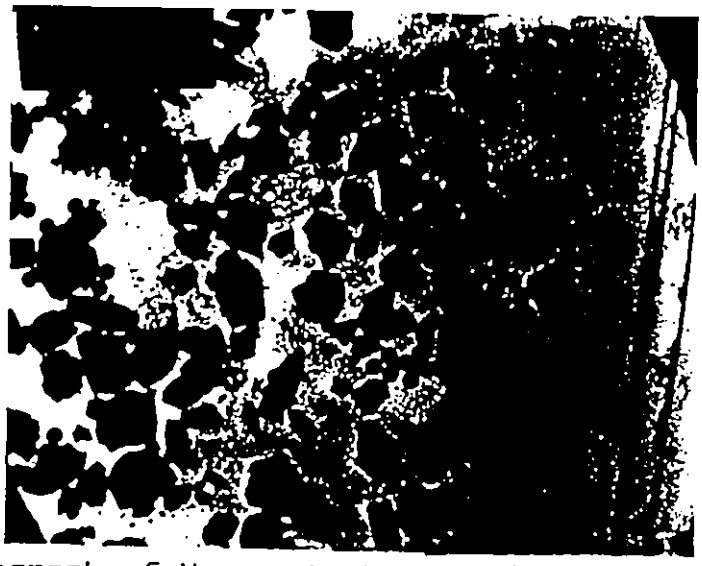

Fig 3.4 Micrograph of Na-mordenite 9630X

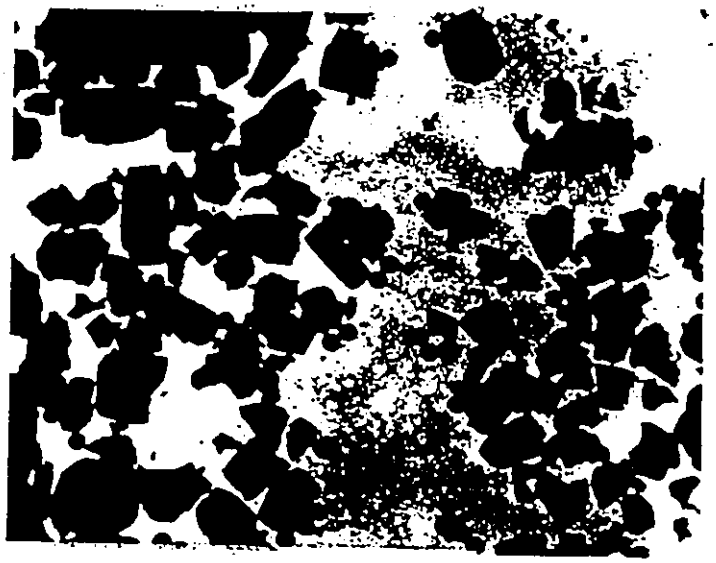

Fig 3.5 Micrograph of H-mordenite 9630X

Fig 3.6 Micrograph of 4A 9630X

shown in Figs. 3.4, 3.5 and 3.6 for zeolites Na-mordenite, H-mordenite and 4A, respectively. More than 500 particles were counted for each zeolite, and the particle sizes were measured directly from the enlarged photographs. The 4A crystals are shown to have the expected cubic shape, but the morphology of the mordenite crystals is less well defined. The crystal structure of mordenite is orthorhombic; however, few particles exhibited the expected rectangular shape. As a result, two measurements were made for each particle; a shortest and a longest edge length, and the mean of these two edge lengths was used in the later particle size distribution calculation.

Particle size distributions for zeolite 4A are presented in Table 3.4. The cumulative weight fractions were plotted against the edge lengths on both normal and log-normal plots, Figs. 3.7 and 3.8, respectively. The log-normal distribution is shown to have a better fit with a weight mean average of 3.27 microns and a standard deviation of 1.86. These values indicate that the 4A particles studied in this work were smaller and had a broader distribution compared to those used by Eagan with a weight mean average of 4 microns and a standard deviation of 1.33. [17]

The particle size distribution data for mordenites are presented in Tables 3.5 and 3.6. Log-normal distribution curves are shown in Fig. 3.9. In general, H-mordenite's data give a better fit, and its particle size on an average is slightly larger than the Na-mordenite (2.98 versus 2.45 microns). Also, H-mordenite has a narrower distribution. The results of the particle size distribution studies are summarized in Table 3.7.

Table 3.4 Particle size distribution data for zeolite 4A

Edge Length (μ)	Wt. Fraction	Cumulative Fraction
0.5	0.0000	0.0000
1.0	0.0380	0.0380
1.5	0.1063	0.1443
2.0	0.0911	0.2355
2.5	0.1089	0.3443
3.0	0.1139	0.4583
3.5	0.0684	0.5266
4.0	0.0532	0.5798
4.5	0.0405	0.6203
5.0	0.0633	0.6836
5.5	0.0557	0.7393
6.0	0.0658	0.8051
6.5	0.0506	0.8557
7.0	0.0405	0.8962
7.5	0.0253	0.9215
8.0	0.0101	0.9317
8.5	0.0101	0.9418
9.0	0.0051	0.9469
9.5	0.0127	0.9595
10.0	0.0000	0.9595
10.5	0.0101	0.9696
11.0	0.0051	0.9747
11.5	0.0101	0.9848
12.0	0.0051	0.9899
12.5	0.0000	0.9899
13.0	0.0025	0.9924
13.5	0.0025	0.9950
14.0	0.0000	0.9950
14.5	0.0000	0.9950
15.0	0.0051	0.9999
15.5	0.0000	0.9999
16.0	0.0025	1.0000

FIG 3.7 4A SIZE DISTRIBUTION, NORMAL DISTRIBUTION

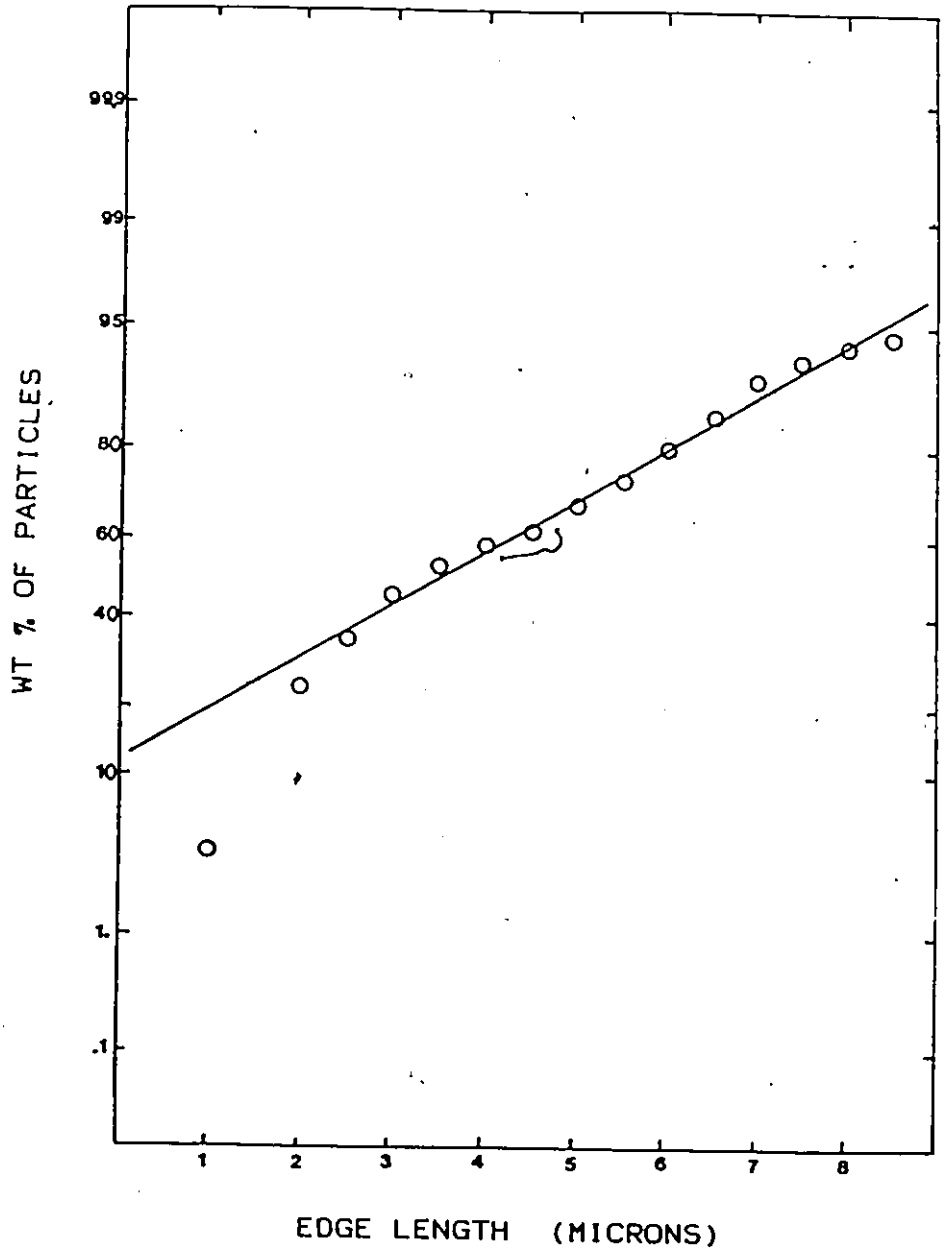

FIG 3.8 4A SIZE DISTRIBUTION, LOG-NORMAL DISTRIBUTION

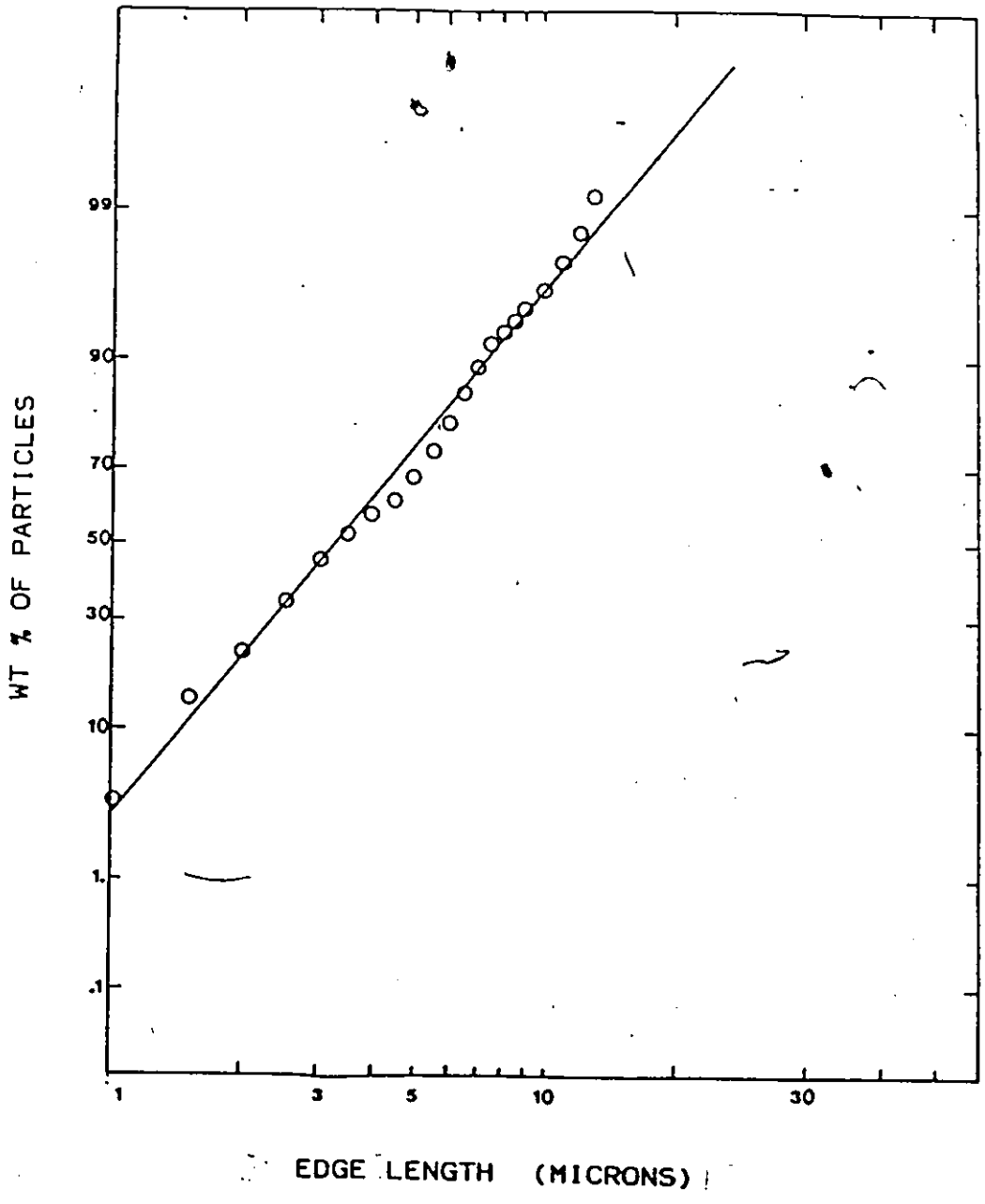

Table 3.5 Particle size distribution data for Na-modenite

Edge Length (μ)	Wt. Fraction	Cumulative Fraction
0.4	0.0000	0.0000
0.8	0.0474	0.0474
1.2	0.0645	0.1119
1.6	0.1369	0.2488
2.0	0.0921	0.3409
2.4	0.1092	0.4504
2.8	0.0869	0.5370
3.2	0.1237	0.6607
3.6	0.0895	0.7502
4.0	0.0546	0.8048
4.4	0.0573	0.8621
4.8	0.0362	0.8983
5.2	0.0362	0.9345
5.6	0.0270	0.9615
6.0	0.0158	0.9773
6.4	0.0112	0.9885
6.8	0.0040	0.9925
7.2	0.0059	0.9984
7.6	0.0007	0.9991
8.0	0.0000	0.9998
8.4	0.0000	0.9998
8.8	0.0000	0.9998
9.2	0.0002	1.0000

Table 3.6 Particle size distribution data for H-mordenite

Edge Length (μ)	Wt. Fraction	Cumulative Fraction
0.5	0.0000	0.0000
1.0	0.0034	0.0034
1.5	0.0542	0.0576
2.0	0.1061	0.1637
2.5	0.1727	0.3365
3.0	0.1219	0.4583
3.5	0.1580	0.6161
4.0	0.1264	0.7427
4.5	0.1072	0.8499
5.0	0.0632	0.9131
5.5	0.0226	0.9357
6.0	0.0260	0.9617
6.5	0.0147	0.9764
7.0	0.0079	0.9843
7.5	0.0068	0.9911
8.0	0.0012	0.9923
8.5	0.0012	0.9935
9.0	0.0012	0.9945
9.5	0.0012	0.9957
10.0	0.0012	0.9969
10.5	0.0023	0.9992
11.0	0.0007	0.9999

FIG 3.9 Na, H-MORDENITE SIZE DISTRIBUTION, LOG-NORMAL DISTRIBUTION

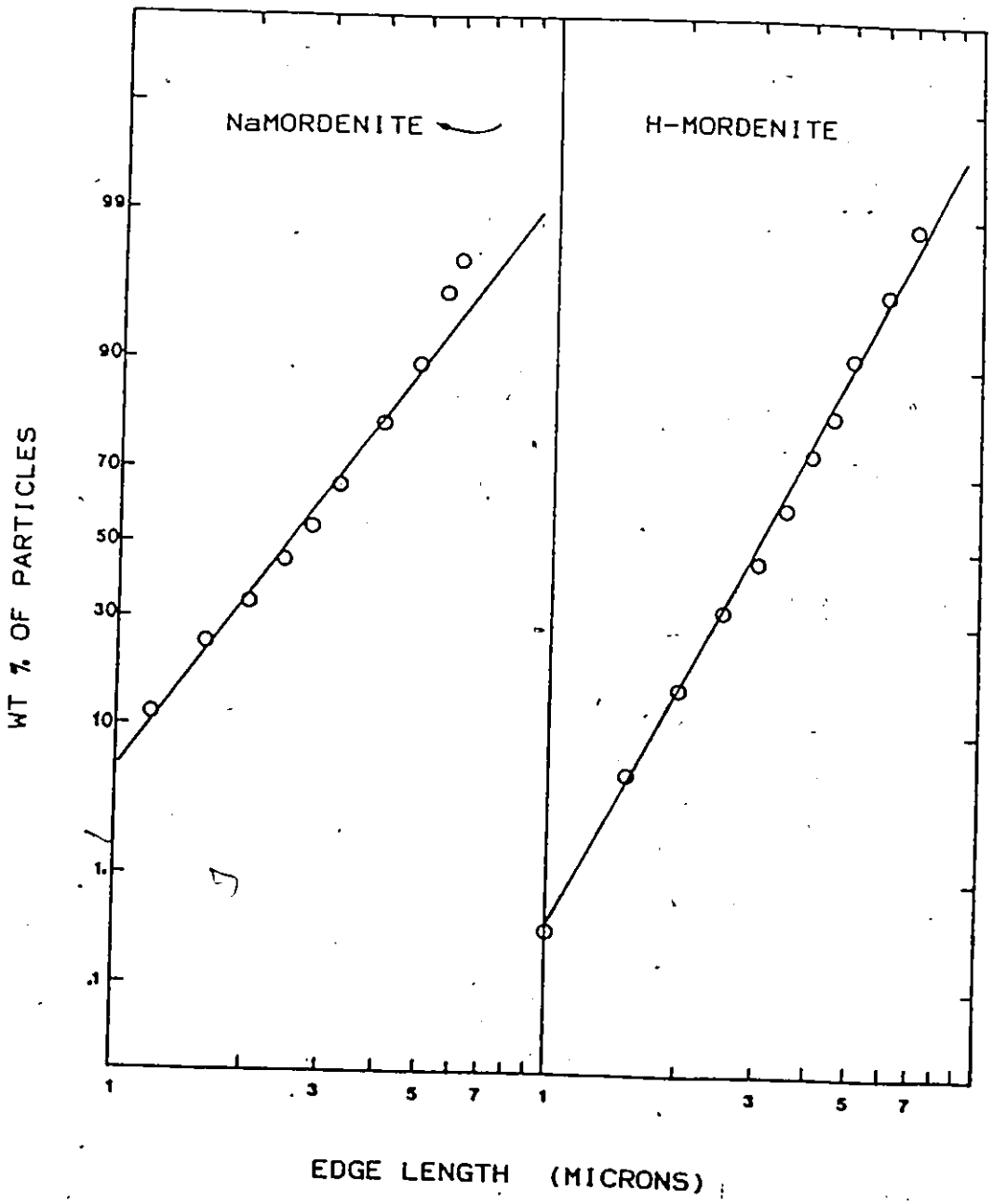

Table 3.7 Summary of particle size distribution results

ZEOLITE	NO. OF PARTICLE COUNTED	WEIGHTED MEAN (edge length,)	STANDARD DEV.
4A	515	3.27	1.86
Na-Mord.	760	2.45	1.76
H-Mord.	443	2.98	1.49

CHAPTER IV

EQUILIBRIUM AND KINETIC RESULTS

4.1 EQUILIBRIUM

Equilibrium isotherms of ethane, ethylene and carbon dioxide on zeolites 4A, Na-mordenite and H-mordenite are shown in Figures 4.1 through 4.7. Experimental data were tested against a 2-dimensional virial equation of increasing inverse integer-powers of ($A-\sigma$), where A is the area per molecule and σ is a constant related to the cross-sectional area of the molecules in a closely packed condition. The final equation as developed in Appendix (A-2) is of the form

$$\ln (P/\chi)-\chi=\ln K +(\beta/\sigma)\chi(2+\chi)+(\gamma/\sigma^2)\chi^2(1.5+\chi) \qquad 4.1$$

where P is the equilibrium pressure, ln K, β/σ and γ/σ^2 are the first, second and third virial coefficients, respectively. χ is equal to $\theta/1-\theta$, and θ is chosen to be Q/Qs where Q is the equilibrium amount adsorbed. Qs is the volume of sorbate with a liquid density at its normal boiling point equal to the volume of the accessible pores in the zeolites; 0.281 cc/g and 0.165 cc/g for the respective zeolites 4A and mordenites. For CO_2, Qs was calculated by taking its solid density at sublimation point of -78°C.

In the present work, the equilibrium sorption data were fitted by non-linear least squares to the 3-constant virial equation first and, if the third virial coefficient (γ/σ^2) of a given sorbate at most of the temperatures studied was found not to be significantly different from zero according to a standard statistical t-test, then, the data were re-fitted to a 2-constant equation by setting γ/σ^2 to zero. Overall, the inclusion of the third term improves the goodness of fit only marginally. However, in cases where the values of γ/σ^2 were found to be appreciably different from zero,

for example, the adsorption isotherms of CO_2 on 4A and ethane on Na-mordenite, the presence of a third constant had the effect of causing the values of other parameters to vary erratically with temperatures. As a result, all of the isotherms obtained in this study were correlated with the 2-constant virial equation.

In Figures 4.1 to 4.7, calculated isotherms are shown as the solid curves. Values of the virial coefficients estimated by least squares are presented in Table 4.1 As shown, the virial equation correlated the experimental isotherms reasonably well. Anderson, et al. [1] reported that isotherms with a point of inflection could be adequately described with a 3-constant virial equation. The present form of the virial equation used in this study is superior to the standard virial equation in terms of A^{-1} proposed by Kiselev [28] and Barrer[7]; evidently, the equations they developed do not have the necessary form of fitting the commonly obtained isotherms unless four or five coefficients were used. Moreover, the present virial equation describes well the nearly rectangular isotherms of CO_2 and C_2H_4. The Langmuir equation usually predicts adsorption values lower than the experimental at large pressure, whereas Freundlich equations are also normally inappropriate for these rectangular isotherms.

The value of the saturation adsorption, Qs, was chosen in an arbitrary but reasonable way. In the mordenite case, no attempt was made to distinguish pore volume differences between the two cationic forms. Furthermore, we have taken Qs to be independent of temperature. However, Eagan [17], in a study of permanent gases adsorption on 4A zeolite, made a systematic search for the best value of Qs and found the virial equation to be insensitive to the actual value of Qs used; the values of Qs obtained

FIG 4.1 ETHANE ISOTHERMS ON H-MORDENITE ZEOLITE

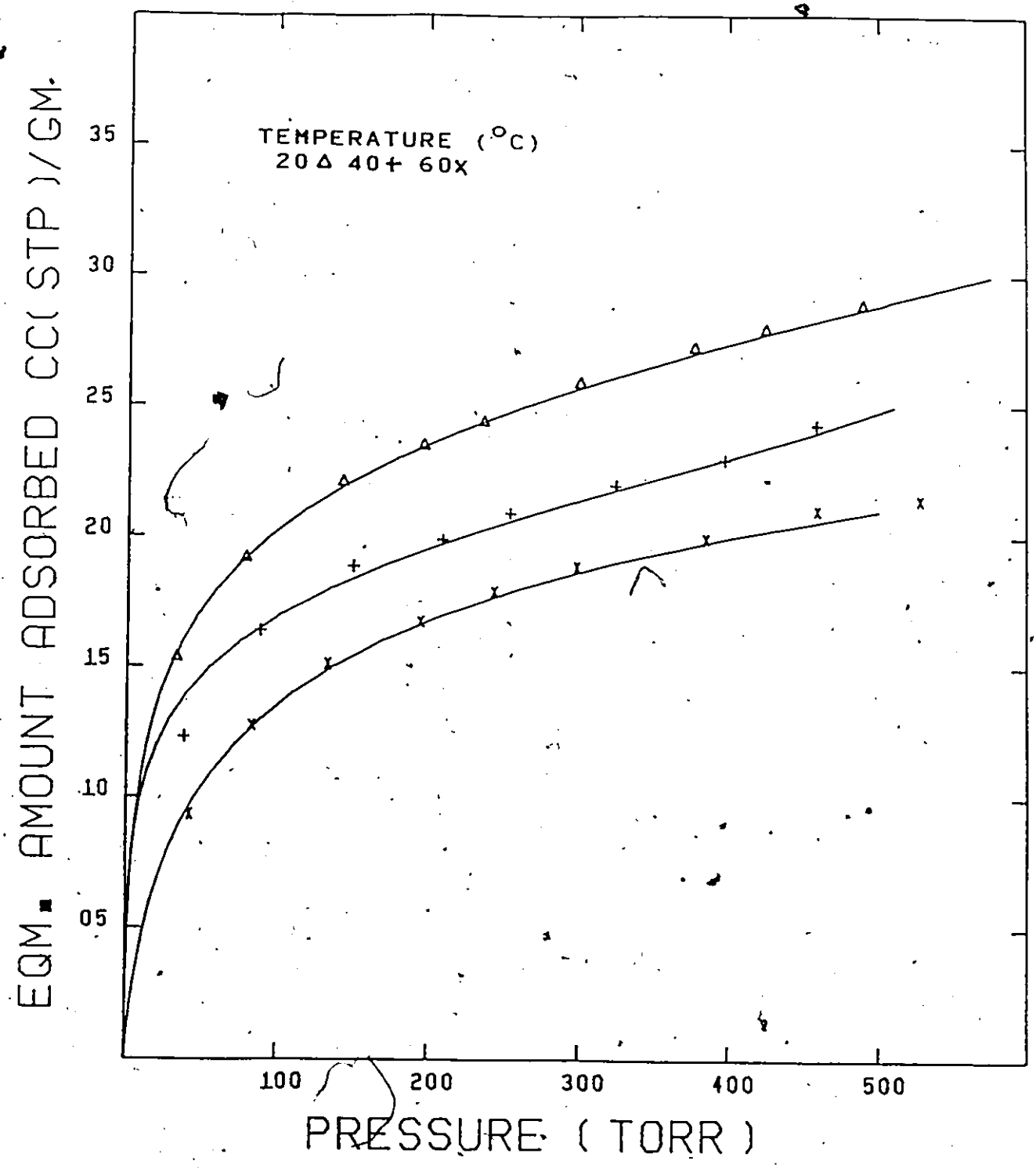

FIG 4.2 ETHANE ISOTHERMS ON Na-MORDENITE ZEOLITE

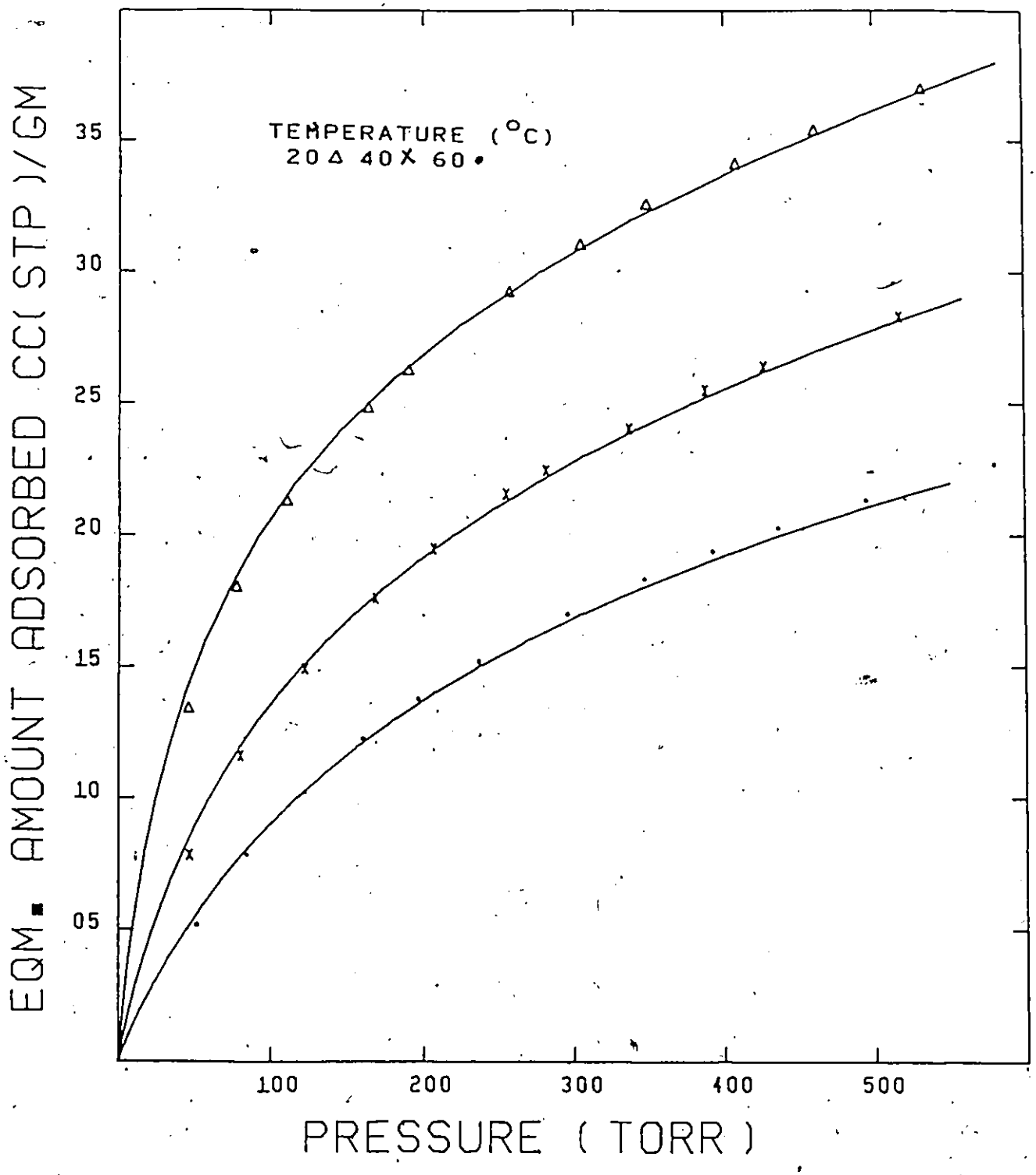

FIG 4.3 CARBON DIOXIDE ISOTHERMS
ON H-MORDENITE ZEOLITE

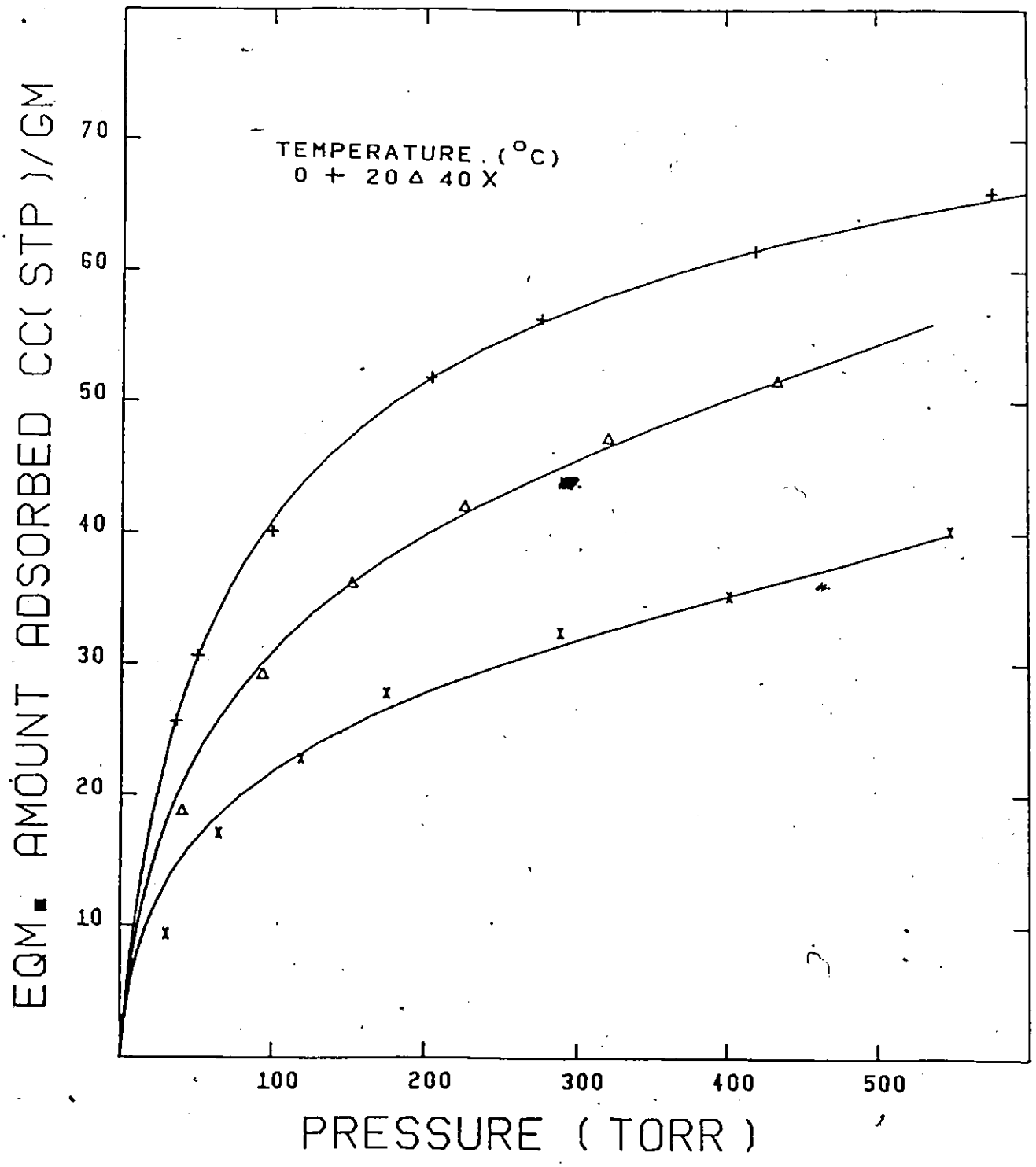

FIG 4.4 ETHANE ISOTHERMS ON NaA ZEOLITE

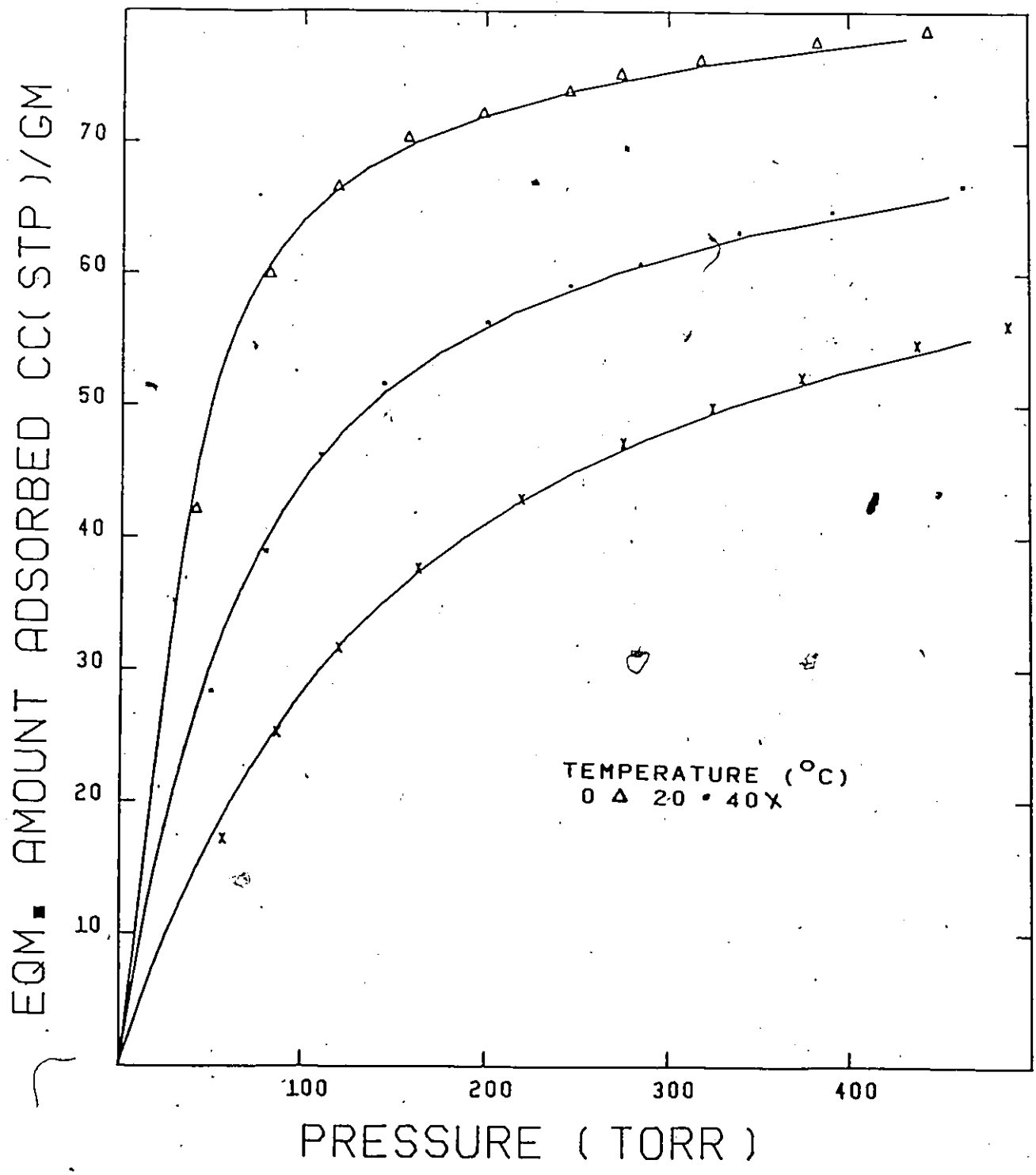

FIG 4.5 CARBON DIOXIDE ISOTHERMS ON NaA ZEOLITE

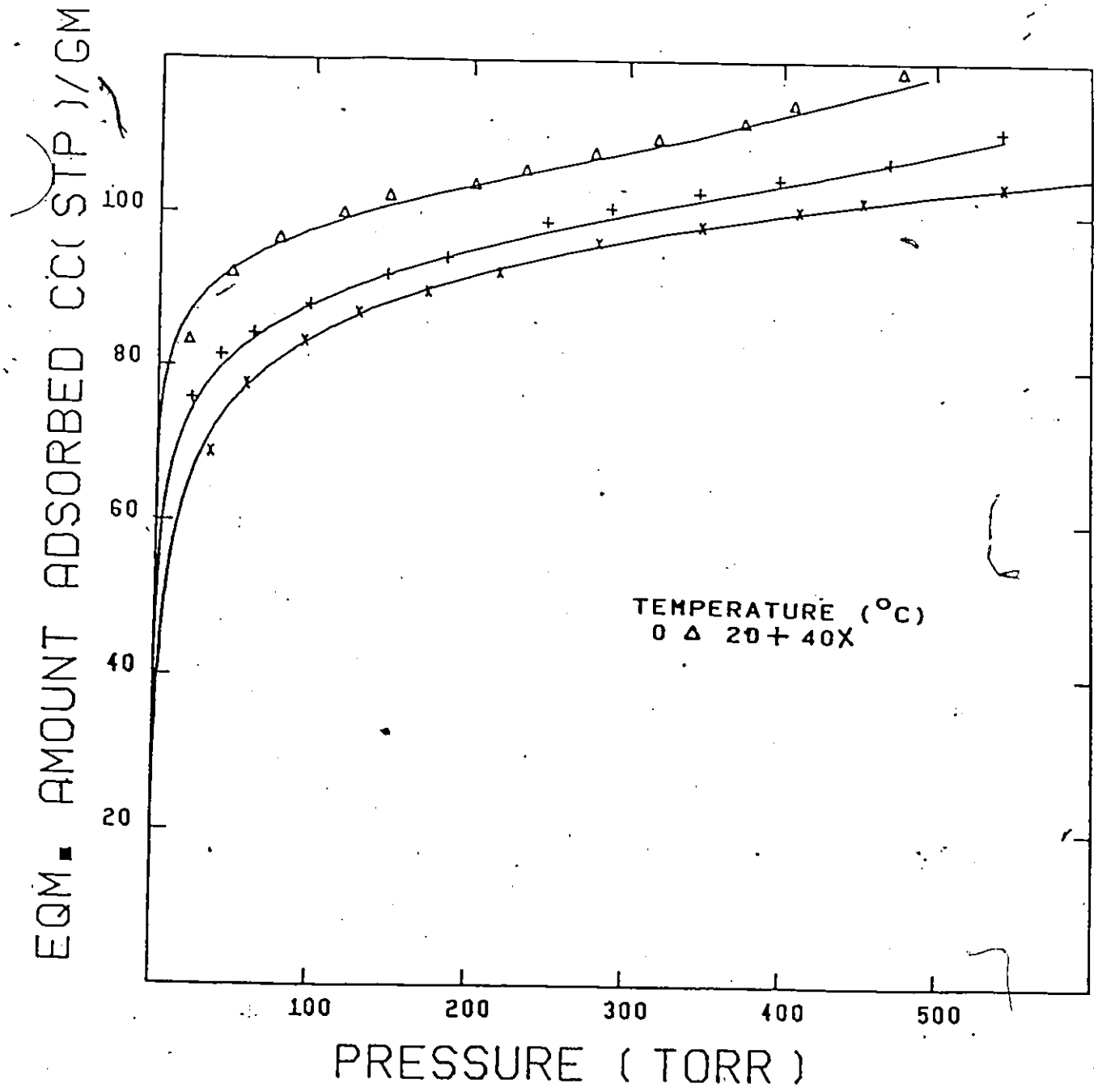

FIG 4.6 CARBON DIOXIDE ISOTHERMS ON Na-MORDENITE ZEOLITE

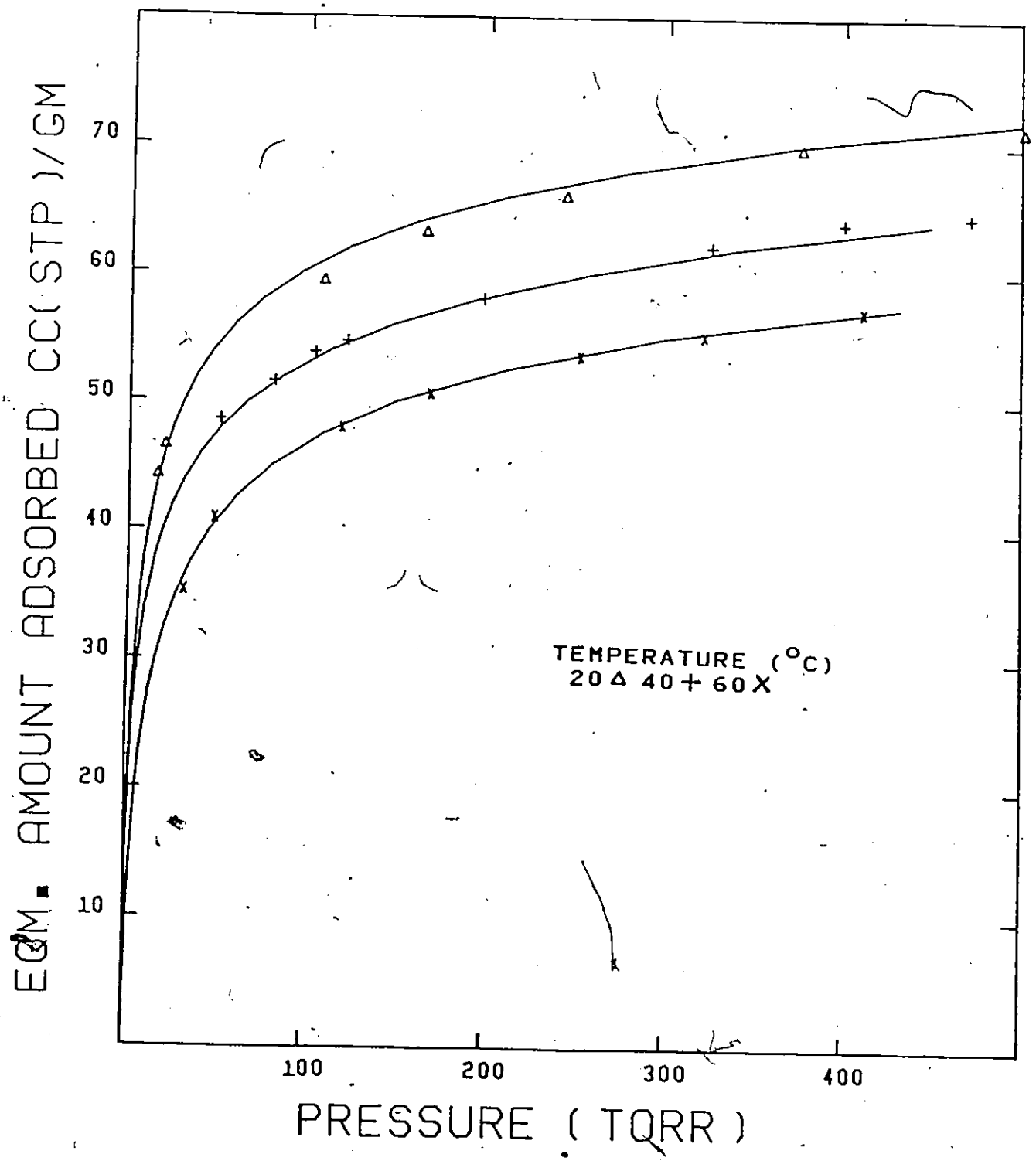

FIG 4.7 ETHYLENE ISOTHERMS ON NaA ZEOLITE

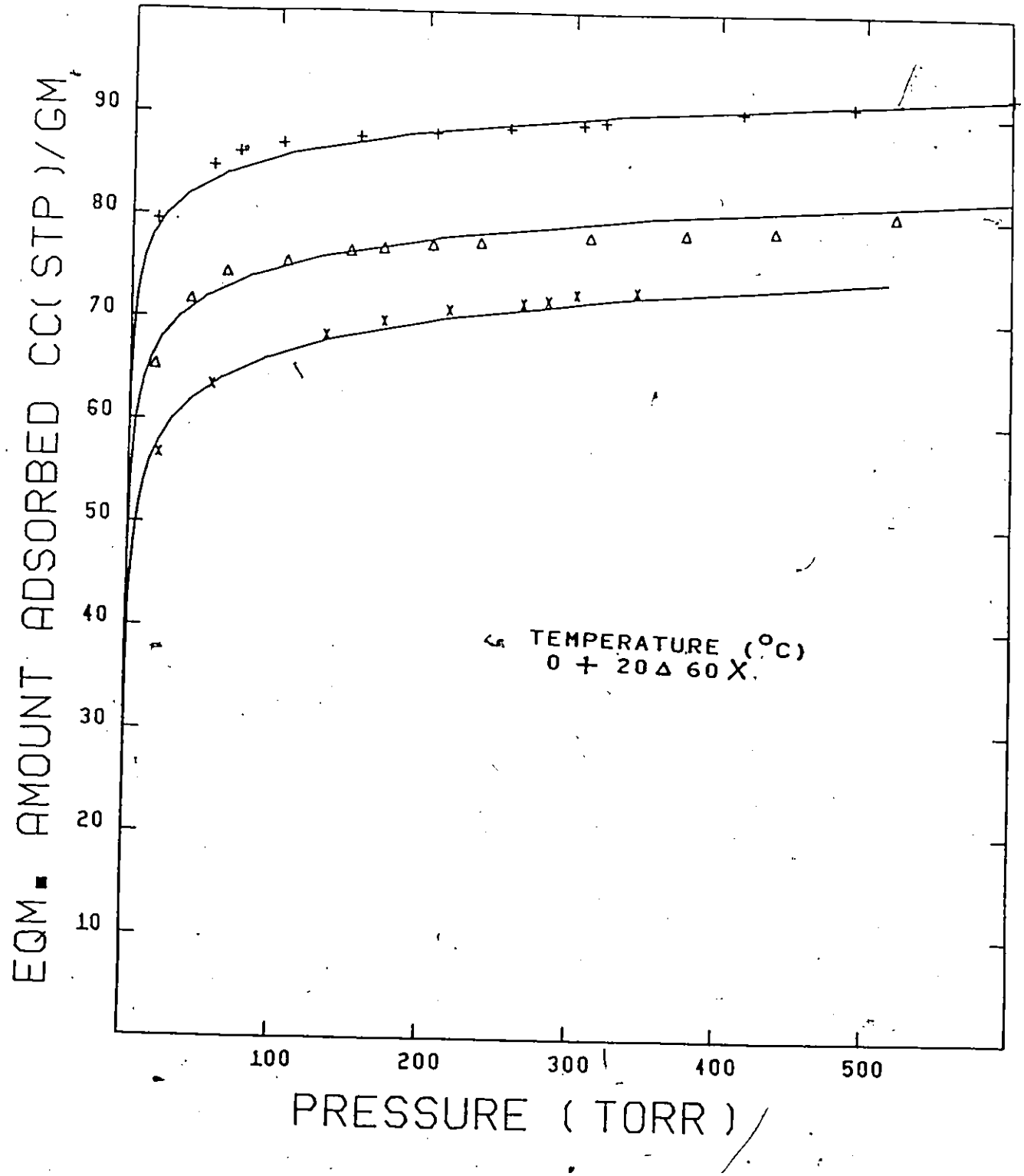

Table 4.1 Least Squares Parameter Values in Virial Equation

Least squares parameter values are given first, followed by 95% (+ or -) confidence limits. Qs values are in cc(STP)/g of dehydrated zeolites.

Zeolite	Gas (Qs)	Temp. (°C)	Least Square Parameter Values Ln K	β/σ
NaA	CO_2	0.0	2.363 , 0.757	1.248 , 0.338
		20.0	3.819 , 0.595	0.810 , 0.276
	(246.26)	40.0	3.022 , 0.223	1.466 , 0.115
Na-mord		20.0	2.469 , 0.366	0.993 , 0.136
	(144.62)	40.0	2.745 , 0.285	1.263 , 0.127
		60.0	2.803 , 0.148	1.789 , 0.087
H-mord		20.0	4.998 , 0.171	0.289 , 0.070
		40.0	5.897 , 0.282	0.633 , 0.065
		60.0	6.175 , 0.348	0.719 , 0.038
NaA	C_2H_4	0.0	-4.933 , 1.890	5.267 , 0.937
		20.0	-2.943 , 1.526	5.845 , 0.966
	(212.73)	40.0	-1.569 , 0.695	5.852 , 0.552
NaA	C_2H_6	0.0	2.646 , 0.374	1.005 , 0.154
		20.0	4.505 , 0.161	0.751 , 0.100
	(164.95)	40.0	5.478 , 0.093	0.707 , 0.067
Na-mord.		20.0	4.549 , 0.279	2.076 , 0.300
	(96.85)	40.0	4.847 , 0.467	2.746 , 0.673
		60.0	5.089 , 0.122	3.387 , 0.198
H-mord.		20.0	5.548 , 0.126	0.372 , 0.087
		40.0	6.190 , 0.079	0.527 , 0.081
		60.0	6.621 , 0.028	0.914 , 0.042

from a non-linear least square parameter search method varied by as large as ten times of the original value in some instances and as little as half in other cases without significantly improving the goodness of fit.

The first virial coefficient, ln K, is related to the reciprocal of the Henry's Law constant and, as such, it is a measure of sorbate-zeolite interaction; small values of K indicate strong interaction. The adequacy of Eqn. 4.1 in describing a given isotherm can further be tested from the linearity of the curves in plotting ln K against the reciprocal absolute temperature. Fig. 4.8 shows these plots are essentially smooth curves exhibiting little curvature. In terms of the sorbate-zeolite interaction, the magnitude of ln K shows that both C_2H_4 and CO_2 have a stronger interaction with the zeolite electrostatic field than ethane. This may be the reflection of the π-electrons and quadrupole moment properties associated with the two respective molecular species. For a given sorbate, however, the sorbate-zeolite interactions are approximately the same for 4A and Na-mordenite, both having sodium as the cation, Table 4.1.

Physical significance can also be attached to the higher virial coefficients, and β/σ is usually interpreted in terms of the adsorbate-adsorbate molecular interaction; negative values indicate an attractive interaction enhancing adsorption and positive values, repulsion. Positive values were consistently obtained for all isotherms, indicating a net dominating adsorbate-adsorbate repulsion which may have been the result of the strong adsorbate-zeolite interaction, Table 4.1

The isosteric heats of adsorption, q_{st}, as a function of amount adsorbed were calculated from the experimental isostere using the usual Clapeyron equation

FIG 4.8 LN K Vs 1/T

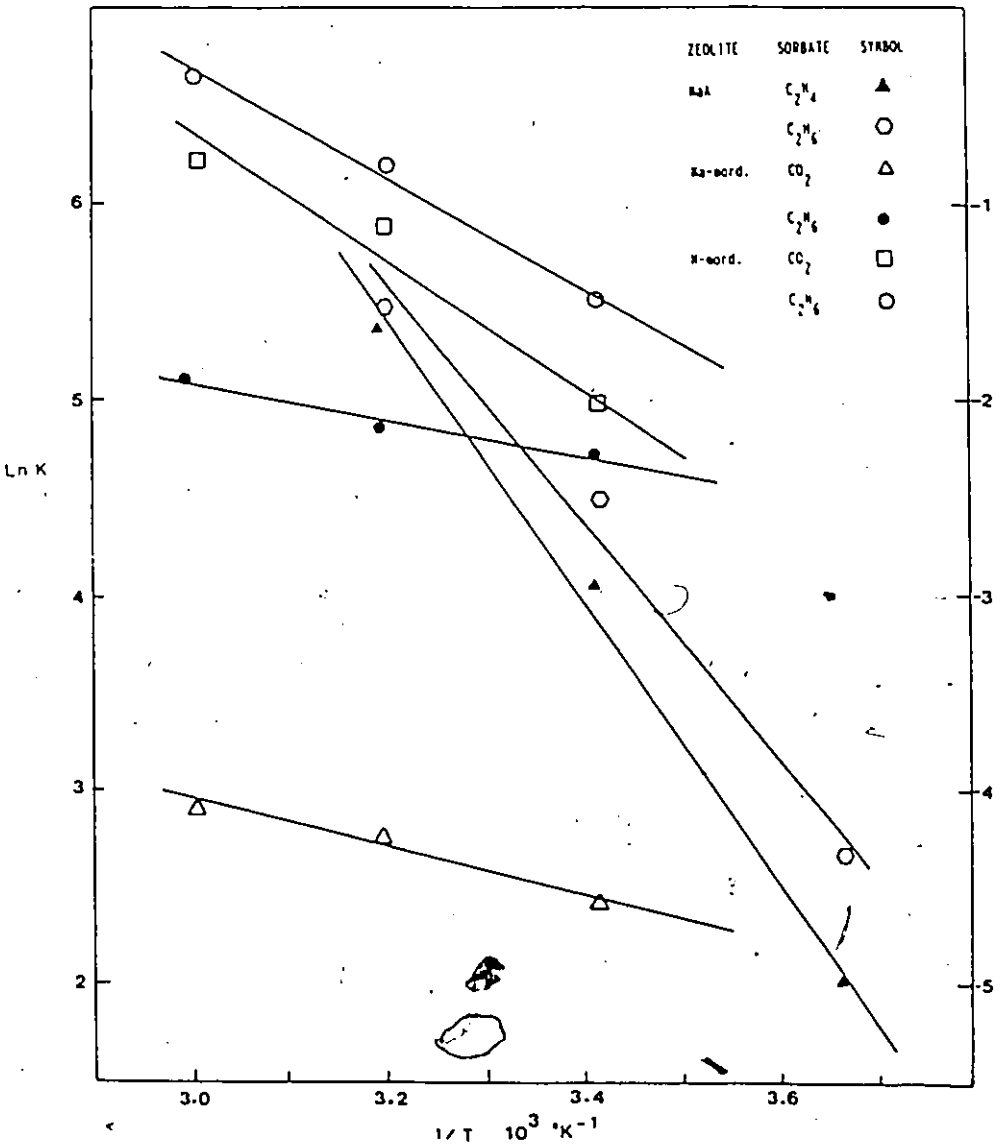

$$q_{st} = -R \left(\partial \ln P / \partial (1/T) \right)_Q \qquad 4.2$$

Results are shown in Fig. 4.9. With the exception of CO_2 on 4A, calculated heat of sorption values generally show very little concentration dependency. Values of q_{st} can be compared with the isosteric heat of sorption data from the literature: For adsorption of ethane on zeolite. 4A, Kondis and Dranoff [30] determined a slightly higher value of 29.3 KJ/mole whereas Brandt and Rudluff [10] obtained a value of 25.8 KJ/mole, which agrees well with the value of 26 KJ/mole obtained in this study. Sheth and Dranoff [52] quoted a q_{st} value of 39.33 KJ/mole in adsorption of ethylene on 4A, this is lower than the 54.0 KJ/mole determined in the current study. However, their reported value was calculated from an isotherm that consisted of only three data points. For ethane adsorption on H-mordenite, Barrer [8] calculated a value of 38.5 KJ/mole which is higher than the 31.5 KJ/mole reported here. Barrer and Murphy [9] also determined the initial isosteric heat for CO_2 adsorption on Na- and H-mordenite zeolites to be 65 KJ/mole and 46 KJ/mole, respectively. Although these values are significantly higher than ours, their heat of sorption showed a strong concentration dependency and decreased drastically with increasing amount of sorption, whereas our values remain essentially constant with concentration. In fact, with the exception of CO_2 on 4A, the isosteric heats obtained in this work show very little dependence upon concentration. For adsorptions of ethane on 4A, CO_2 on H-mordenite, a slight upward curvature can be seen with increasing concentration; this may have been the result of the repulsive adsorbate-adsorbate interaction as indicated by the +ve sign of the second virial coefficient mentioned in the previous section.

A comment on the adsorption of CO_2 on zeolite 4A is in order; Fig. 4.9

FIG 4.9 ISOSTERIC HEAT Vs AMOUNT ADSORBED

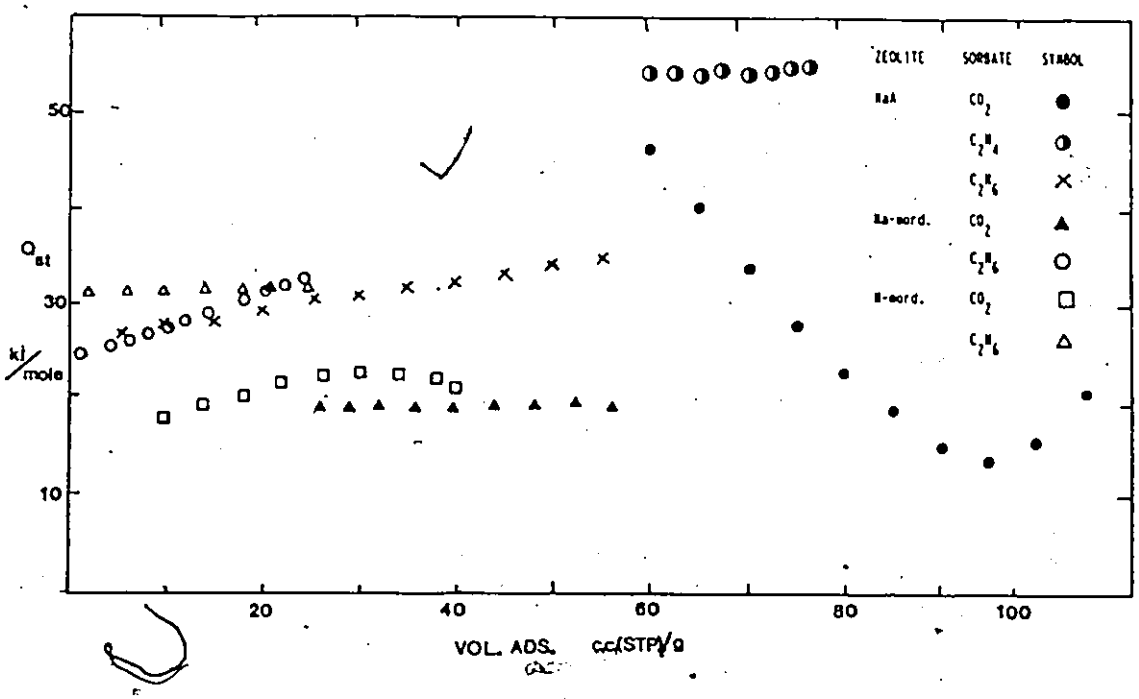

shows an initial decrease in heats of adsorption with concentration followed by an increase. This phenomenon was also reported by Eagan [17]. He attributed the initial decrease in heat to the reduction of the interaction energy per molecule between the CO_2 molecules and zeolite surface and suggested that the subsequent increase at higher concentration was due to the formation of semi-solid adsorbed phase with enhanced interaction between adjacent CO_2 molecules.

4.2 KINETIC DATA

4.2.1 SINGLE COMPONENT DIFFUSION RATES

Single component sorption rates of carbon dioxide, ethylene and ethane on zeolites 4A, Na- and H-mordenite were measured at temperatures of 273 K, 293 K, 313 K and 333 K. Diffusivities were calculated by matching the sorption uptake curves to the solutions of Ficklan diffusion equation for cubic particles with size distribution effects taken into consideration, Appendix A-3. Results are summarized in Table 4.2.

Several important points are suggested by the data of Table 4.2: It should be noted first that the diffusivities of adsorption are consistently higher than those of desorption. Secondly, for a given molecule, the diffusion rate increases in the order from zeolite 4A, Na- to H-mordenite. Thirdly, for a given zeolite, diffusivity increases in the sequence of ethane, ethylene and carbon dioxide for sorption on 4A, whereas the reverse order is observed for sorption of the same molecules in both mordenite zeolites

Some comparison of diffusivities determined in this work with those available in the literature can be made; Carter and Husain [13] studied the

Table 4.2 Fick's Law Diffusivity of Adsorption into Pre-evacuated Zeolites and Desorption in Pure Helium.

Zeolite	Diffusant	Diffusion direction	Diffusivity 10^{+13} cm^2/sec			
			0.0°C	20.0°C	40.0°C	60.0°C
NaA	CO_2	ADS.	17.63	21.77	23.38	-
		DES.	0.57	3.00	4.84	-
	C_2H_4	ADS.	3.77	16.46	23.18	-
		DES.	0.24	1.94	5.26	
	C_2H_6	ADS.	0.84	2.26	-	-
		DES.	0.44	1.37	-	-
Na-mord.	CO_2	ADS.	-	51.87	60.80	79.75
		DES.	-	6.28	8.45	21.98
	C_2H_4	ADS.	-	93.70	137.4	120.32
		DES.	-	18.07	15.92	43.00
	C_2H_6	ADS.	-	246.7	310.8	385.67
		DES.	-	69.27	126.80	193.00
H-mord.	CO_2	ADS.	73.77	99.77	130.27	-
		DES.	24.13	51.28	87.62	-
	C_2H_6	ADS.	121.97	204.50	317.67	-
		DES.	83.47	174.50	300.70	-

sorption rate of carbon dioxide on a fixed bed of zeolite A pellets. The reported value of diffusivity of 1.44×10^{-10} cm^2/sec at 25°C and a pressure of 1.25 atm is somewhat higher than the value of 0.21×10^{-10} cm^2/sec reported in this study. Their data, however, may have been complicated by the mass and heat transfer resistances within the zeolite pellets. Yucel and Ruthven [57] found a wide range of diffusion coefficients in a study of adsorption of carbon dioxide on zeolite 4A with varying crystal sizes. However, the activation energies obtained were similar. Moreover, the diffusivity showed a high degree of concentration dependency; at a comparable CO_2 partial pressure to this work, the diffusivity values varied from a high of 4.0×10^{-9} cm^2/sec to a low of 1.8×10^{-11} cm^2/sec. Brandt and Rudloff [10] measured the diffusion rate of ethane in various cationic forms of Linde A type zeolites. The calculated diffusion coefficients corresponding to 4A also showed a concentration sensitivity; D/R^2 obtained varied from 9.3×10^{-4} sec^{-1} to 4.4×10^{-4} sec^{-1} determined from the initial and late portions of the rate curve, respectively. A similar study of ethane sorption on zeolite 5A conducted by Loughlin and Ruthven [45] indicated a positive concentration dependency of the diffusivity. Also, they reported good agreements in values of D/R^2 measured in sorption on zeolite crystals and pellets thus suggesting a lack of difference in the basic diffusional resistance between the two samples. Sheth and Dranoff [52] carried out sorption experiment of ethylene on 4A in a flow system. Results obtained show an average value of D/R^2 over 9 runs to be 1.31×10^{-3} sec^{-1}. This value is high when compared to the present study. Their experimental set up was similar to the current work, although sorption runs were measured at a higher temperature of 75°C.

Table 4.2 shows the diffusion rate of a particular sorbate molecule increases in the order from zeolite 4A, Na-mordenite to H-mordenite. this trend paralleled the increasing pore aperture size from 4A to H-mordenite. The diffusion rate increased because the larger pores offer a greater degree of mobility freedom by decreasing the steric interaction between the sorbate molecule and the zeolitic framework. Loughlin and Ruthven [33] found the ethane diffusivity in various cationic forms of zeolite A followed the order of cation sizes; diffusion coefficient decreases with increasing cationic radii. This is because the exchangeable cations usually obstruct the window apertures between the adjacent zeolite cavities, and the reduction in the cation size thus removes some of the obstruction and causes in effect an increase in the size of the diffusion channels which then resulted in a greater molecular mobility for the diffusing molecules.

For sorption on zeolite 4A, the diffusivity is shown to increase in the order of ethane, ethylene and carbon dioxide, Table 4.2. This trend seems at first at odds with the expectation that with the enhanced interaction between the adsorbate and zeolitic eletrostatic field, for example, carbon dioxide with its strong quadrupole moment, the molecular mobility would be reduced. Table 3.3 lists some pertinent physical properties of molecules studied in this work. Of particular interest is the minimum molecular cross-sectional area. In systems where the critical diameter of the diffusing molecule closely approaches to that of the zeolite aperture size, the lattice framwork itself, in relation to other effects such as the electronic interaction, may become the dominant factor in determining the controlling resistance to molecular flow. Zeolite 4A - sorbate combinations are apparently one of these systems where the diffusivity decreases markedly

with increasing critical cross-sectional area. Thus, CO_2, being the smallest molecule, exhibited the highest rate. The strong correlation of molecular diameter with pore size has been reported in the literature: Nelson and Walker [40] in a study of propane sorption on Linde A zeolite, reported propane diffusivity in CaA (effective pore diameter, 5A) to be 4 times larger than in NaA (effective pore diameter, 4A). Barrer and Ibbitson [6] observed that the diffusion coefficients of hydrocarbon gases in analcite and chabazite decreased with increasing molecular weight. Ruthven [45] also reached the same conclusion in a study of light hydrocarbons sorption on zeolite 5A.

The steric effect mentioned above should nevertheless diminish with an increase in the relative size between the zeolite pores and diffusate molecular diameter. For small molecules diffusing in large port zeolites, the zeolitic framework structure itself offers a reduced steric resistance to the passage of diffusates and other factors such as the electronic interaction arising from the molecular quadrupole moment, dipole, π-bond interaction with the zeolitic electrostatic field may gain sufficient magnitude to become the controlling factor in determining diffusion rates. Thus, diffusion rates of carbon dioxide, ethylene and ethane in large port mordenite zeolites (Na-mordenite, 6-7A, H-mordenite, 9-10A) are expected to be in the reverse order of that observed for the zeolite 4A, i.e., ethane, being a relatively inert molecule, has the least interaction, and should have the highest rate, whereas, CO_2, with its strong qrudrupole moment, should exhibit the lowerest rate, which is consistent with the experimental results.

The values of the effective diffusion coefficients calculated from

adsorption and desorption uptake curves are shown to be vastly different. Thus, it reflects the anisotropic nature of the zeolite diffusion mechanism, Table 4.2. Desorption rates in general are much smaller than the adsorption rates for all molecules and zeolites studied. Other workers have reported the similar phenomena; For ethylene sorption on 4A, Sheth and Dranoff [52] found a ratio of 1.72 between adsorption and desorption rates. Satterfield and Frabetti [49] reported the diffusion coefficient of desorption varied from three to six times smaller than those of adsorption in sorption studies of C_1 to C_4 paraffins on Na-mordenite. Garg and Ruthven [22] investigated this phenomenon in a theoretical model simulation and concluded that the non-linearity of the isotherms and the observed concentration dependency of the diffusivity could have a significant impact on the respective sorption rates; for a large differential change in sorbate concentration, their simulated results showed a significant divergence between adsorption and desorption curves with the desorption rate being much smaller. Ebeley [20] also reported similar observations in a study of light paraffin hydrocarbon sorption on 5A. However, the difference may have been further magnified by thermal effects.

The direct comparison of adsorption and desorption rate curves are shown in Figs. 4.10 through 4.17. These figures (Z-plots) are the result of plotting the fractional approach to equilibrium values, Z, of the respective adsorption and desorption curves against each other at equal sorption time. Comparing sorption rates by plotting in this fashion has the advantages of demonstrating precisely and clearly the differences between the adsorption and desorption rates. Also, since the diagonal line serves as a reference, the degree of the rate differences may be evaluated from the distance

FIG 4.10 SINGLE COMPONENT Z-PLOT OF CARBON DIOXIDE ON NaA

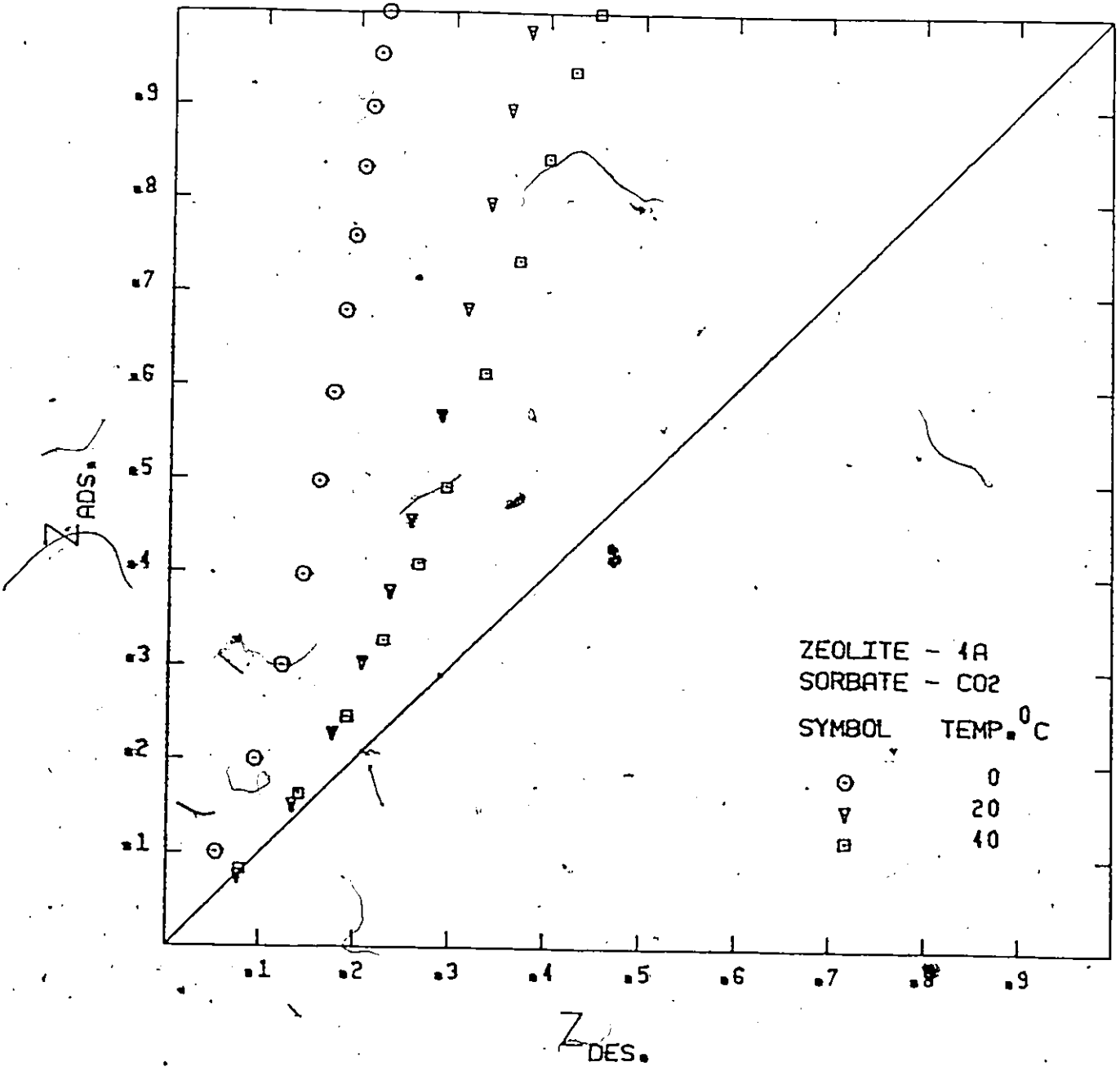

FIG 4.11 SINGLE COMPONENT Z-PLOT OF ETHYLENE ON NaA

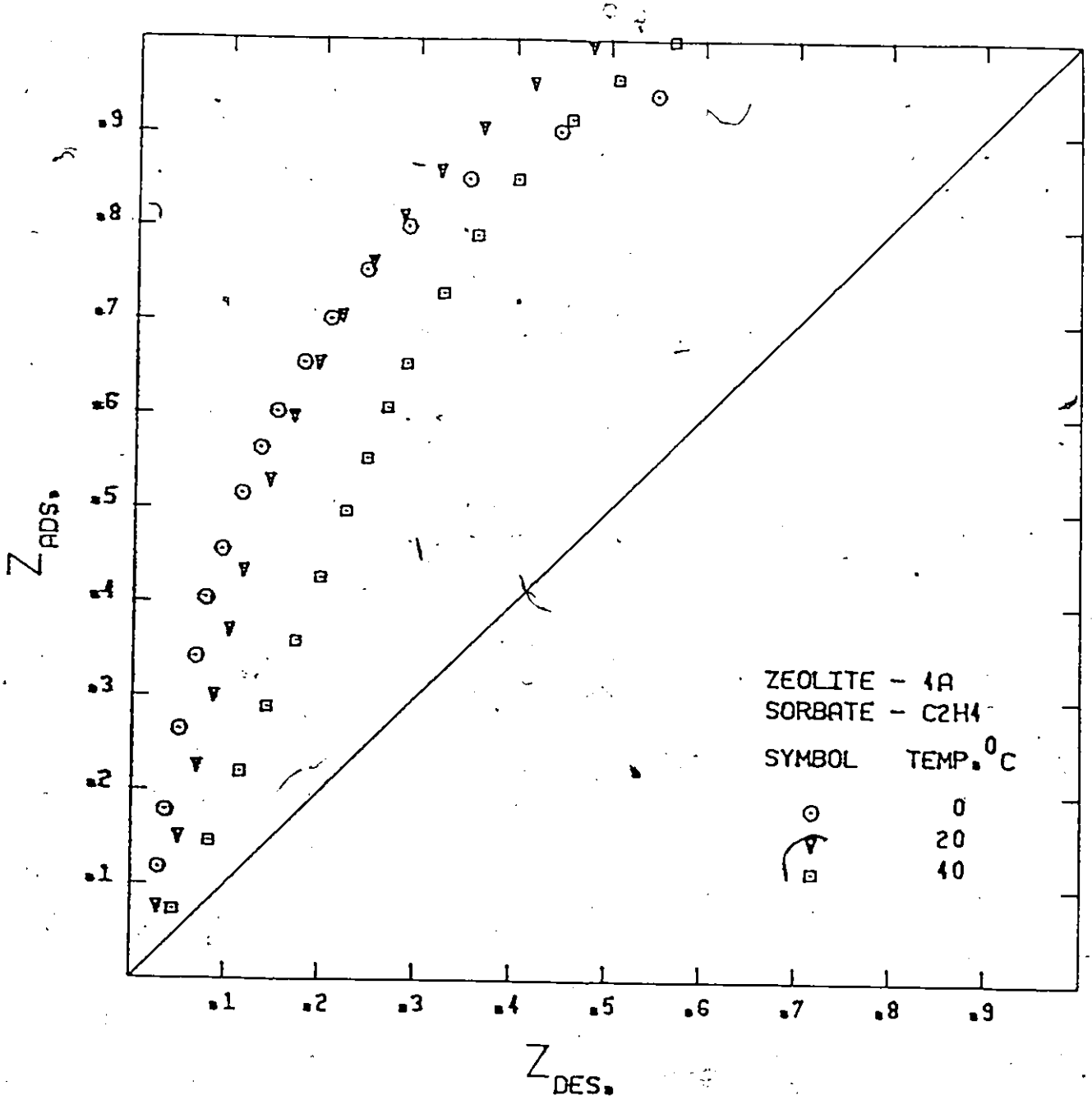

FIG 4.12 SINGLE COMPONENT Z-PLOT OF ETHANE ON NaA

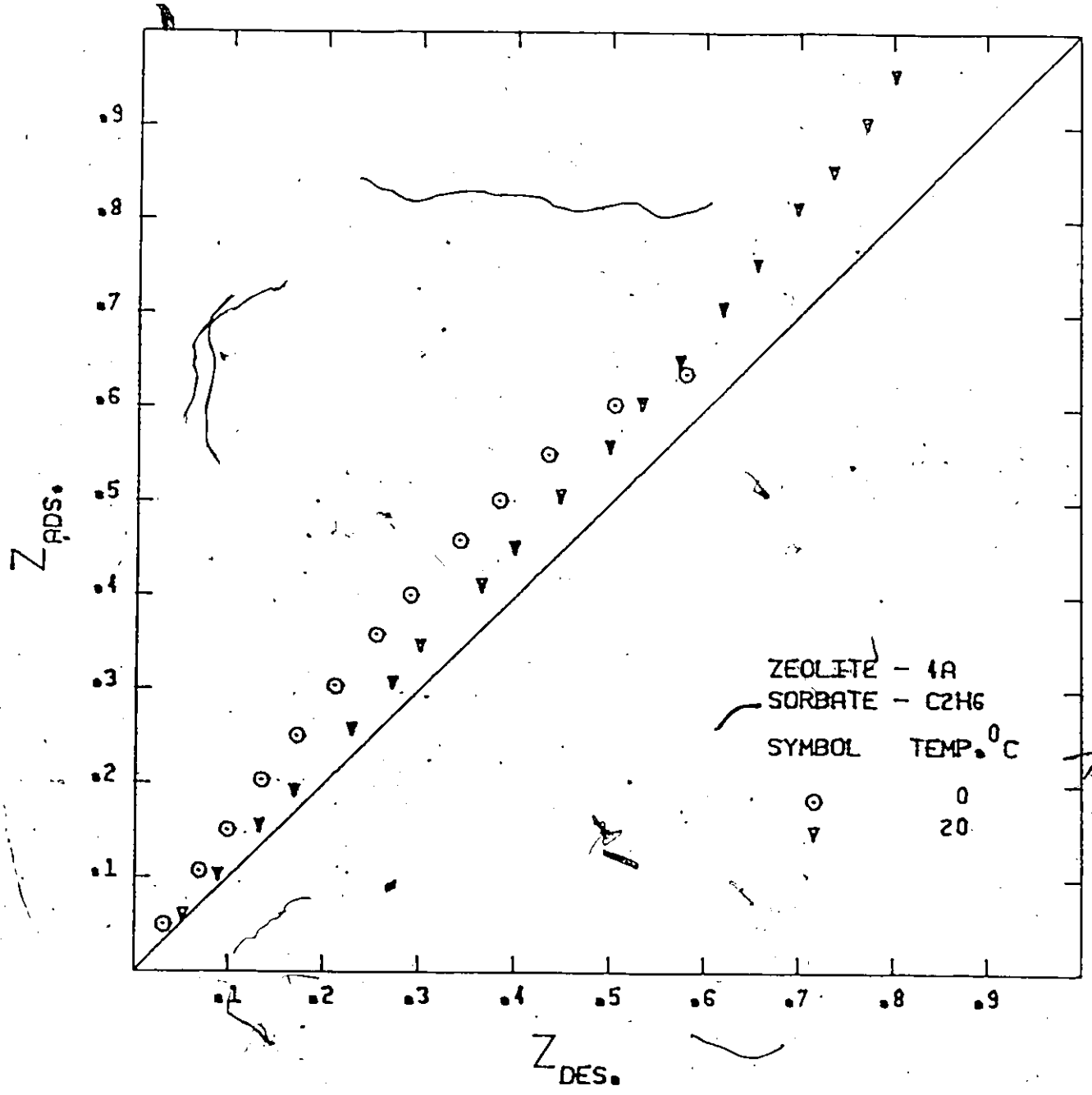

FIG 4.13 SINGLE COMPONENT Z-PLOT OF CARBON DIOXIDE ON Na-MORDENITE

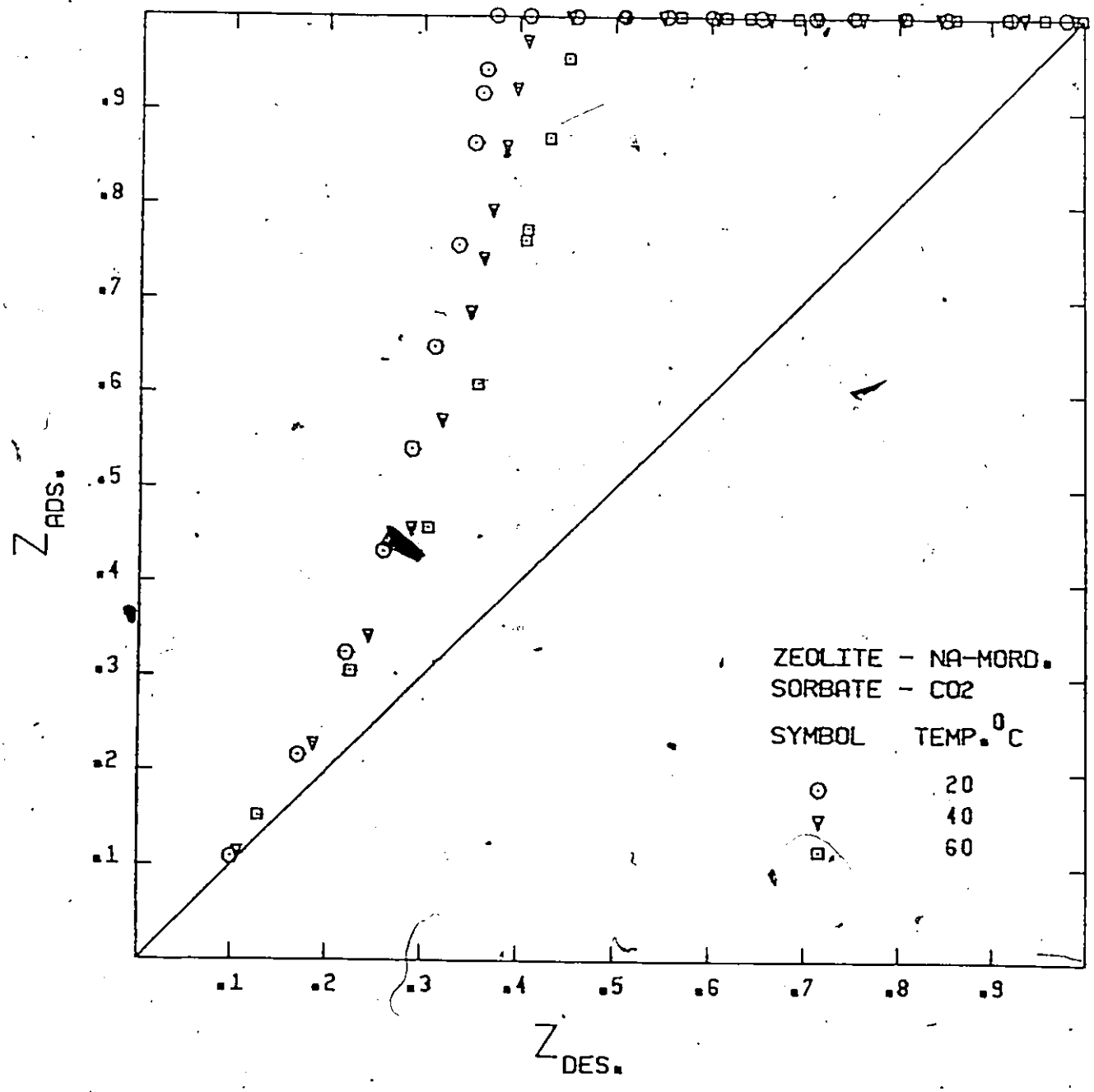

FIG 4.14 SINGLE COMPONENT Z-PLOT OF ETHYLENE ON Na-MORDENITE

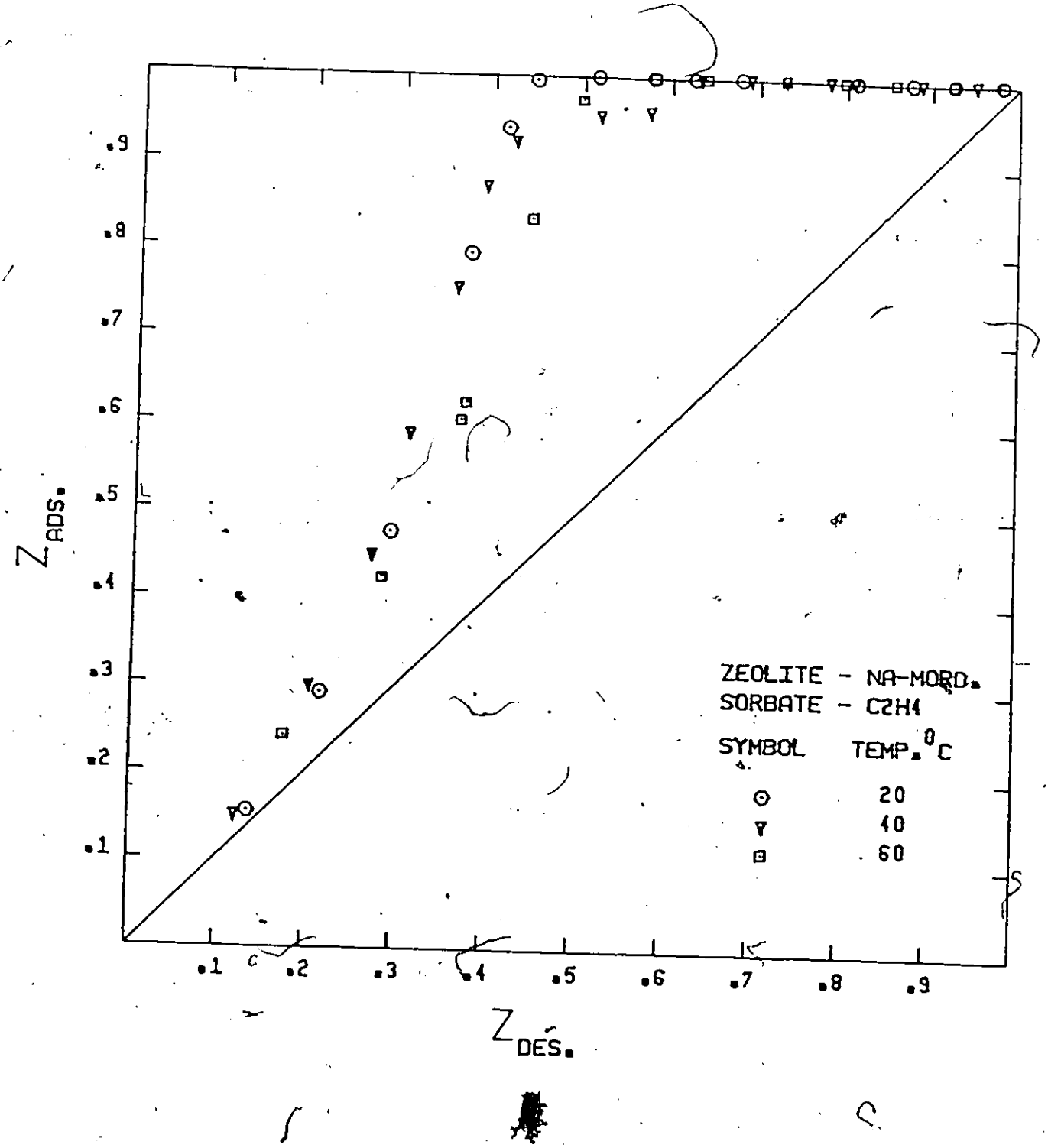

FIG 4.15 SINGLE COMPONENT Z-PLOT OF ETHANE ON Na-MORDENITE

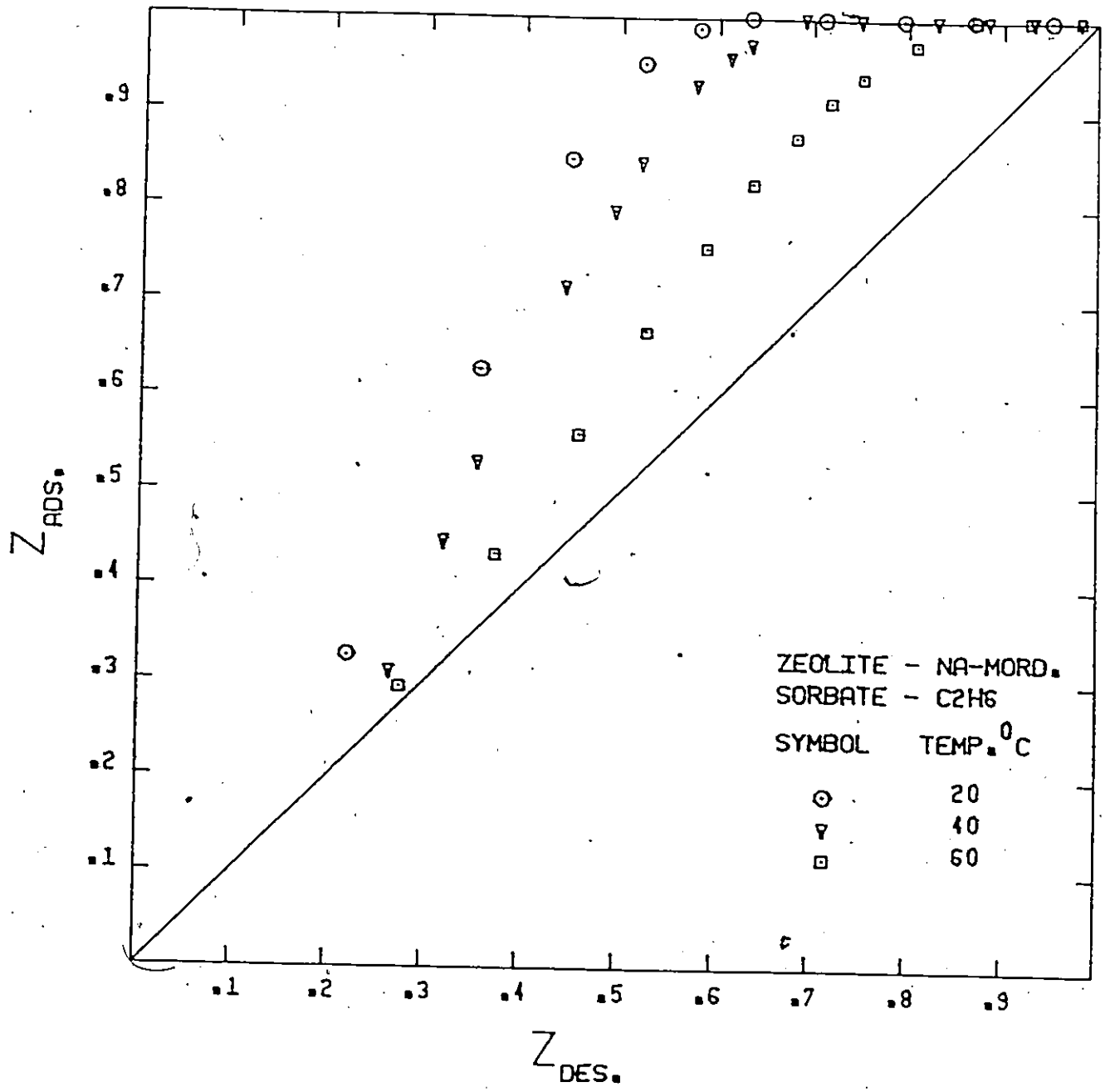

FIG 4.16 SINGLE COMPONENT Z-PLOT OF CARBON DIOXIDE ON H-MORDENITE

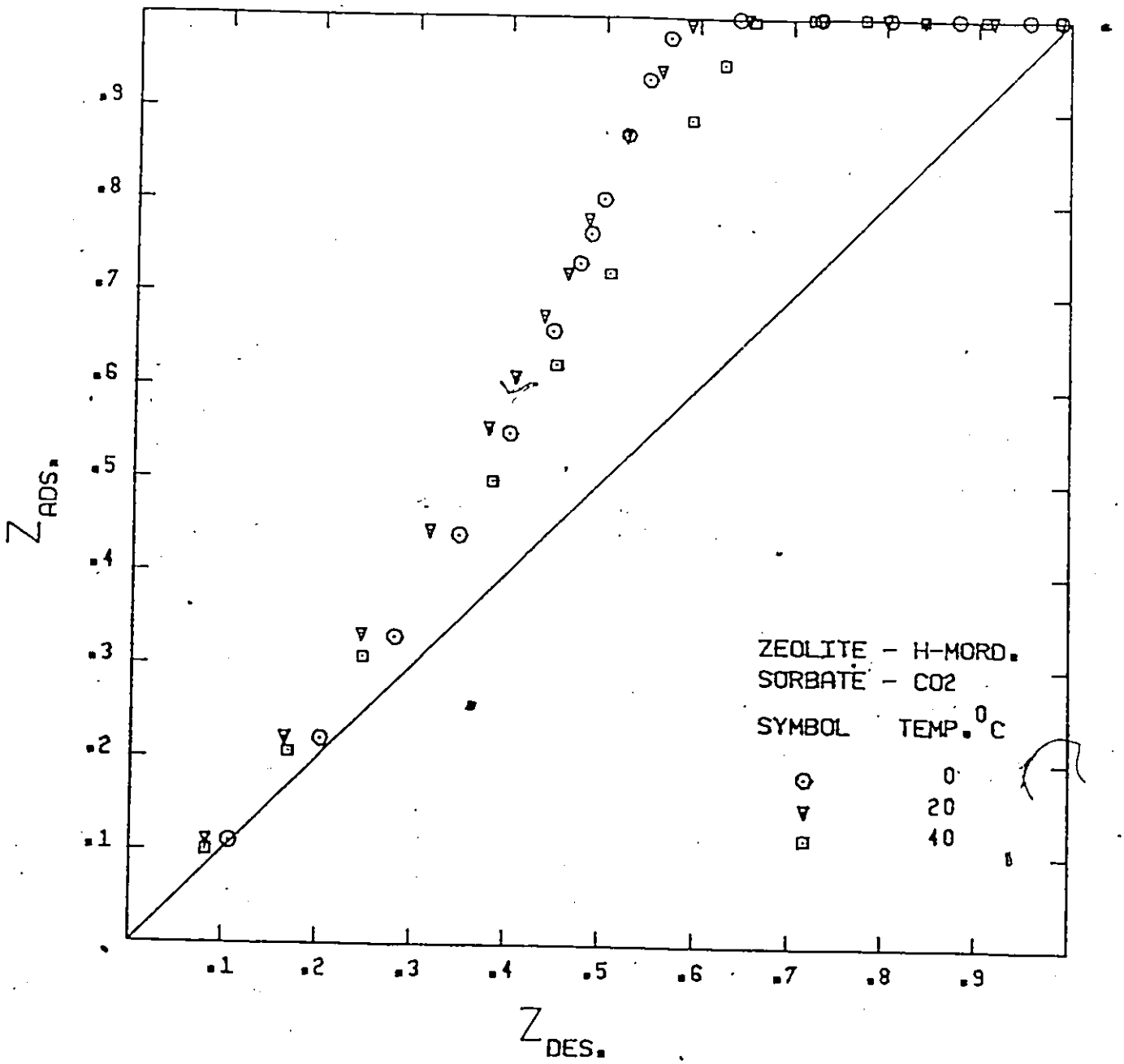

FIG 4.17 SINGLE COMPONENT Z-PLOT OF ETHANE ON H-MORDENITE

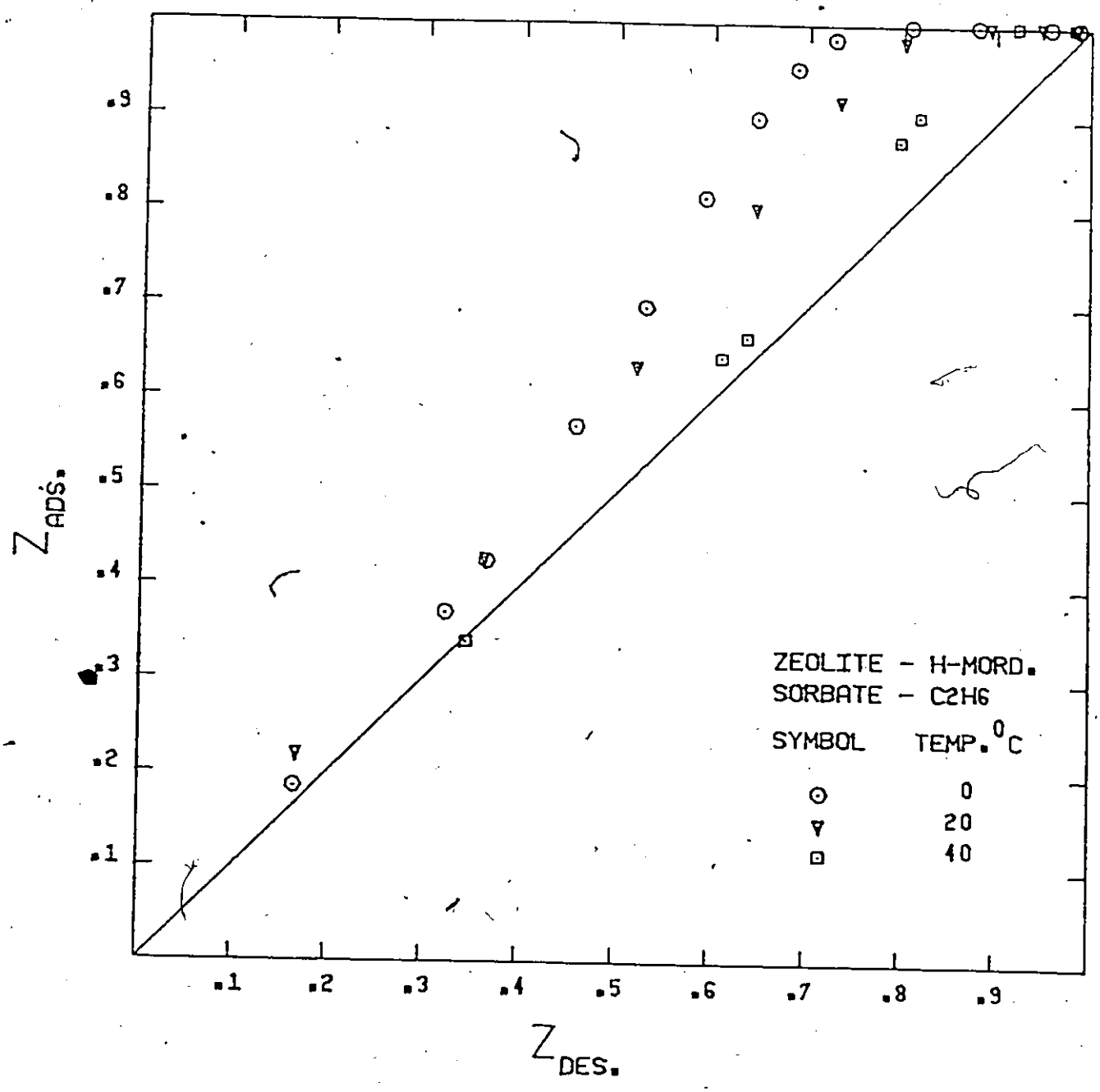

between the curves and this line. Moreover, the Z curves reveal a continuous relationship between adsorption/desorption rates at the various fractional uptakes. As can be observed, all Z-plot curves lie consistently in the upper triangular section indicating that in general, the adsorption rate to be the larger one. Table 4.3 lists the ratio of adsorption/desorption diffusivity calculated from the non-linear least squares fitting of the rate curves to the simple Fick's law model. Overall, the ratio can be seen to decrease with increasing temperature, however, since the calculated diffusion coefficient represents an average value for the entire rate curve and closer examination of the Z-plots reveals that in some instances some overlapping and cross-over of the curves, for example, Figs. 4.11 and 4.14, which complicates the physical interpretation. Moreover, the validity of the simple Fick's law model when applied to zeolitic diffusion has been subjected to some controversy. Thus, it is felt that the temperature trend may not necessarily represent the result of some significant physical properties.

4.2.2 MULTIPLE COMPONENT COUNTER DIFFUSION

The sorption and catalytic applications of zeolitic molecular sieves frequently involve the counter-diffusion of different species within a zeolite framework structure. For example, in catalytic processes, the simultaneous diffusion of reactants and products must occur. The presence of diffusion limitations can significantly alter the activity and selectivity of a zeolite-based catalyst. Accordingly, the knowledge and the understanding of counter-diffusion are an important aspect in the overall design of a catalytic process. Although, the literature is inundated with

Table 4.3 Ratio of Adsorption/Desorption Diffusivities

Zeolite	Diffusant	Temp. (°C)	$F=D_{ads.}/D_{des.}$	F_{avg}
NaA	CO_2	0.0	30.93	
		20.0	7.26	14.34
		40.0	4.83	
	C_2H_4	0.0	15.71	
		20.0	8.48	9.53
		40.0	4.41	
	C_2H_6	0.0	1.91	
		20.0	1.65	1.78
		40.0	-	
Na-mord.	CO_2	20.0	8.26	
		40.0	7.20	6.36
		60.0	3.63	
	C_2H_4	20.0	5.19	
		40.0	8.63	5.54
		60.0	2.80	
	C_2H_6	20.0	3.56	
		40.0	2.45	2.67
		60.0	2.00	
H-mord.	CO_2	0.0	3.06	
		20.0	1.95	2.14
		40.0	1.49	
	C_2H_6	0.0	1.46	
		20.0	1.17	1.23
		40.0	1.06	

Table 4.4 Activation Energy of Adsorption and Desorption

Zeolite	Diffusant	Diffusion Direction	Activation Energy (KJ/mole)
NaA	CO_2	ADS.	5.063
		DES.	46.07
	C_2H_4	ADS.	32.10
		DES.	55.19
	C_2H_6	ADS.	32.75
		DES.	37.97
Na-mord.	CO_2	ADS.	4.44
		DES.	25.06
	C_2H_4	ADS.	5.06
		DES.	17.57
	C_2H_6	ADS.	9.06
		DES.	20.84
H-mord.	CO_2	ADS.	10.08
		DES.	22.072
	C_2H_6	ADS.	16.99
		DES.	22.76

equilibrium and kinetic studies of single sorbate systems, little attention has been given to the very important subject of zeolitic counter-diffusion. Nonetheless, most of the published works related to this subject have reported that the counter-diffusion rates to be smaller than the corresponding single sorbate system for the same molecular species. However, the comparisons have been frequently based on the values of diffusivity calculated from sorption rate curves with little regard given to the actual diffusional direction, and since it is well known that zeolite diffusion mechanism is highly anisotropic, as demonstrated in the previous section, a more meaningful comparison should be the diffusion and counter-diffusion rate of a particular molecular species migrating in the same direction, i.e. adsorptive counter-diffusion versus unidirectional adsorption, and desorptive counter-diffusion rate versus unidirection desorption rate.

UNIDIRECTION ADSORPTION - ADSORPTIVE COUNTER-DIFFUSION

In our investigation of the counter-diffusion phenomenon, the unidirection (single component sorption kinetics) sorption rates were first established in a preliminary study as described in the previous section. Following this, we then proceeded to study the counter-diffusion effect by loading the zeolite with a particular sorbate, a second sorbate was subsequently allowed to come into contact with the zeolite now containing the presorbed molecules. The progress of both the adsorption rate of the counter adsorbate and the desorption rate of the presorbed species were monitored simultaneously. A more detailed description of the experimental procedures is given in the experimental section. The fractional approach to equilibrium of the adsorptive counter diffusate ($Z_{c.ads}$) can

then be plotted against the corresponding fractional approach to equilibrium of the unidirection adsorption of the same molecule (Z_{ads}) at equal sorption time. The result of these plots are shown in Figures 4.18 to 4.25 inclusive. Qualitative interpretations of the plots are as follows; if there has been no adsorbate/desorbate interaction, then, the experimental data points would be expected to fall on the diagonal line. However, if the interaction is significant, then appreciable deviation from the 45^{o} line would occur and the distance between the Z-curves and the diagonal line could be a direct measure of the degree of interaction. Also, the region where the Z-curves fall is important; for example, if the Z-curves lie within the upper left-hand triangle, the effect of the presorbed molecule upon the counter-adsorbate is regarded as a negative one, i.e. a retardation of the binary adsorption rate. But if the Z-curves are in the lower right-hand triangle, then, the effect is considered to be a positive one, i.e. rate enhancement.

For CO_2-4A system, where CO_2 is the counter adsorbate, the presence of either C_2H_4 or C_2H_6 as the presorbed molecule is shown to have a negative effect, Fig 4.20. The adsorptive counter diffusion rate of CO_2 is smaller than the corresponding unidirection adsorption rate into a pre-evacuated 4A zeolite. The degree of influence exerted by the C_2H_4 and C_2H_6 upon CO_2 adsorption rate however differs. C_2H_4 has a greater impact causing the Z-curve to depart farther away from the reference diagonal line. Sorption temperature can also be seen to be a relevent parameter and the retardation of the counter adsorption rate is less at higher temperature. The temperature effect becomes less obvious for the reversed sorbate sequence of C_2H_4-4A and C_2H_6-4A systems, but the influence of the presorbed CO_2 is

FIG 4.18 BINARY COMPONENT Z-PLOT OF ETHYLENE ADSORPTION ON NaA

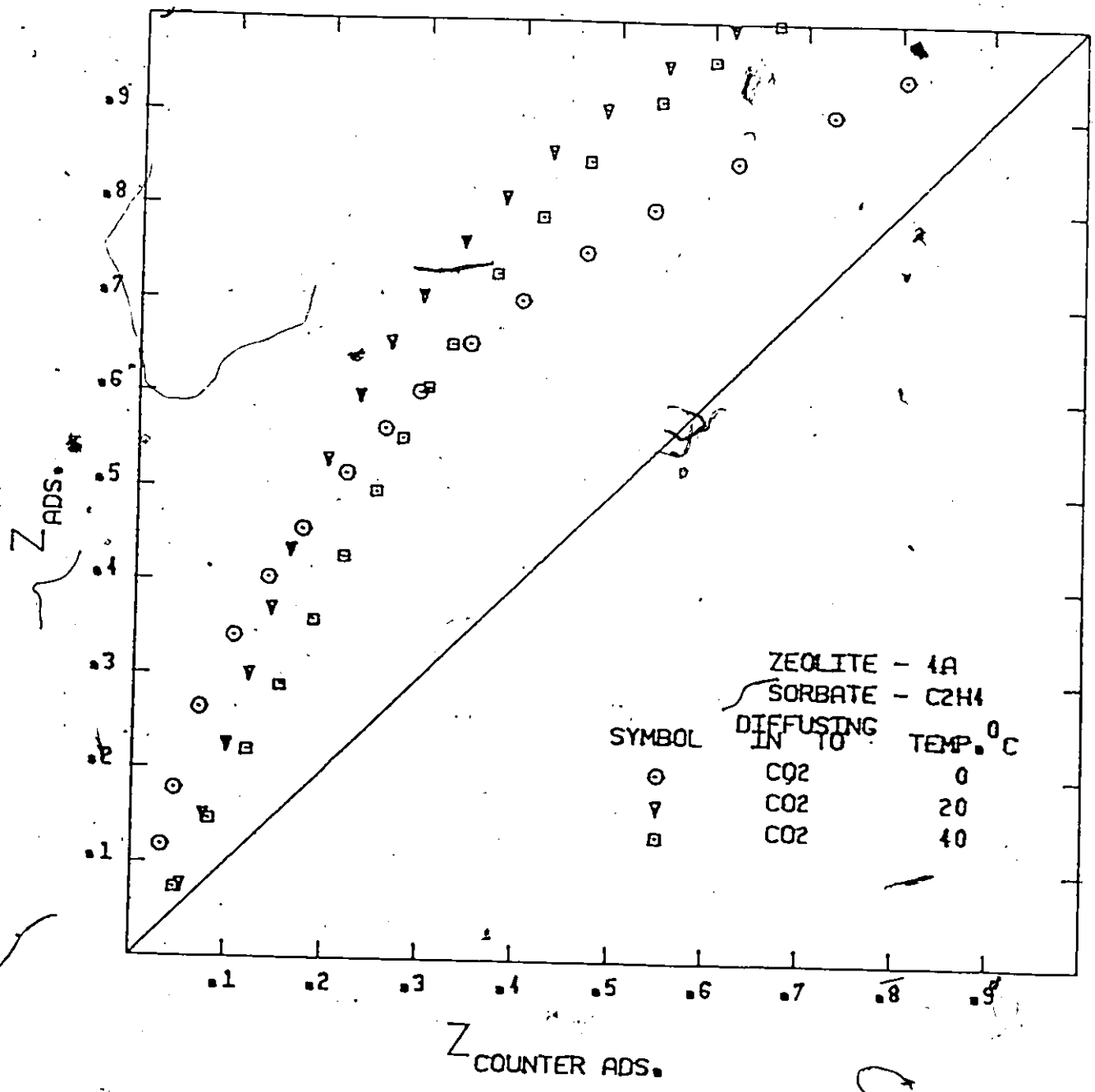

FIG 4.19 BINARY COMPONENT Z-PLOT OF ETHANE ADSORPTION ON NaA

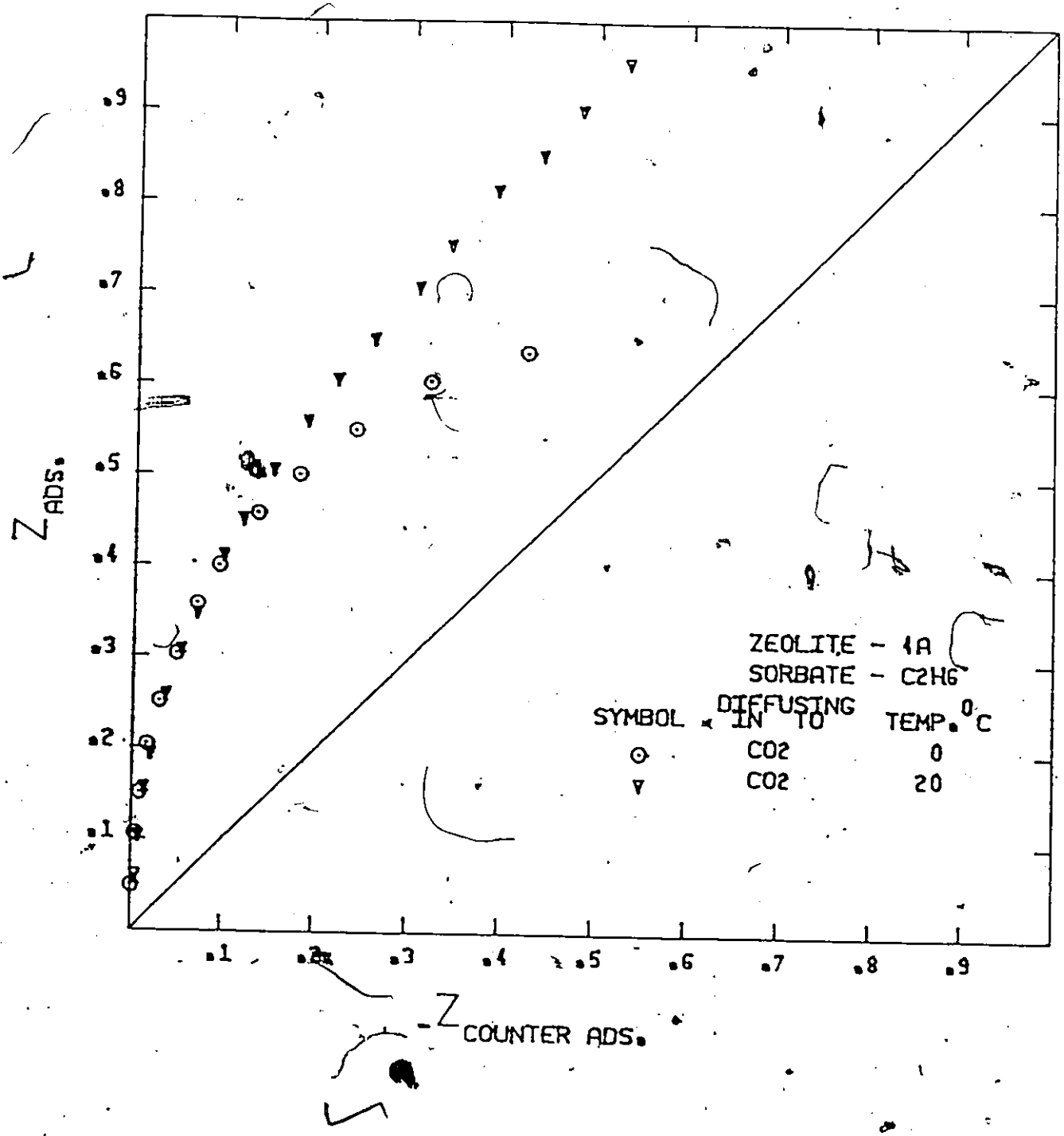

FIG 4:20 BINARY COMPONENT Z-PLOT OF CARBON DIOXIDE ADSORPTION ON NaA

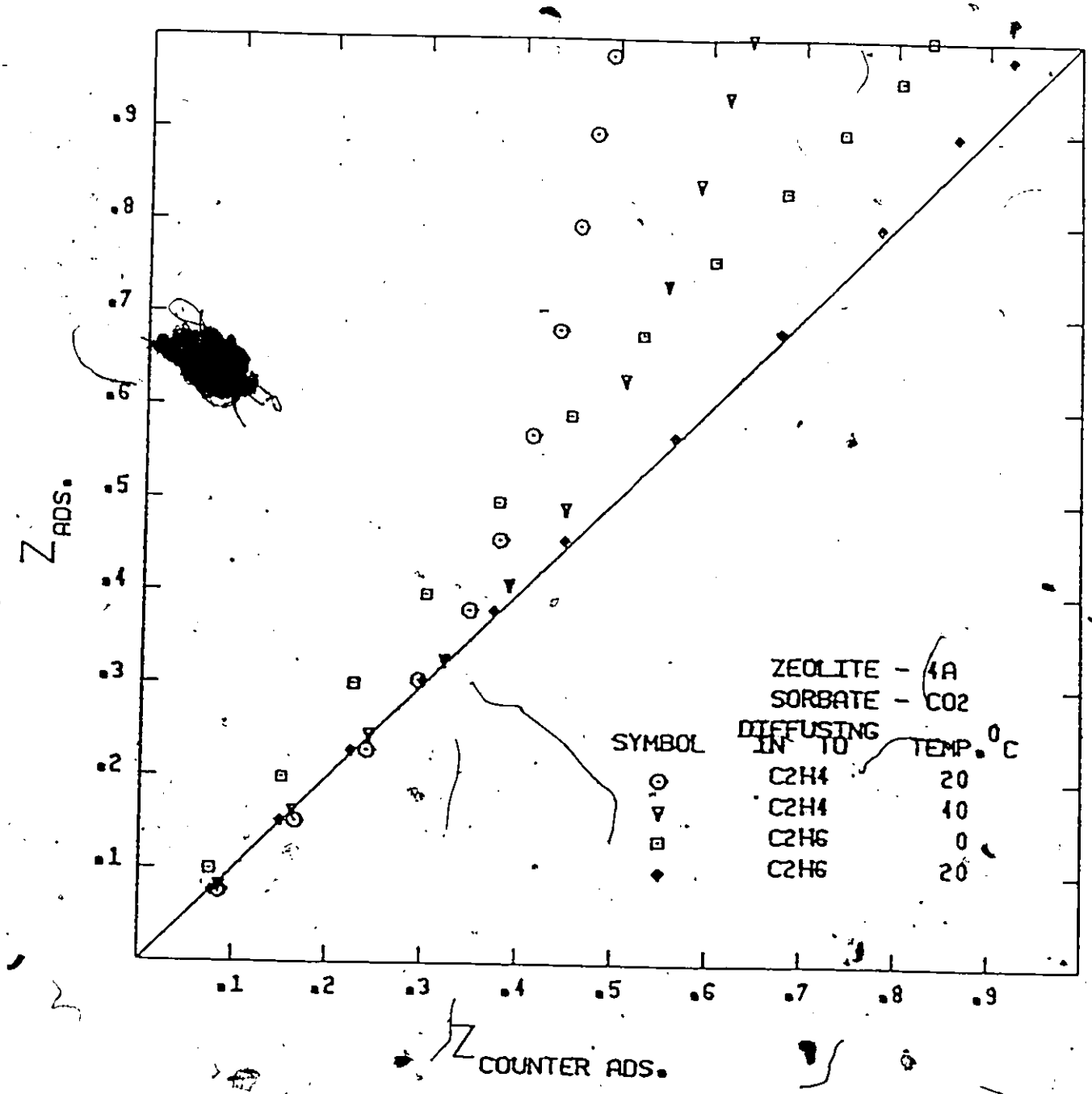

FIG 4.21 BINARY COMPONENT Z-PLOT OF CARBON DIOXIDE ADSORPTION ON Na-MORDENITE

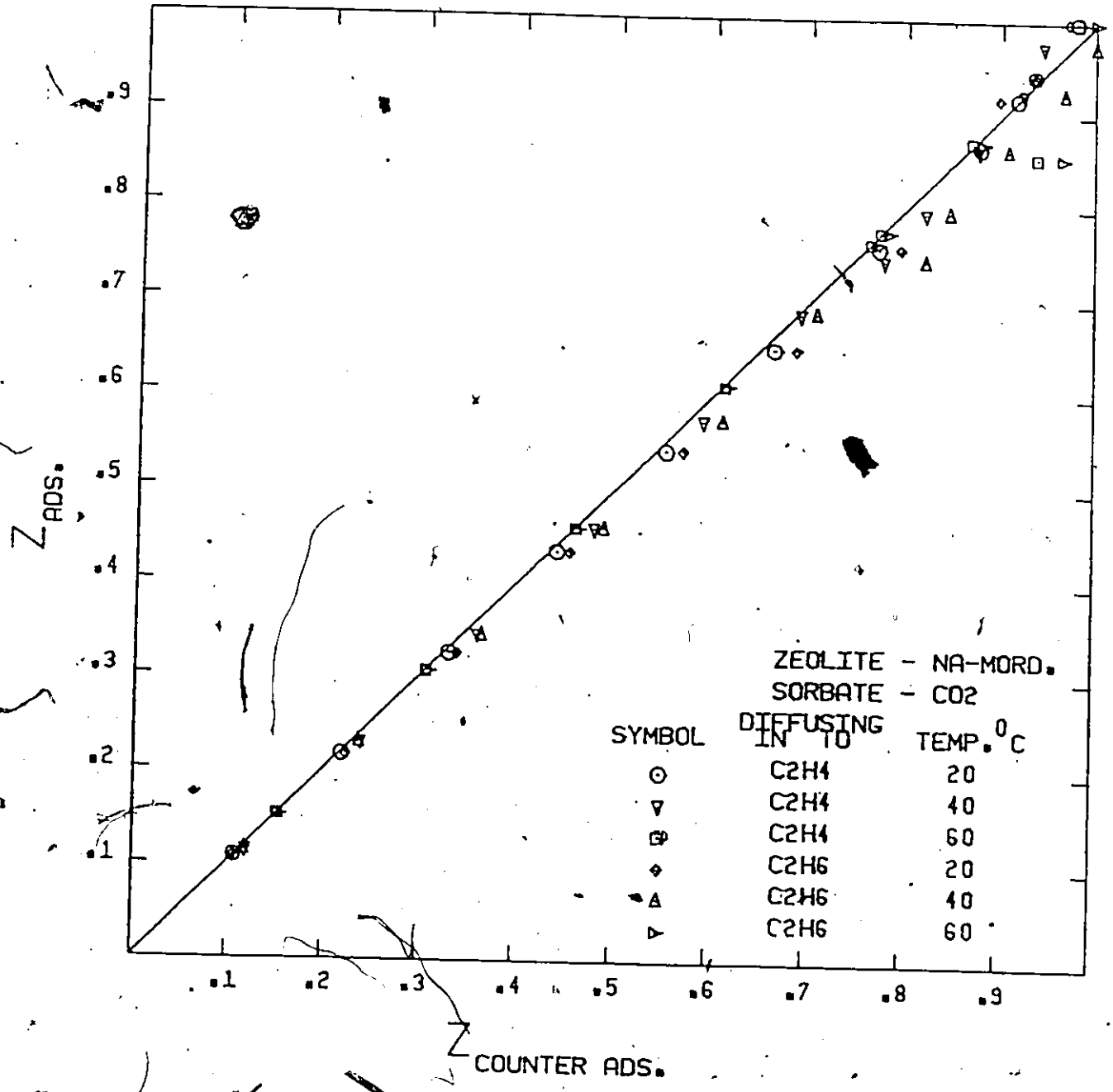

FIG 4.22 BINARY COMPONENT Z-PLOT OF ETHYLENE ADSORPTION ON Na-MORDENITE

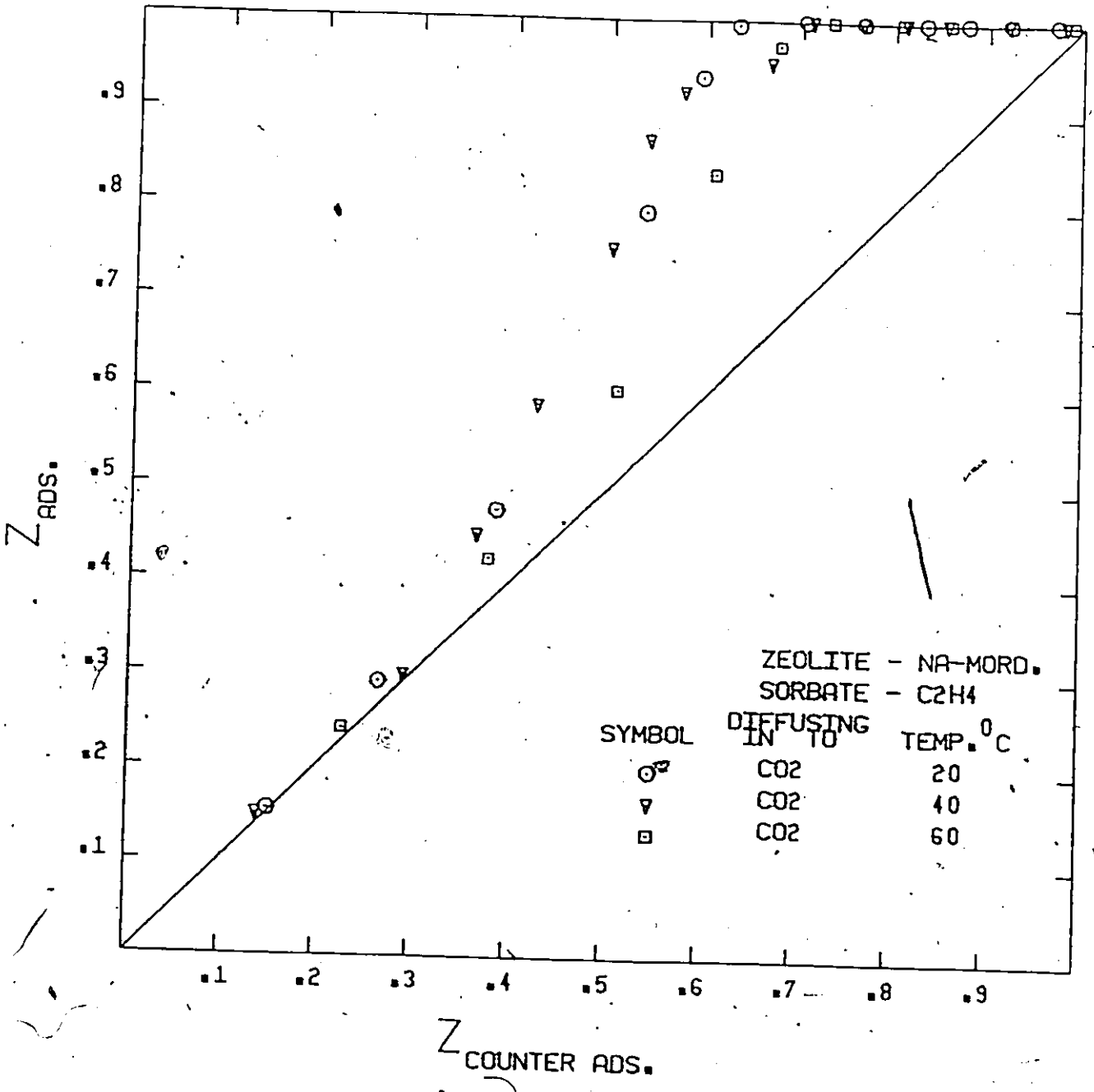

FIG 4.23 BINARY COMPONENT Z-PLOT OF ETHANE ADSORPTION ON Na-MORDENITE

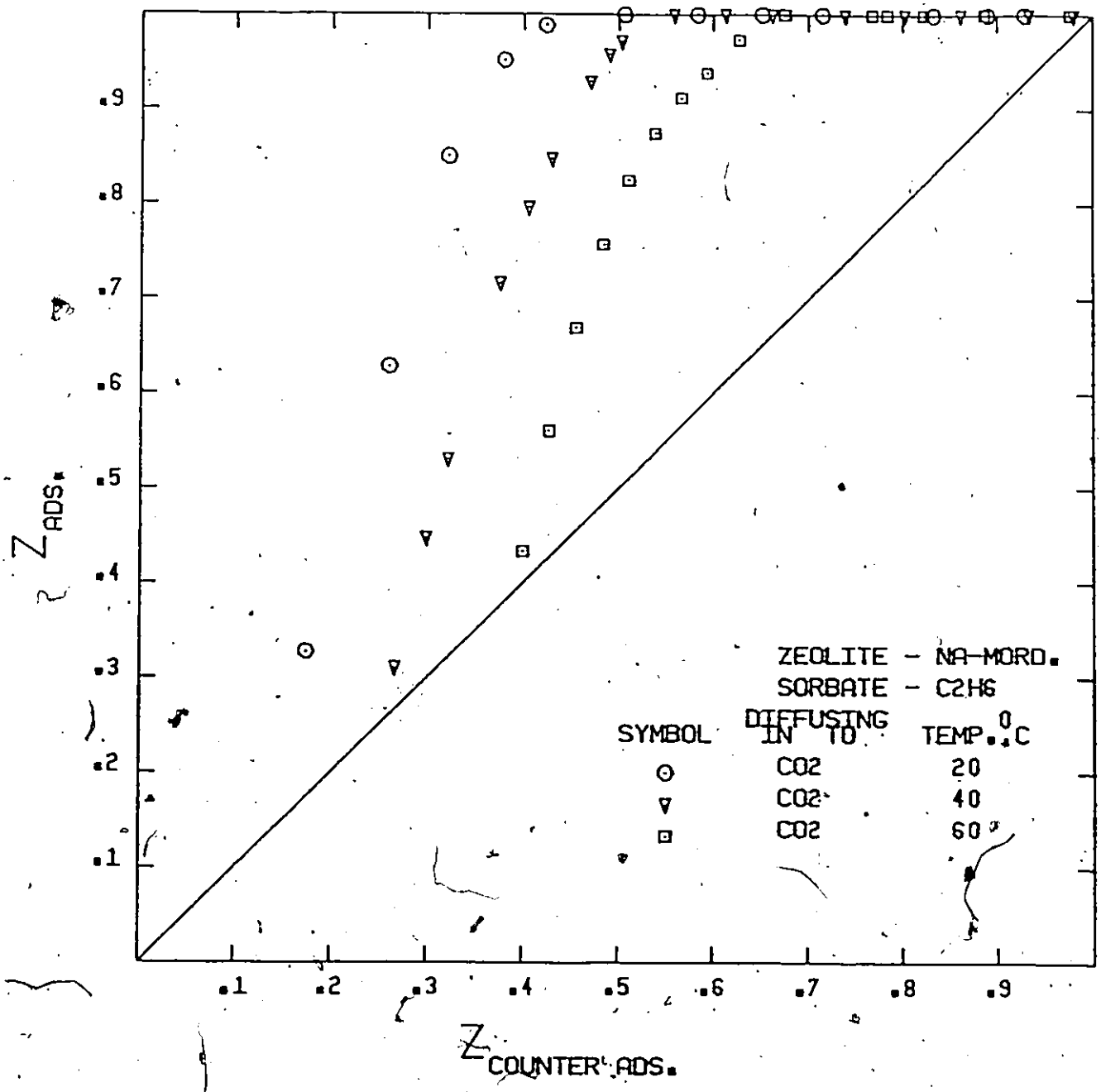

FIG 4.24 BINARY COMPONENT Z-PLOT OF CARBON DIOXIDE ON H-MORDENITE

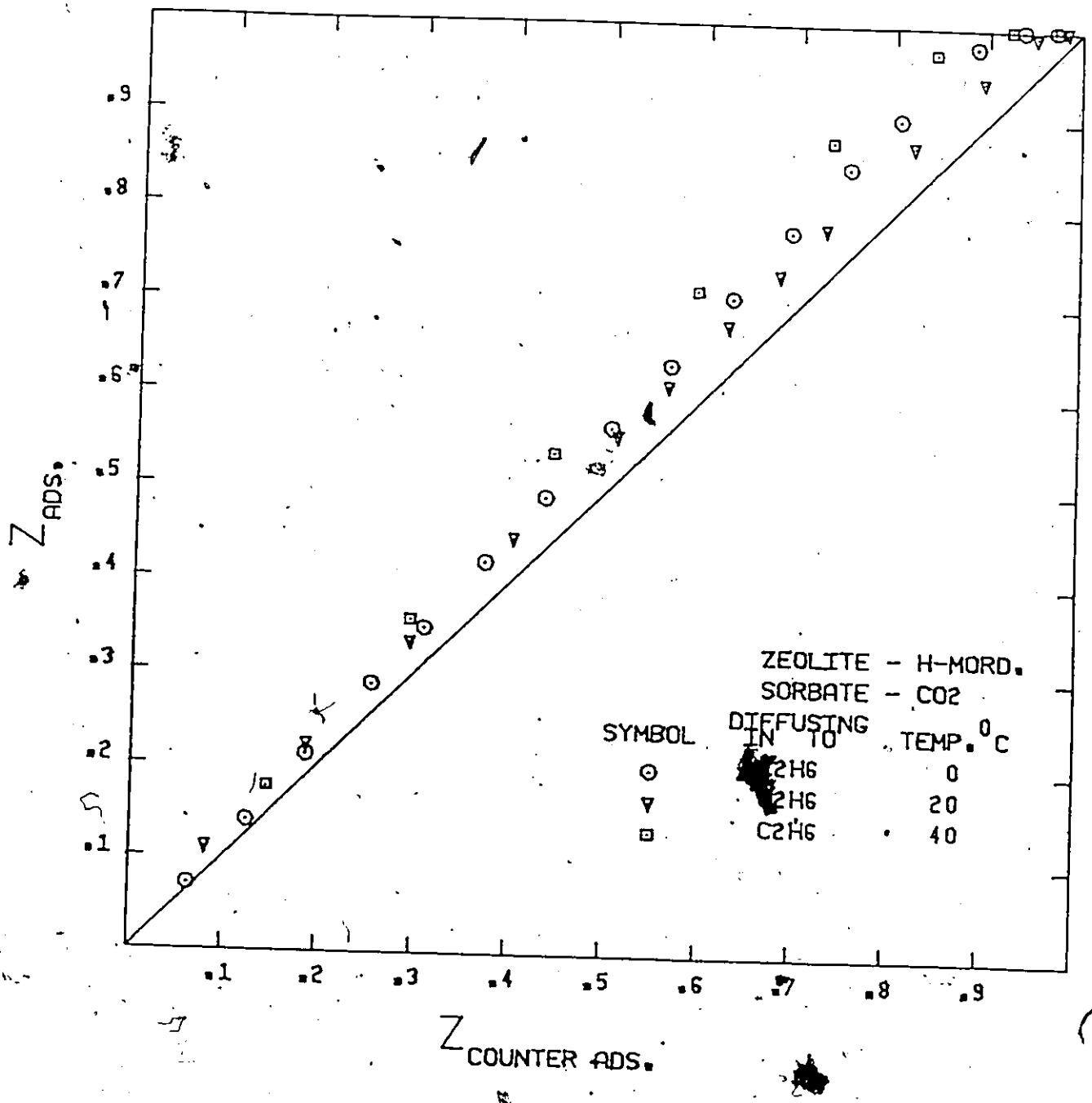

FIG 4.25 BINARY COMPONENT Z-PLOT OF ETHANE ADSORPTION ON H-MORDENITE

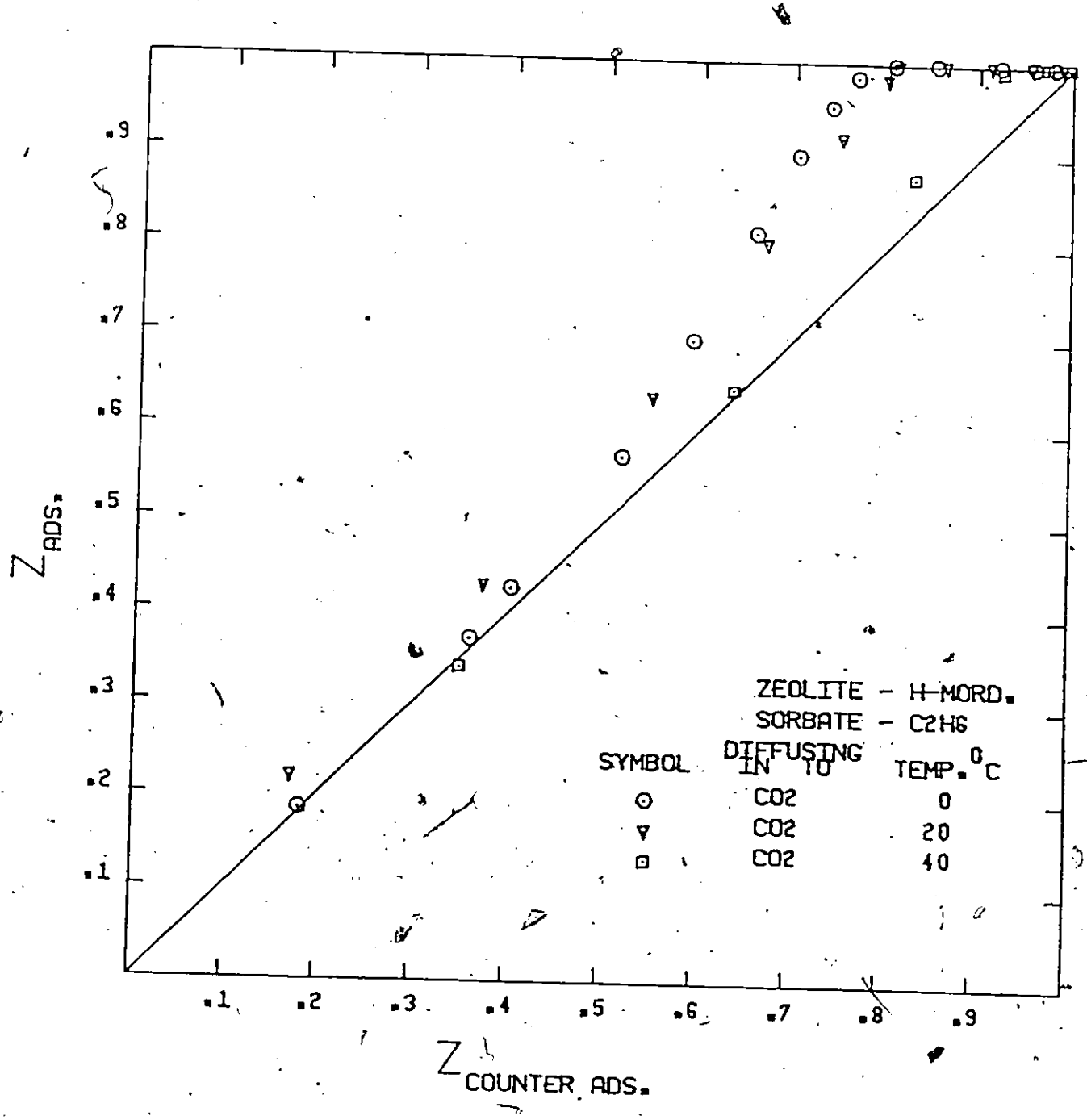

shown to have a similar negative impact upon the adsorptive counter diffusion rates of C_2H_4 and C_2H_6, Figs. 4.18 and 4.19.

For CO_2-Na-mordenite system, where CO_2 is the counter adsorbate molecule diffusing against C_2H_4 and C_2H_6, the effect of the presorbed molecules on the adsorption rate of CO_2 is a minimal one; the Z-curves lie very close to the reference diagonal line, Fig 4.21. Closer inspection of this figure reveals that the Z-curves are actually in the positive region which suggests an adsorption rate enhancement effect. However, the deviation of the Z-curves from the 45° line is slight, and considering the experimental uncertainties of 5-15%, calculated from the repeated runs, the effect is judged to be insignificant. The same comment can not be given to the reversed sorbate sequence of the C_2H_4- and C_2H_6-Na-mordenite systems, Figs 4.22 and 4.23, where the presorbed CO_2 molecules exert a significant negative impact on the adsorption rates of C_2H_4 and C_2H_6. This is parallel with the observations made on the 4A systems of the same sorbate gas pairs. In counter diffusion studies made on the H-mordenite systems, Figs. 4.24 to 4.25, the same retardation of the counter adsorbate diffusion rate by the presorbed species is again consistently observed. However, the degree of rate retardation is less when compared to either the 4A or Na-mordenite systems.

It is quite clear from the experimental results that the diffusion rate of a given sorbate can vary substantially depending whether it is involved in a single or binary sorption system. The adsorptive counter-diffusion rates were in general smaller than the unidirectional adsorption rate of the same molecule into a pre-evacuated zeolite. However, the extent of the influence by the presorbed molecules on counter adsorption rates differed

considerably depending on the type of zeolite as well as the specific sorbate pairs involved.

The pertinent question to ask should therefore be, how to describe the adsorbate-desorbate and/or sorbate-zeolite interactions that could have given rise to the observed phenomena. First we consider the counter-diffusion case in the 4A systems; Structurally, the size of the zeolite 4A conducting channel is extremely narrow. In addition, there is the interference of cations. About two-thirds of the cations are located near the window aperture and these locations are the most likely preferential sorption sites. Molecules interacting with the cations may block further the window openings making it impossible for two molecules diffusing in opposite direction to pass each other. If we take CO_2-C_2H_4-4A system as an illustration, the first molecule being the counter adsorbate and the second, the presorbed molecule and thus the desorbing component, an adsorbate CO_2 molecule will probably first encounter and collide with a C_2H_4 molecule at the window aperture. Momentum transfer from the CO_2 to C_2H_4 may occur which could resulted in the slowing down of the CO_2 molecule. Since this leading CO_2 molecule is followed by a train of CO_2s, the retardation of its rate will affect all subsequent ones thus resulting in the overall reduction of the adsorption rates.

From a purely steric point of view, since the sum total of the minimum cross-sectional areas of both CO_2-C_2H_4 and CO_2-C_2H_6 sorbate pairs exceeded the free diameter of the 4A window size, consequently, neither component of the molecular pairs could pass each other at the constrictive openings. Also, since ethane molecule is slightly larger and heavier than ethylene, one would expect that the molecular collisions with ethane would result in a

greater reduction of the adsorptive diffusion rate of CO_2. Examination of the diffusivity data do not support this argument, Table 4.5; ethylene is shown to have a greater rate retardating effect than ethane. Hence, some other physical properties may be involved. Moore and Katzer [39] suggested that the strength of interaction between the presorbed molecules and zeolites could affect the counter diffusion rate of the adsorbate molecules. Such strength of interaction may be indicated by the degree of preferential adsorption of one compound over the other and, may be measured in terms of the amount of equilibrium uptake; large fractional uptake indicates a stronger interaction. Indeed, ethylene was adsorbed to a greater extent than ethane, 83.4 cc(STP)/g versus 30.62 cc(STP)/g, on zeolite 4A at 273°K. The strength of interaction may also be indicated by the values of heat of sorption; 56.0 KJ/mole and 27.0 KJ/mole for ethylene and ethane, respectively. The enhanced interaction between ethylene and zeolite electrostatic field is probably due to the Π electrons. The larger uptake of ethylene also implies that there were more ethylene molecules present in the zeolite, and therefore, the probability of CO_2/C_2H_4 encounter should be proportionally higher. Furthermore, since the structure of zeolite 4A is 3-dimensional, the incoming CO_2 molecules could conceivably avoid the less available ethane molecules by choosing diffusion paths with unblocked windows, whereas in the ethylene case, such avoidance of molecular encounter may not be possible because most of the window sites were occupied. Moreover, the equilibrium uptake decreases with increasing temperature as a result of the exothermic nature of the sorption process. Therefore, the number of the presorbed molecules decreases accordingly, which then resulted in a larger fraction of the unoccupied window sorption

Table 4.5 Adsorption Unidirection Diffusivity ($D_{ads.}$) and Counter-direction Diffusivity ($D_{c.ads.}$)

Zeolite	Molecule Diffuing in (Primary focus)	Molecule Diffusing out	Diffusivity (10^{11} cm^2/min) 0.0°C	20.0°C	40.0°C	60.0°C
NaA	CO_2	-	10.58	13.06	14.03	-
	CO_2	C_2H_4	-	1.827	6.708	-
	CO_2	C_2H_6	9.732	13.29	-	-
	C_2H_4	-	2.263	11.69	13.47	-
	C_2H_4	CO_2	0.518	2.54	4.77	-
	C_2H_6	-	0.506	1.33	-	-
	C_2H_6	CO_2	0.112	0.14	-	-
Na-mord.	CO_2	-	-	31.12	36.48	47.85
	CO_2	C_2H_4	-	31.52	38.77	39.23
	CO_2	C_2H_6	-	38.92	30.93	39.14
	C_2H_4	-	-	56.22	82.46	72.19
	C_2H_4	CO_2	-	25.25	18.94	53.60
	C_2H_6	-	-	148.0	186.5	231.4
	C_2H_6	CO_2	-	18.1	43.3	77.25
H-mord.	CO_2	-	44.26	55.43	78.16	-
	CO_2	C_2H_6	33.03	44.21	69.49	-
	C_2H_6	-	73.18	122.7	190.6	-
	C_2H_6	CO_2	50.89	101.9	204.2	-

sites, thus, at elevated temperatures, the probability of encounter between adsorbate/desorbate should be lowered and the effect of the adsorbate/desorbate interaction reduced. In fact, this is observed, for example, the equilibrium uptake of the presorbed ethane at 20°C was limited to 12.2 cc(STP)/g; comparison of the adsorptive counter diffusion of CO_2 against ethane and its unidirectional diffusion coefficients shows little difference, 13.29×10^{-13} cm^2/sec and 13.06×10^{-13} cm^2/sec, respectively.

The zeolite pore dimension in relation to the diffusate molecular size seems to be an important parameter in determining adsorbate/desorbate interaction. In small pore zeolites such as 4A, the narrow aperture size may force the encounter of the two molecular species. For counter-diffusion in large port zeolites, e.g. mordenite, where the sum of the cross-sectional area of the diffusate pairs studied in this work was less than the free diameter of the conducting channels, molecules should be capable of passing each other and adsorbate/desorbate interaction should also be reduced. Table 4.6 compares the unidirectional adsorption rate to adsorptive counter diffusion rate in terms of the diffusivity ratio; for the same sorbate pair at the same temperature, the ratio decreases in the order of zeolite 4A, Na-mordenite and almost approach unity with H-mordenite. This is parallel with the increase in pore size from 4.2A to 6.8A to 10A for the respective zeolites. One approach to ascertain the steric effect in large port zeolites is to increase the diffusate molecular size. Katzer and Satterfield studied the counter diffusion of the much larger aromatic molecules, cumene and benzene in H-mordenite; they reported the adsorptive counter diffusion rate to be two orders of magnitude lower. [48] Satterfield and Cheng [47] also investigated the counter diffusion of aromatic and naphthalenic hydrocarbons

Table 4.6 Ratio of $D_{ads.}/D_{c.ads.}$

Zeolite	Molecule Diffusing in (Primary focus)	Molecule Diffusion out	$D_{ads.}/D_{c.ads.}$ 0.0°C	20.0°C	40.0°C	60.0°C
NaA	CO_2	-	1.0	1.0	1.0	-
	CO_2	C_2H_4	-	7.15	2.09	-
	CO_2	C_2H_6	1.09	0.98	-	-
	C_2H_4	-	1.0	1.0	1.0	-
	C_2H_4	CO_2	4.37	4.60	2.82	-
	C_2H_6	-	1.0	1.0	-	-
	C_2H_6	CO_2	4.52	9.64	-	-
Na-mord.	CO_2	-	-	1.0	1.0	1.0
	CO_2	C_2H_4	-	0.99	0.96	1.22
	CO_2	C_2H_6	-	0.80	1.18	1.22
	C_2H_4	-	-	1.0	1.0	1.0
	C_2H_4	CO_2	-	2.23	4.35	1.35
	C_2H_6	-	-	1.0	1.0	1.0
	C_2H_6	CO_2	-	8.22	4.31	3.00
H-mord.	CO_2	-	1.0	1.0	1.0	-
	CO_2	C_2H_6	1.34	1.25	1.12	-
	C_2H_6	-	1.0	1.0	1.0	-
	C_2H_6	CO_2	1.44	1.20	0.93	-

in Type Y zeolites and found the effective diffusivity under the counter diffusion condition to be less by factors of 10^{-1} to 10^{-3} in relation to the unidirectional diffusion into an initially empty pore structure.

UNIDIRECTION DESORPTION - DESORPTIVE COUNTER-DIFFUSION

Comparisons of the unidirection desorptive diffusion rate and the desorptive counter-diffusion rate of the same molecule were made in a similar fashion by plotting the respective fractional equilibrium uptakes (Z_{des}, $Z_{c.des}$) against each other at equal sorption time. Results of these plots are shown in Figures 4.26 to 4.33. In contrast to the adsorptive diffusion process, Z-desorption curves in general lie in the lower right-hand triangular region suggesting a positive rate enhancement effect, i.e. the desorption rate of the presorbed component was increased in the presence of a counter adsorbate. One exception to the above observation was the C_2H_6-CO_2-4A system, where ethane was the presorbed component and carbon dioxide, the counter adsorbate. Fig. 4.28 shows the Z-desorption curve of this system deviated substantially above the reference diagonal line which indicating an opposite effect of retardation of ethane desorption rate. A more detailed discussion concerning this unique system will be given in a later section.

For CO_2 desorption on zeolite 4A, Fig. 4.26 shows clearly that ethylene as a counter adsorbate increased the desorption rate of the presorbed CO_2 and rendering its Z-desorption curve to depart significantly away from the reference diagonal line. The degree of the desorption rate enhancement however decreases with increasing sorption temperature. When ethylene was replaced with ethane, the enhancement effect became less pronounced. At a lower temperature of $0^{\circ}C$, there is some weak evidence pointing to a positive

FIG 4.26 BINARY COMPONENT Z-PLOT OF CARBON DIOXIDE DESORPTION ON NaA

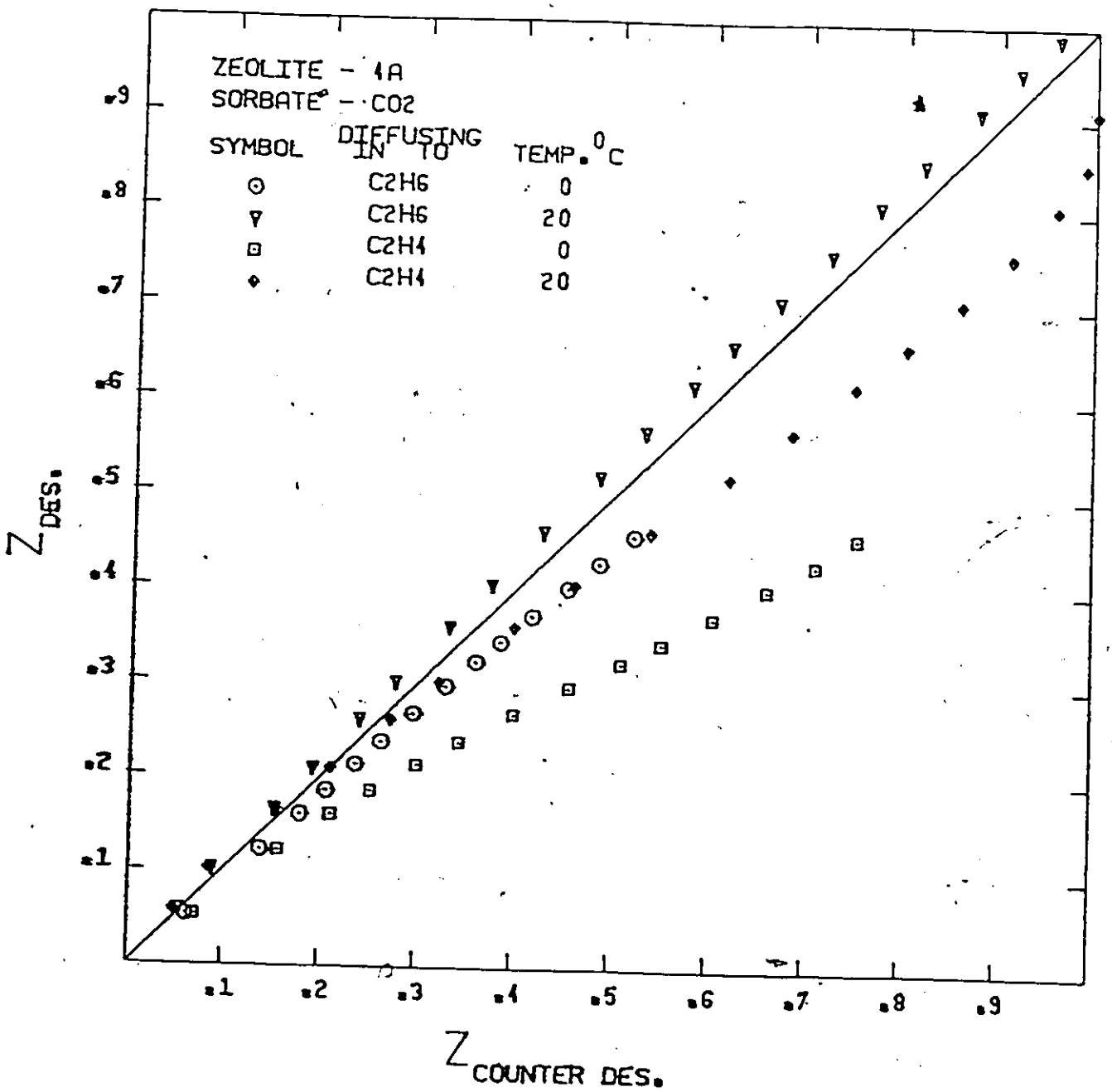

FIG 4.27 BINARY COMPONENT Z-PLOT OF ETHYLENE DESORPTION ON NaA

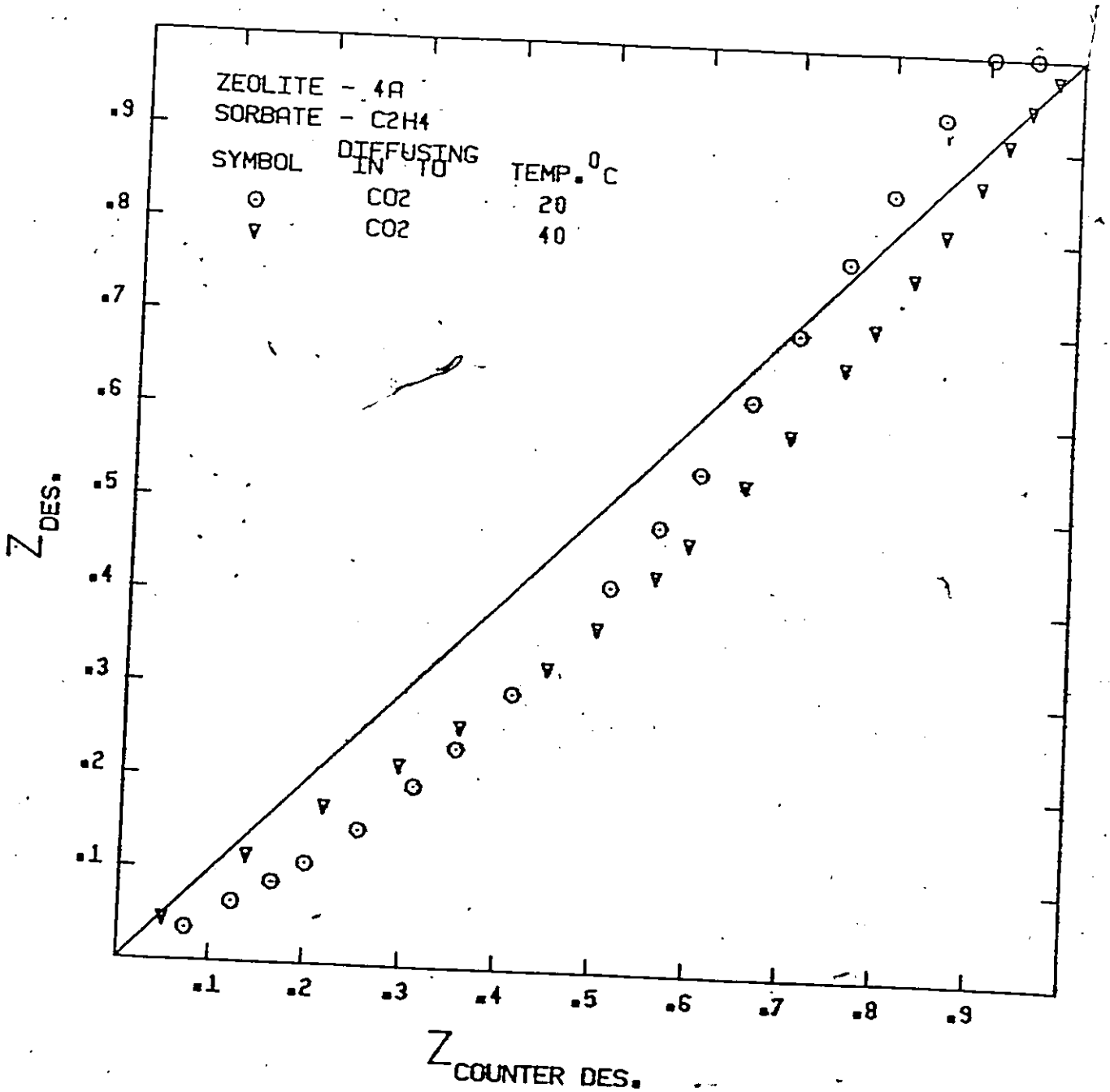

FIG. 4.28 BINARY COMPONENT Z-PLOT OF ETHANE DESORPTION ON NaA

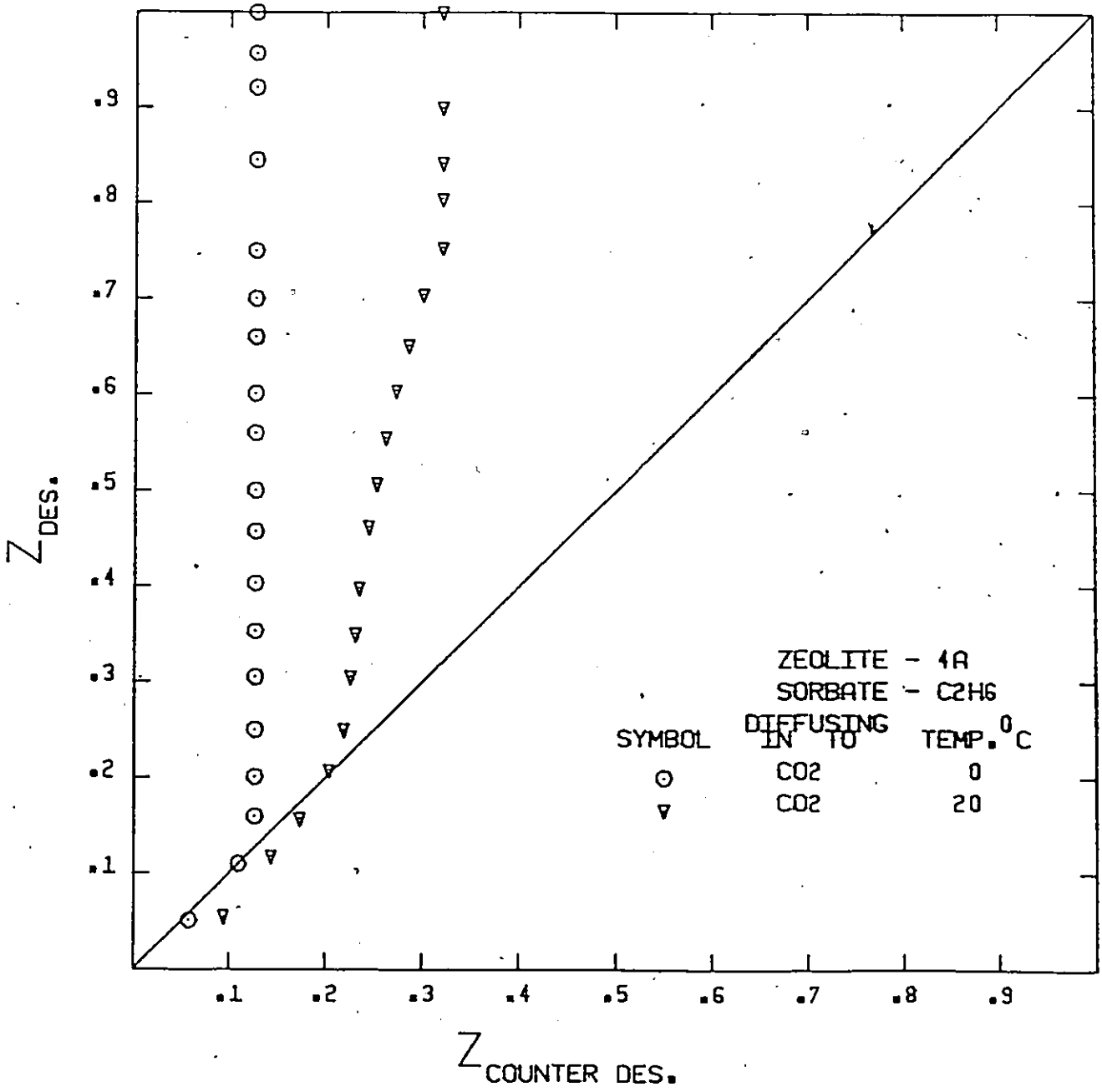

FIG 4.29 BINARY COMPONENT Z-PLOT OF CARBON DIOXIDE DESORPTION ON Na-MORDENITE

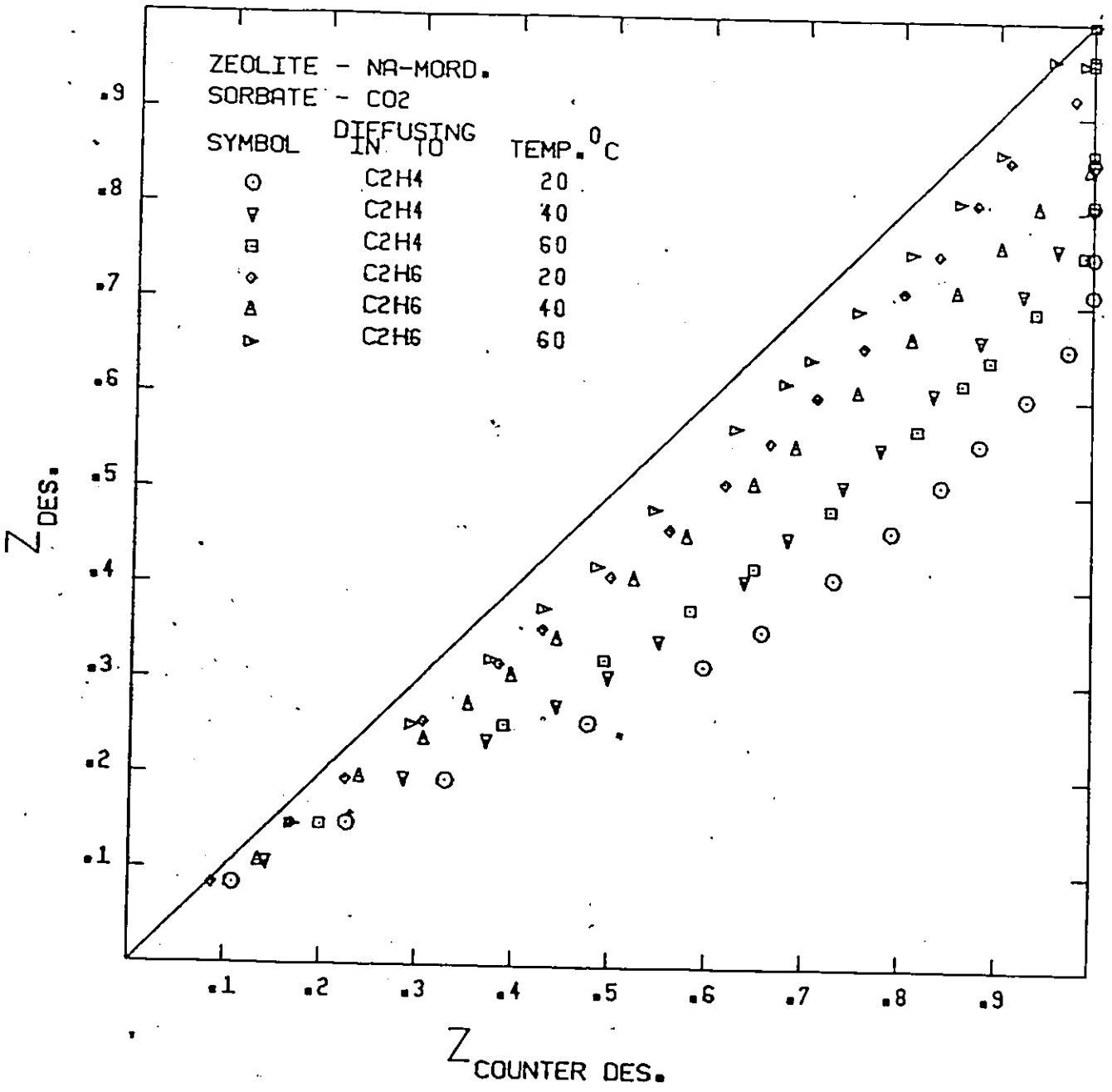

FIG 4.30 BINARY COMPONENT Z-PLOT OF ETHYLENE DESORPTION ON Na-MORDENITE

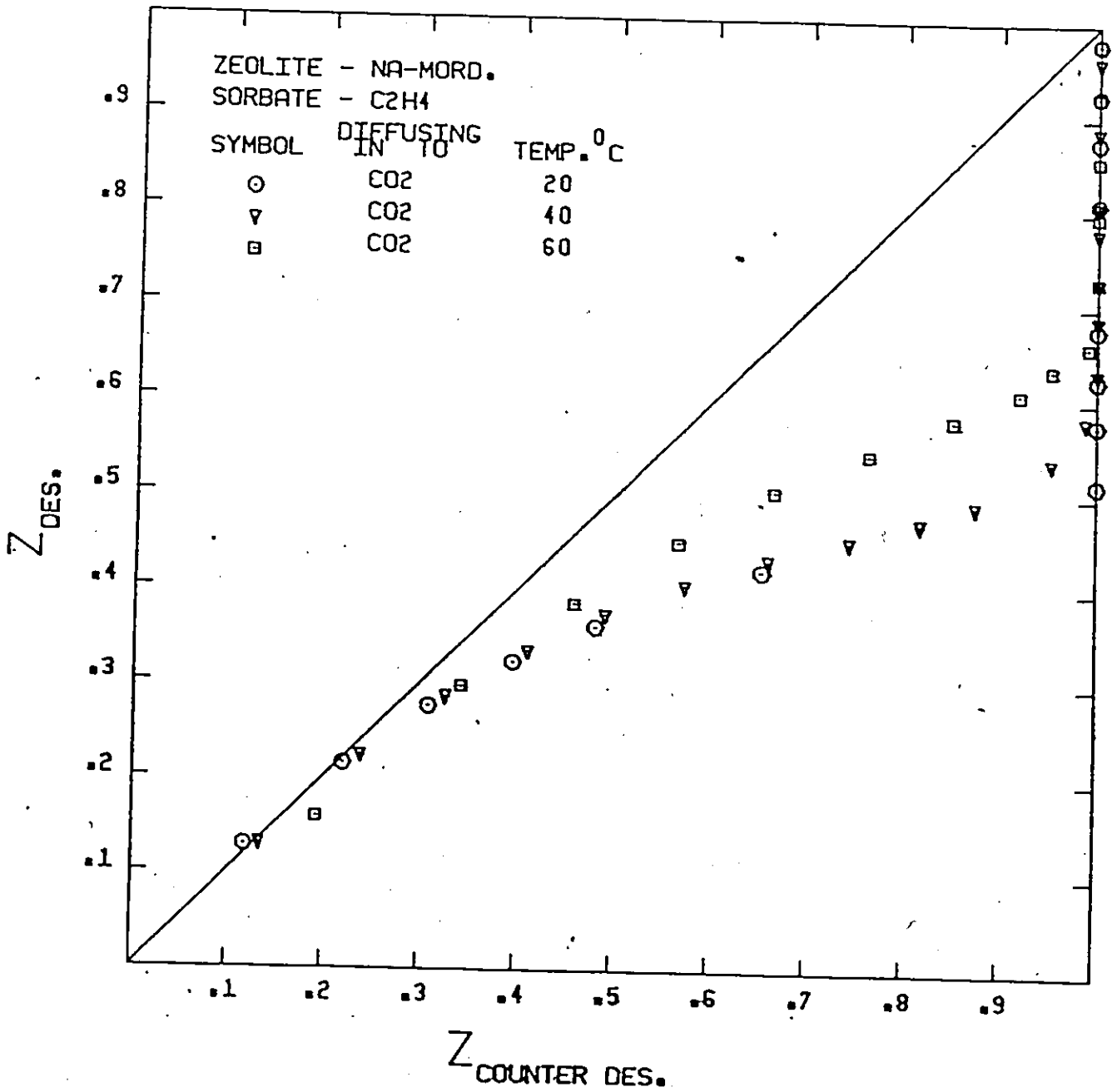

FIG 4.31 BINARY COMPONENT Z-PLOT OF ETHANE DESORPTION ON Na-MORDENITE

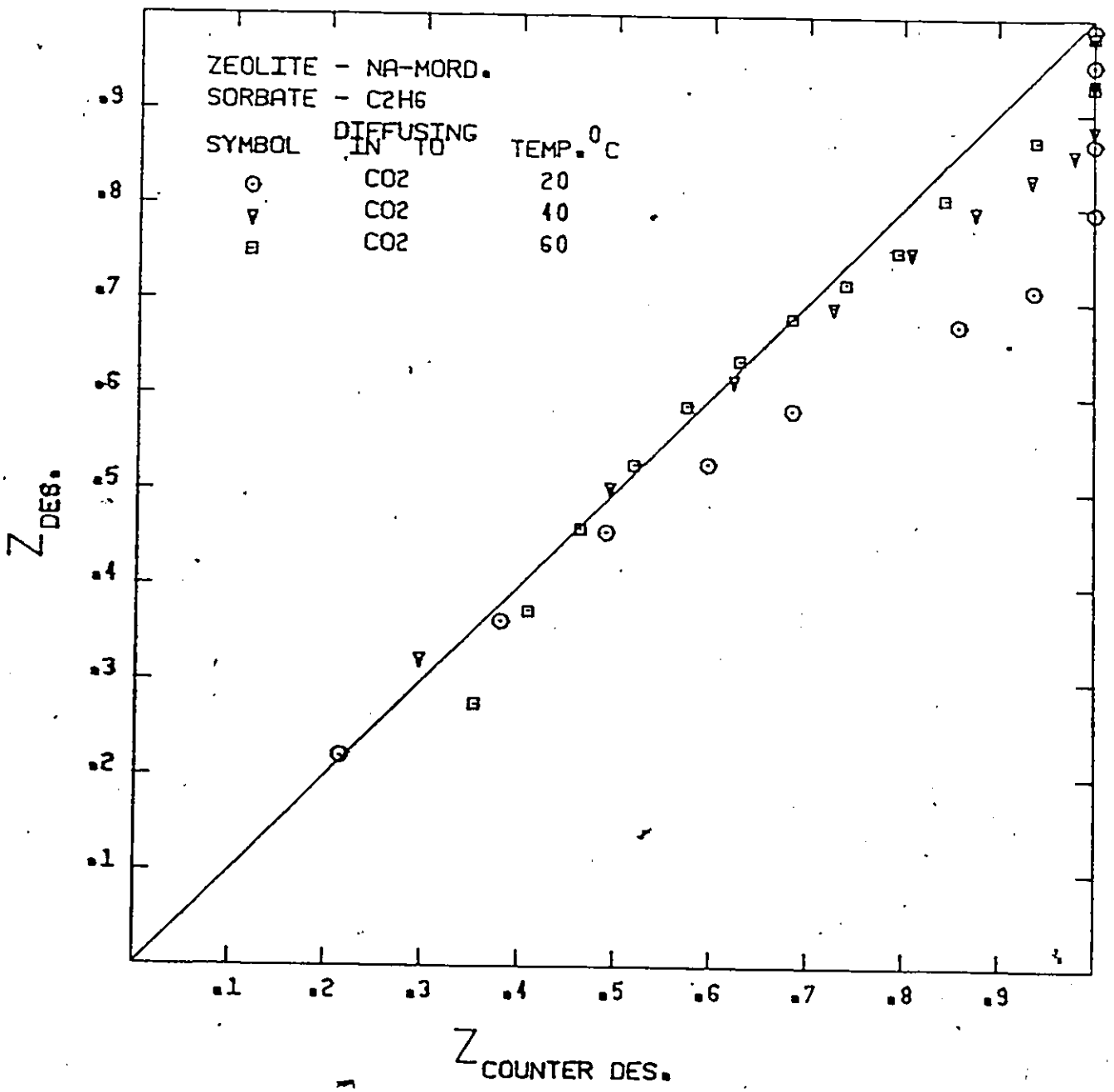

FIG 4.32 BINARY COMPONENT Z-PLOT OF CARBON DIOXIDE DESORPTION ON H-MORDENITE

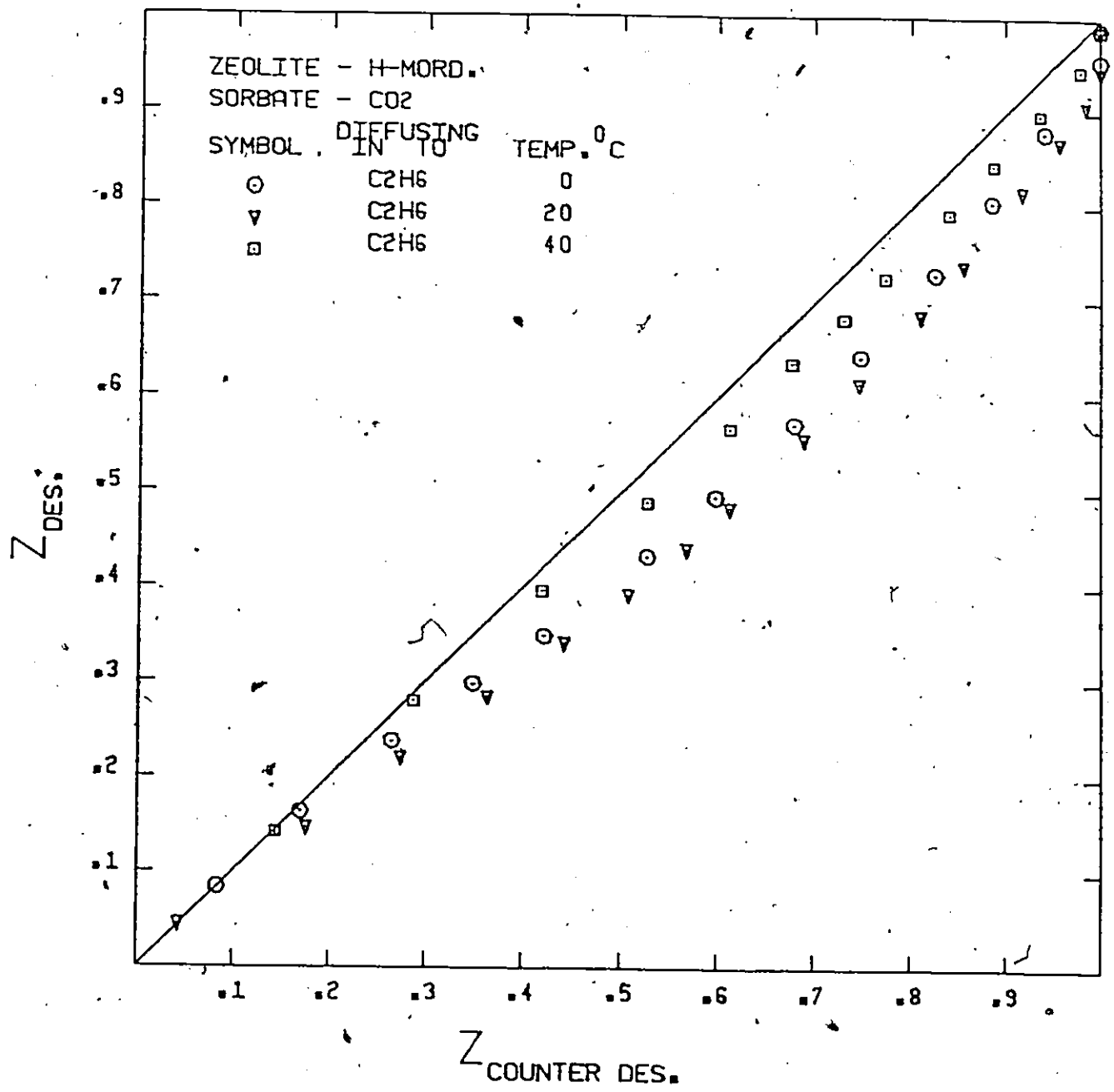

FIG 4.33 BINARY COMPONENT Z-PLOT OF ETHANE DESORPTION ON H-MORDENITE

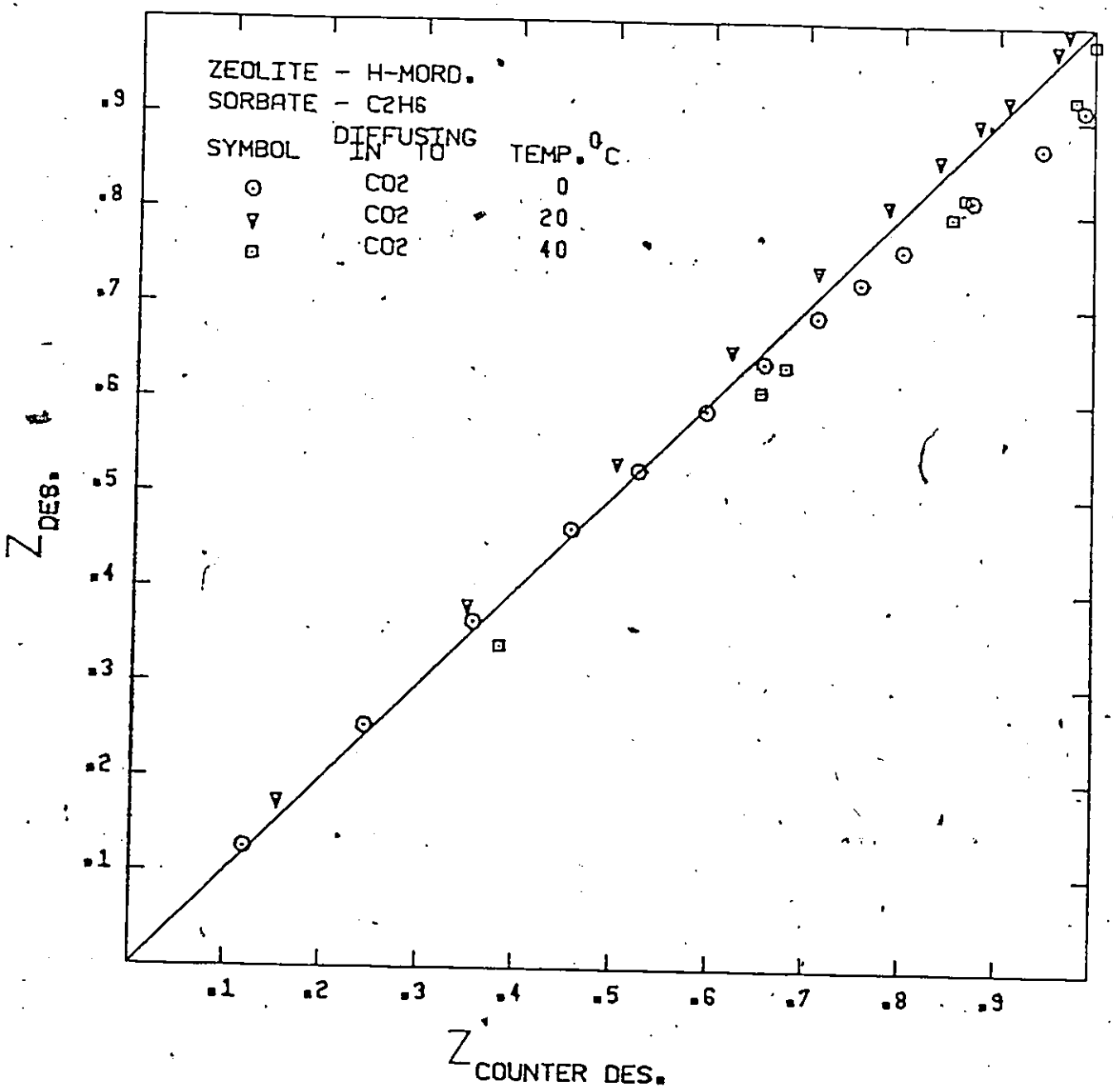

effect by the ethane molecule. But at a higher temperature of 20 ^{o}C, such positive influence diminishes and seems to reverse itself. The Z-curve is observed to lie slightly above the reference line. However, considering the experimental uncertainties involved, little physical significance can be ascribed to this observation. Thus, the ethane effect on the CO_2 desorption rate is regarded to be negligible.

Perhaps the result of negligible effect of ethane adsorbate on CO_2 desorption rate is not too surprising if one considers the equilibrium uptake of ethane; in contrast to ethylene, the quantity of ethane adsorbed at our experimental conditions is relatively small, 30.62 cc(STP)/g and 12.22 cc(STP)/g at 0^{o}C and 20^{o}C respectively. These values correspond to a coverage of 2.38 and 0.95 molecule/cavity for the two temperatures studied. Since adsorbate-desorbate interaction could profoundly affect the kinetic rates of the respective diffusates, the degree of influence of one sorbate on another should therefore be proportional to the number of molecules involved. A reduction in the number of molecules would cause a reduction in the overall interaction. Although zeolite pore structure is an important factor in determining the adsorbate-desorbate interaction and in small port zeolite such as 4A, the narrowness of the window aperture would force the encounter of the two molecules, but, unlike zeolite mordenite, the pore structure of 4A is also 3-dimensional containing internal cavities that are interconnected to each other through six window openings. Since the number of ethane molecules available was insufficient to occupy all the window sorption sites, thus, it is conceivable that a presorbed CO_2 molecule could avoid the encounter with the ethane molecules by choosing an unblocked route.

Table 4.7 Desorption Unidirection Diffusivity ($D_{des.}$) and Counter-desorption Diffusivity ($D_{c.des.}$)

Zeolite	Molecule Diffusing out (Primary focus)	Molecule Diffusing in	Diffusivity (10^{11} cm^2/min) 0.0°C	20.0°C	40.0°C	60.0°C
NaA	CO_2	-	0.344	1.80	2.904	-
	CO_2	C_2H_4	1.532	3.49	-	-
	CO_2	C_2H_6	0.483	1.69	-	-
	C_2H_4	-	0.144	1.162	3.153	-
	C_2H_4	CO_2	-	1.556	5.099	-
	C_2H_6	-	0.263	0.822	-	-
	C_2H_6	CO_2	0.156	0.118	-	-
Na-mord.	CO_2	-	-	3.77	5.07	13.19
	CO_2	C_2H_4	-	24.93	19.86	42.75
	CO_2	C_2H_6	-	6.77	11.74	17.81
	C_2H_4	-	-	10.84	9.55	25.80
	C_2H_4	CO_2	-	32.20	46.64	55.74
	C_2H_6	-	-	41.56	76.08	115.8
	C_2H_6	CO_2	-	55.86	78.19	145.5
H-mord.	CO_2	-	14.48	30.77	52.37	-
	CO_2	C_2H_6	22.30	40.58	64.67	-
	C_2H_6	-	50.08	104.7	180.0	-
	C_2H_6	CO_2	54.82	92.13	195.2	-

The above argument is consistent with the observation made on the CO_2-C_2H_4-4A system; ethylene was adsorbed to a greater extent than ethane, 83.4 cc(STP)/g and 71.7 cc(STP)/g at 0^oC and 20^oC respectively. The probability of molecular encounter and collision between the adsorbate ethylene and desorbate CO_2 is therefore significantly higher. Such collision may result in the transferring of momentum from the mobile adsorbate, causing it to slow down, and to the relatively stationary desorbate molecule making it to desorb at a greater rate than would be in the absence of such condition. The losing and gaining of momentum for the respective diffusates paralleled with the increase and decrease in the activation energies of diffusion; Table 4.8 shows a decrease in the desorption activation energy for the presorbed component as well as a corresponding increase in the adsorption activation energy for the counter adsorbate, whenever there is the involvement of a secondary component.

The reversed sorbate gas sequence of the C_2H_4-CO_2-4A system exhibited a similar rate enhancement effect, Fig. 4.27, where ethylene was the presorbed component and CO_2, the counter adsorbate. However, when ethylene was replaced with ethane, the rate enhancement effect disappeared, Fig. 4.28. Moreover, the counter adsorbate CO_2 had a strong negative impact on the desorption rate of ethane and causing its Z-desorption curve to depart significantly into the upper triangular region. The apparent retardation of ethane desorption rate can be seen in the calculated effective diffusivities listed in Table 4.7, where the desorptive counter diffusion coefficient for ethane is substantially smaller than its unidirection value. Another interesting aspect of the C_2H_6-CO_2-4A system is the phenomenon of trapping; in counter diffusion experiment performed at 0^oC, approximately 80% of the

Table 4.8 Comparison of Activation Energy of Diffusion

Zeolite	Diffusant	Diffusion Direction (Against)	Activation Energy (KJ/mole)
NaA	CO_2	ADS.	5.063
		C.ADS. C_2H_4	49.58
		C.ADS. C_2H_6	10.38
		DES.	46.07
		C.DES. C_2H_4	27.36
		C.DES. C_2H_6	37.45
	C_2H_4	ADS.	32.10
		C.ADS. CO_2	39.77
		DES.	55.19
		C.DES. CO_2	45.24
	C_2H_6	ADS.	32.75
		C.ADS. CO_2	8.33
		DES.	37.97
		C.DES. CO_2	-
Na-mord.	CO_2	ADS.	4.44
		C.ADS. C_2H_4	8.67
		C.ADS. C_2H_6	10.21
		DES.	25.06
		C.DES. C_2H_4	21.09
		C.DES. C_2H_6	19.66
	C_2H_4	ADS.	5.06
		C.ADS. CO_2	15.27
		DES.	17.57
		C.DES. CO_2	11.30
	C_2H_6	ADS.	9.06
		C.ADS. CO_2	29.66
		DES.	20.84
		C.DES. CO_2	18.28
H-mord.	CO_2	ADS.	10.08
		C.ADS. C_2H_6	13.14
		DES.	22.72
		C.DES. C_2H_6	18.95
	C_2H_6	ADS.	16.99
		C.ADS. CO_2	24.64
		DES.	22.76
		C.DES. CO_2	22.43

presorbed ethane molecules was trapped. The amount of trapping was confirmed and recovered in a subsequent experiment by passing helium over the zeolite 4A. Trapping is uniquely observed for the C_2H_6-CO_2-4A system and does not seem to affect other sorbate pairs in either zeolites 4A or mordenites. Trapping could have been the cumulative result of the following factors: First, the overwhelming number of the counter adsorbate CO_2 molecules in the zeolite could effectively block all the window openings, which could seal off the conducting channels and thus preventing the ethane molecules from escaping. Second, since CO_2 is a strongly adsorbed species, and is 50% heavier than ethane, the lighter and relatively inert ethane molecule may not be able to induce the CO_2 to dislodge from the window sorption site and thus preventing the exchange of positions to occur in the larger internal cavities.

The above reasoning is consistent with the observation that when the sorbate gas pair sequence is reversed, there was no trapping of the CO_2, because the relatively small number of ethane adsorbate molecules could not effectively block all the channel passageways.

Counter-diffusion of sorbate pairs studied in this work readily occurred in both mordenite zeolites. No trapping of the presorbed species was observed. The structure of mordenite is one-dimensional and hence, unlike the 3-dimensional 4A structure, adsorbate and desorbate could not avoid each other by taking a different route. However, because the free pore diameter of both mordenites is larger than the sum total of the cross-sectional area of the diffusates, passing of the molecules migrating in opposite direction could occur thus resulting in the lack of trapping effect. For counter-diffusion in Na-mordenite, the pore structure was

apparently not sufficiently large so that some interaction between adsorbate/desorbate remained. Again, the result of such interaction is one of the desorption rate enhancement, Figs. 4.29 to 4.31. The activation energy of the counter desorbate is similarly shown to be reduced in comparison with the unidirection diffusion of the same species which indicates a lowering of the diffusion barrier, Table 4.8. With a further enlargement of the pore size openings, counter diffusion in H-mordenite was expected to occur at an even more rapid pace and with a minimum interaction between the diffusing molecules. Indeed, Figs. 4.32 and 4.33 show the Z-desorpton curves to be close to the reference diagonal line and this observation is further supported by the similar values of the activation energies for desorption and counter-desorption in H-mordenite, Table 4.8.

4.3 TRAPPING

The unique trapping phenomenon observed for the C_2H_6-CO_2-4A system was further investigated in a series of counter-diffusion experiments performed at 0^oC. Ethane was loaded into the zeolite 4A to various degrees by changing the gas phase concentration. Table 4.9 shows a comparison of the equilibrium uptakes at three concentration settings studied in the flow system with the values obtained from the ethane isotherm obtained from the static BET system. As shown, the two systems are quite compatible Data in the last colume of Table 4.9 show that a complete removal of the presorbed ethane molecules is possible through passing of pure helium. However, when helium was replaced with a 5% CO_2-He gas mixture, trapping of the presorbed ethane occurred, Table 4.10. The percentage or the fractional amount of the initially loaded ethane molecules that were able to desorb increased with decreasing

Table 4.9 Equilibrium uptake of Ethane At Various Levels of Gas Phase Concentration At 0°C

Gas Phase (%)	Partial Pressure (mm Hg)	EQM.(Isotherm) Vol. Ads. cc(STP)/g	EQM. (Flow) Vol. Ads. cc(STP)/g	Total Vol. Des. in He cc(STP)/g
54.0	410.4	77.7	78.12	76.99
36.2	275.12	75.0	71.37	71.58
19.6	148.96	69.0	-	-

Table 4.10 Trapping Of Presorbed Ethane In Presence Of Carbon Dioxide At 0°C

Volume in cc(STP)/g

Counter Adsorbate	Ethane %	Total Vol. Adsorbed	Vol. Desorbed	Vol. Trapped	Vol. Recovered	% Vol. Trapped
5% CO_2	54.0	77.57	52.61	24.96	24.27	32.18
5% CO_2	36.2	70.93	47.81	24.12	22.94	34.0
5% CO_2	19.6	67.10	36.80	30.82	30.29	45.10
10% CO_2	19.6	68.85	38.45	30.40	29.87	44.15

amount of the initial loading, but the total quantity of the trapped ethane remains relatively constant. Trapping, however, is not a permanent process, because virtually all of ethane was recovered in subsequent experiments through passing of pure helium. Although the absolute amount of ethane trapped seems to be constant, a larger amount of the presorbed ethane at higher initial loading was able to counter desorb. This is perhaps the reflection of the steeper concentration gradient which resulted in a stronger driving force for desorption. Data shown in the last two rows of Table 4.10 indicate that a change in the concentration of the counter adsorbate, CO_2, did not affect the total trapped amount. This may have been the consequence of the rather rectangular isotherm of CO_2, i.e. the equilibrium amount of the sorbed phase was insensitive to the gas phase concentration variation.

CHAPTER V

KINETIC MODEL SIMULATION

5.1 INTRODUCTION

Diffusion in zeolite has been widely modeled after the simple Fick's law model in which the intrinsic mobility of a given diffusate molecule is often characterized by a single parameter, the diffusion coefficient D; i.e.

$$\partial C/\partial t = D\partial^2 C/\partial x^2 \qquad 5.1$$

with the appropriate boundary conditions. Most of the single component kinetic data apparently can be adequately correlated with Eqn. 5.1, if due consideration is given to the zeolite particle shape, size distribution, concentration dependency of the diffusivity as well as the temperature effect in the case of the non-isothermal sorption experiments. However, when this simple model is applied to the multicomponent sorption system, it would not yield information at a fundamental level because the equation does not provide terms that could be used to account for molecular interaction, for example, adsorbate/desorbate interaction. Nonetheless, kinetic data of the multicomponent systems can still be fitted to this model although caution must be exercised in the interpretation of results; the diffusion coefficient represents no more than an empirical parameter. The important aspects of the multicomponent sorption in relation to the industrial applications have been noted in the previous sections. Unfortunately, with the exception of the tracer diffusion studies, very few attempts have been made in the past in the qualitative and quantitative analysis and

interpretation of these important systems.

5.2 MULTICOMPONENT DIFFUSION MODEL BASED ON CHEMICAL POTENTIAL DRIVING FORCE

One quantitative description of the multicomponent sorption process was proposed by Karger and Bulow [26], in which the zeolite diffusion model is based on the thermodynamics of irreversible processes. For a binary component system, the formulation of the model starts with the definition of fluxes, J_1 and J_2 for the two components

$$J_1 = -L_{11} \text{ grad } \mu_1 - L_{12} \text{ grad } \mu_2$$

$$J_2 = -L_{22} \text{ grad } \mu_2 - L_{21} \text{ grad } \mu_1 \qquad 5.2$$

where L_{12} and L_{21} are cross coefficients, and L_{11} and L_{22} are straight coefficients. μ_1 and μ_2 are chemical potentials for component 1 and 2, respectively. Karger and Bulow [26] simplified Eqn. 5.2 by eliminating the cross coefficients, i.e., ($L_{12}=L_{21}=0.0$). The chemical potential terms are related to the partial pressures through a standard relationship

$$\mu_i = \mu_i^{\circ} + R\,T \ln P_i \qquad 5.3$$

and the partial pressures P_is in turn are determined from the equilibrium relationship, $P_1=f(C_1,C_2)$. Habgood [24] also started from the principle of irreversible thermodynamics and developed a similar model. He proposed that the velocity of the diffsate is proportional to its chemical potential gradient, i.e.

$$U_A = -L_A \nabla \mu_A \qquad 5.4$$

where L_A is related to the mobility of component A in a mixture containing B. The flux of A is defined as

$$J_A = C_A U_A = - C_A L_A \nabla \mu_A \qquad 5.5$$

Which can then be substituted into the equation of continuity, i.e.

$$d C_A / d t + \nabla J_A = 0 \qquad 5.6$$

The chemical potential μ_A is related to the partial pressure through a conventional expression,

$$\mu_A = \mu_A^{\circ} + R T \ln p_A \qquad 5.7$$

and

$$p_A = f (C_A, C_B) \qquad 5.8$$

where C_A , C_B represent the sorbed phase concentrations of the binary mixture. Habgood used a mixed Langmuir isotherm to establish the functional relationship of Eqn. 5.8, i.e.

$$p_A = C_A / b_A (C_m - C_A - C_B) \qquad 5.9$$

Finally, after the evaluation of the partial derivatives and with the appropriate substitutions, he obtained the basic diffusion equation as

follows: For molecule A,

$$\frac{\partial\theta_B}{\partial t} = \frac{R\,T\,L_B}{(1-\theta_A-\theta_B)}\left[(1-\theta_A)\left(\frac{\partial^2\theta_B}{\partial r^2}+\frac{2}{r}\frac{\partial\theta_B}{\partial r}\right)+\theta_B\left(\frac{\partial^2\theta_B}{\partial r^2}+\frac{2}{r}\frac{\partial\theta_A}{\partial r}\right)\right] + \frac{R\,T\,L_B}{(1-\theta_A-\theta_B)^2}\left[(1-\theta_A)\frac{\partial\theta_B}{\partial r}+\theta_B\frac{\partial\theta_A}{\partial r}\right]\left(\frac{\partial\theta_B}{\partial r}+\frac{\partial\theta_A}{\partial r}\right)$$

and an analogous expression for molecule B. 5.10

$$\frac{\partial\theta_A}{\partial t} = \frac{R\,T\,L_A}{(1-\theta_A-\theta_B)}\left[(1-\theta_B)\left(\frac{\partial^2\theta_A}{\partial r^2}+\frac{2}{r}\frac{\partial\theta_A}{\partial r}\right)+\theta_A\left(\frac{\partial^2\theta_B}{\partial r^2}+\frac{2}{r}\frac{\partial\theta_B}{\partial r}\right)\right] + \frac{R\,T\,L_A}{(1-\theta_A-\theta_B)^2}\left[(1-\theta_B)\frac{\partial\theta_A}{\partial r}+\theta_A\frac{\partial\theta_B}{\partial r}\right]\left(\frac{\partial\theta_A}{\partial r}+\frac{\partial\theta_B}{\partial r}\right)$$

where $\theta_i = C_i/C_m$, and $D_{Ao} = R\,T\,L_A$ and $D_{Bo} = R\,T\,L_B$.

The mathematical models proposed by Habgood and Karger and Bulow in principle provide a strong coupling for the diffusion equations because the chemical potential gradient of one molecular species is a function of the concentration and concentration gradient of both components in a binary mixture. This is in contrast with the conventional concentration gradient based Fick's law model where coupling of the diffusion equation can only be obtained through the equilibrium conditions at the exterior surface.

Round, et al. [42] solved Eqn 5.10 by a finite difference numerical technique. They applied this model to the case of co-diffusion of N_2 and CH_4 in zeolite 4A. Their results showed that although the quantitative correlation was only moderately good, qualitatively, the model was capable of producing all of the pertinent features of the rate curves, which includes a maximum in the N_2 uptake.

In the present work, we are concerned with the counter diffusion phenomenon in zeolites. Accordingly, the usefulness of this chemical potential model can be tested by changing the appropriate boundary conditions. In our computer simulation experiment, Eqn 5.10 was solved by an

explicit finite difference numerical method in which the zeolite crystal was considered to be of spherical shape, with the radius of the particle divided into N equal radial increments. The relevent initial and boundary conditions pertinent to our system are given as follow:

$$\begin{aligned} \theta_A\ (r,0) &= \theta_{Ao} \\ \theta_B\ (r,0) &= \theta_{Bo} \\ \theta_A\ (a,0) &= \theta_{Al} \\ \theta_B\ (a,0) &= \theta_{Bl} \end{aligned} \qquad 5.11$$

and

$$d\theta_A/dr\ (0,t) = d\theta_B/dr\ (0,t) = 0.0$$

Results of the simulation studies are presented in the following section.

As indicated earlier, the type of counter diffusion simulation studied is one in which the zeolite was preloaded to some coverage with one component, B. The desorption of B was induced by passing a gas mixture containing another sorbable component, A. For the purpose of clarity, in any given counter-diffusion simulation experiment, related to the chemical potential model, as described in the following section, A is referred to as the adsorbate molecule while B is the desorbate molecule. The parameters of interest are the values of diffusivities as well as the degrees of coverage or concentration effect of the respective molecules. The objective is to find the condition, i.e., a combination of parameter values, in which the simulation results would match our experimental observations. Evaluation of the model was made by comparing the simulated single component fractional equilibrium uptake values of a particular molecular species to its equilibrium uptakes under the binary condition in the familiar Z-plots.

Fig. 5.1 compares the adsorptive and desorptive equilibrium uptakes of molecules A and B having the identical values of diffusivity and coverages.

FIG 5.1 COMPARISON OF THE SINGLE COMPONENT ADSORPTION/DESORPTION RATES, CHEMICAL POTENTIAL MODEL.

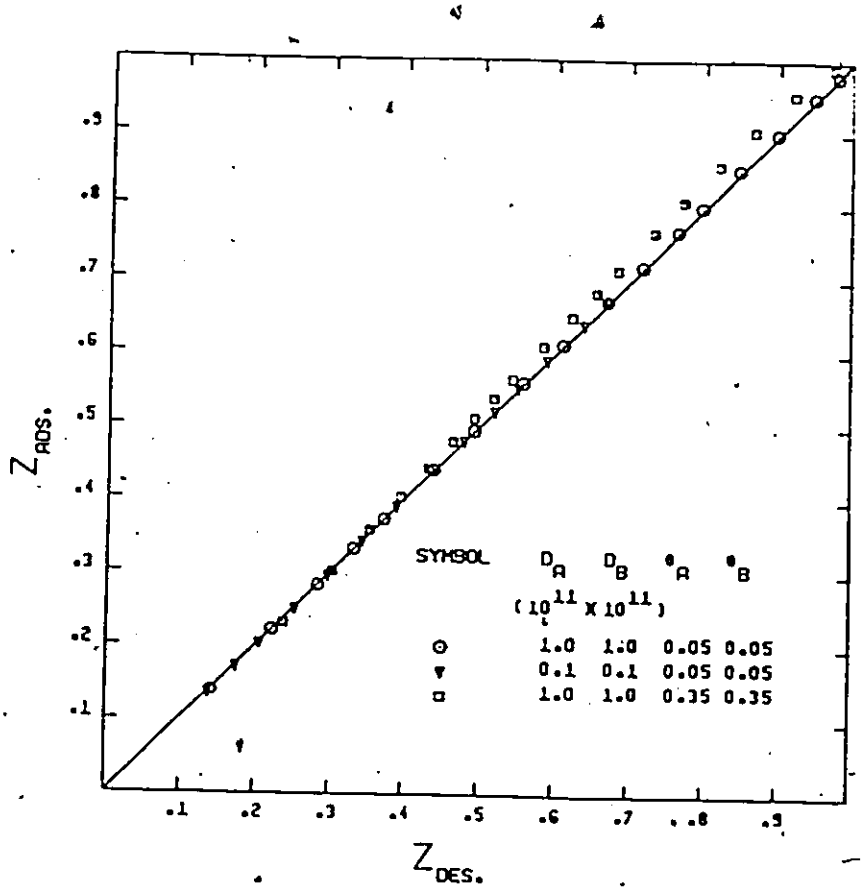

FIG 5.2 BINARY Z-ADSORPTION PLOT, EFFECT OF THE DESORBATE DIFFUSIVITY, CHEMICAL POTENTIAL MODEL.

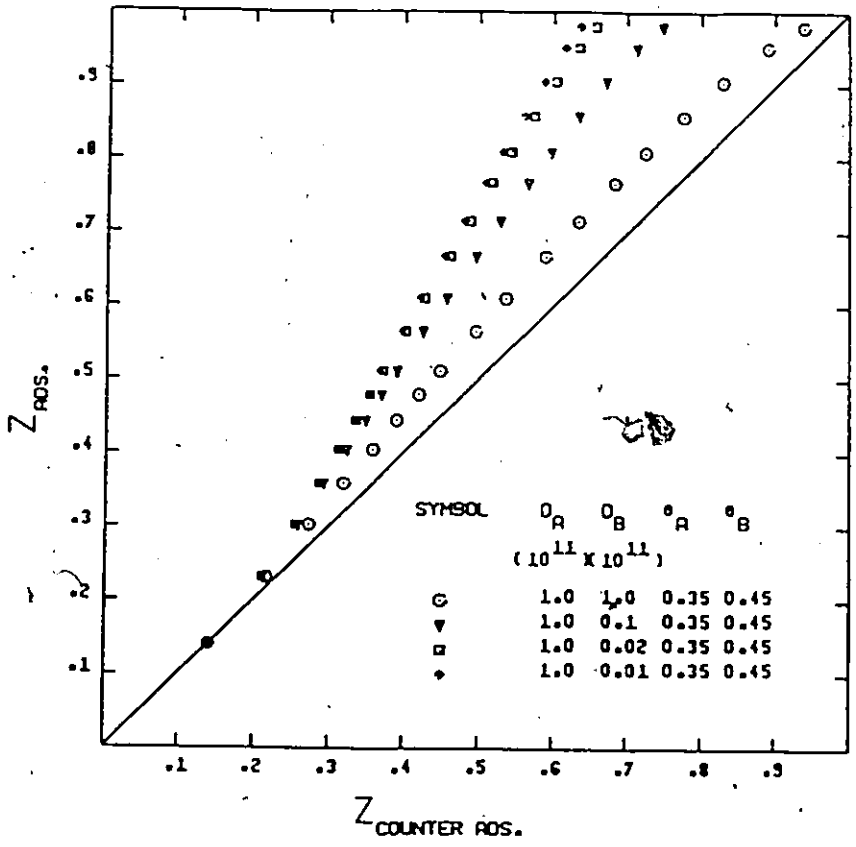

FIG 5.3 BINARY Z-DESORPTION PLOT, EFFECT OF ADSORBATE (A) DIFFUSIVITY, CHEMICAL POTENTIAL MODEL.

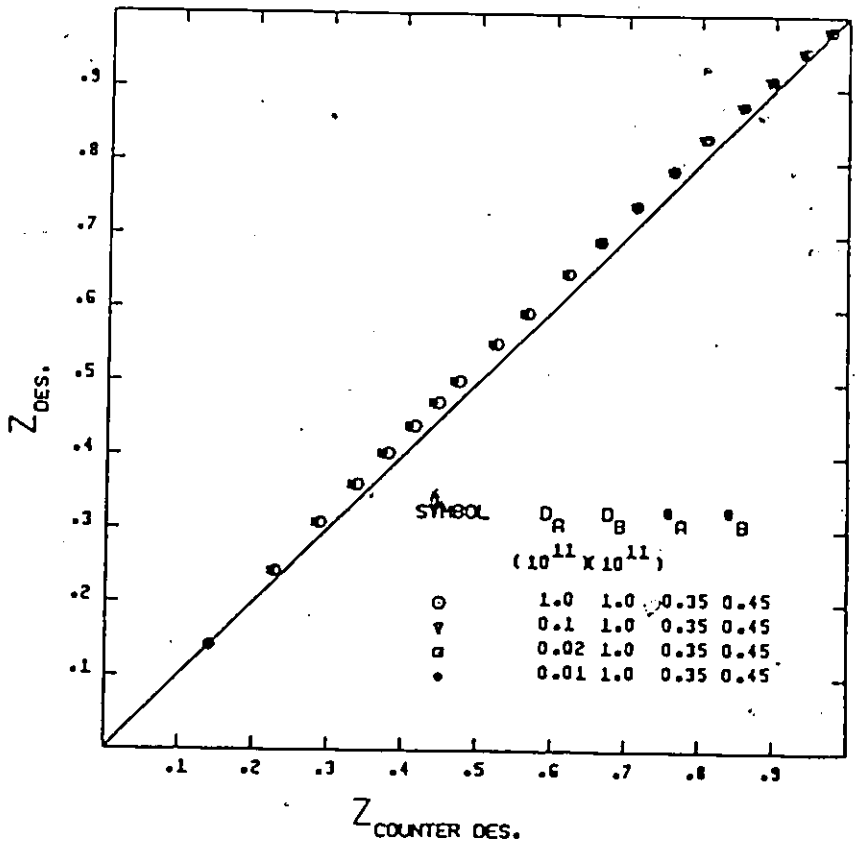

FIG 5.4 BINARY Z-DESORPTION PLOT, LOW LOADING OF B, EFFECT OF ADSORBATE (A) CONCENTRATION, CHEMICAL POTENTIAL MODEL.

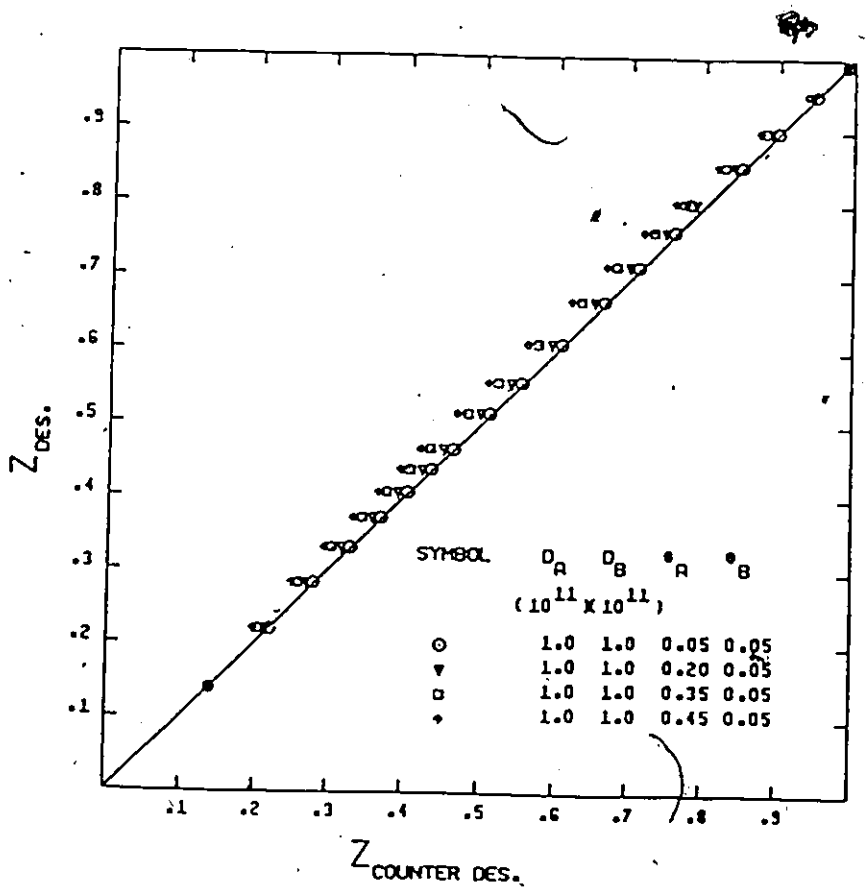

FIG 5.5 BINARY Z-DESORPTION PLOT, HIGH LOADING OF B, EFFECT OF ADSORBATE (A) CONCENTRATION,-CHEMICAL POTENTIAL MODEL.

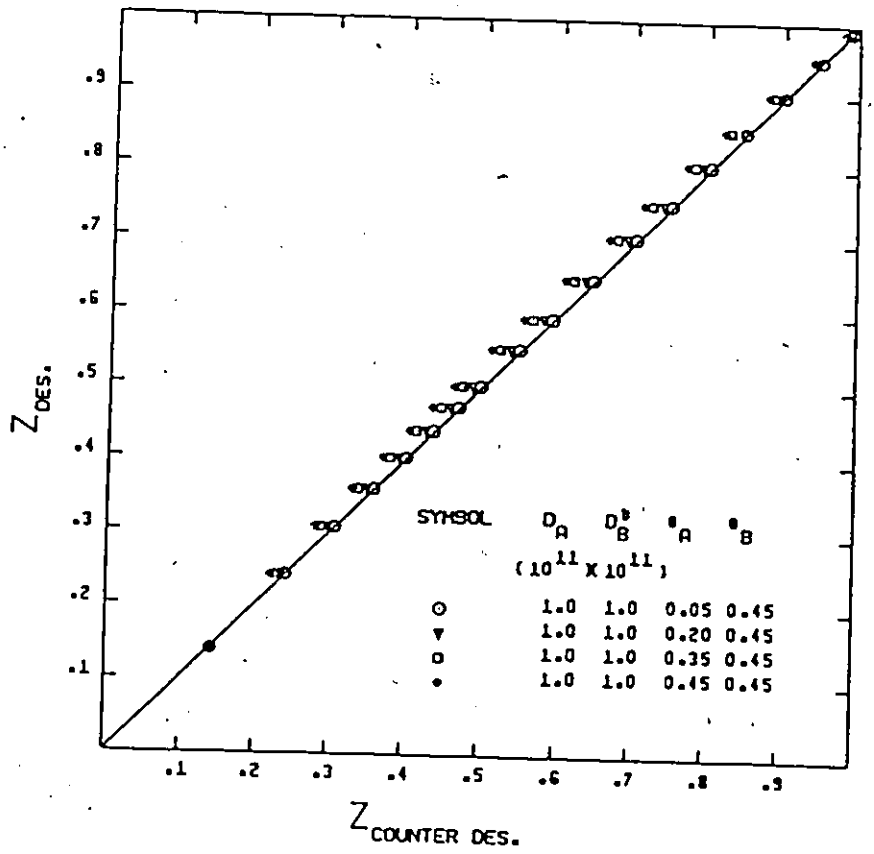

The values of Z_A and Z_B were obtained independently, i.e. in the absence of the other molecule, also, since the parameters are of equal values, i.e. A=B, this simulation experiment represents a single component sorption case. At a low coverage of 0.05, regardless of the diffusivity values, the adsorption and desorption rates are identical as indicated by the overlapping of the Z-curve and the reference line. When the coverage was increased to 0.35, a slight deviation from the 45^{o} line occured. The direction indicates that the desorption rate is slightly lower than the adsorption rate, which qualitatively agrees with our experimental observation. However, the difference is relatively insignificant and attempts to magnify the rate difference by increasing the value of the coverage were unsuccessful.

For the binary sorption case, the effect of the desorbate diffusivity, D_B, on the counter-adsorbate adsorption rate is shown in Fig. 5.2. The diffusivity of A was kept constant while the values of D_B was varied. The simulated Z-adsorption curves shows the presence of B could significantly retard the counter adsorption rate of A eventhough the intrinsic mobility of A remained constant. However, the same comment can not be given to the reversed case where the diffusivity of B was kept at a constant value and the diffusivity of A was varied in the same order as in the previous case, Fig. 5.3. From the desorption point of view, the simulated Z-desorption curves show that the presence of the counter adsorbate A had only a minimal effect on the desorption rate of the presorbed molecule B. Moreover, the overlapping of the curves indicated that the desorption rate of B was insensitive to the values of D_A although D_A was varied by over two orders of magnitude. The effect of the concentration of A, (θ_A), on the desorption

rate, was investigated at two different degrees of loading of B,(θ_B=0.05, 0.45), Figs. 5.4 and 5.5, respectively. The concentration of A does seem to affect the desorption rate of B although it is in a manner of retarding its rate. The desorption rate of B decreases further with increasing concentration levels of A, however, the effect was not as pronounced as that of the counter adsorption case. Comparison of the two figures shows that no significant differences existed between the two sets of Z-curves although the loading of the presorbed component was increased by nine folds.

In summary, the simulation studies of the chemical potential model, when applied to the counter diffusion case, indicated that the model could exhibit some of the pertinent features observed in our experimental studies. For example, the anisotropic nature of the adsorption and desorption precesses. In the binary case, it qualitatively described the retardation of the counter adsorbing component diffusion rate. However, it failed to predict the corresponding rate enhancement effect of the presorbed component in a binary mixture.

5.3 RANDOM WALK MODEL

An adsorption/desorption simulation program was developed by using the principle of random walk. In this program, the zeolite particle is modelled in terms of a single one-dimensional pore channel having open pore mouths at each end. The desorption of a molecular species out of the pore or the adsorption of a sorbate gas into the pore as well as the combination of the simultaneous adsorption/desorption of two species could be simulated.

FIG 5.6 RANDOM WALK MODEL, ● DESORBATE MOLECULE, O ADSORBATE MOLECULE.

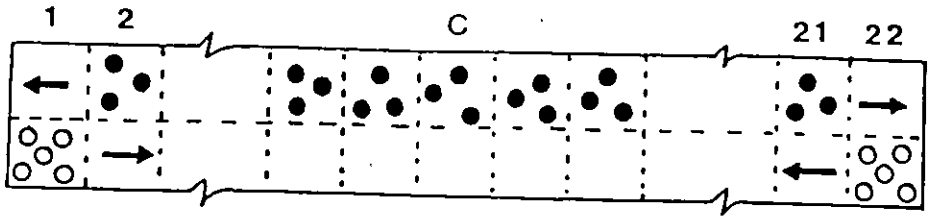

DEFINITION OF IMPORTANT PARAMETERS

CB	-	CRITICAL MOVING VALUE FOR ADSORBATE "B"
BM	-	MAXIMUM NUMBER OF MOLECULES "B" PER CELL
CA	-	CRITICAL MOVING VALUE FOR DESORBATE "A"
AM	-	MAXIMUM NUMBER OF MOLECULES "A" PER CELL
RN	-	RANDOM NUMBER BETWEEN 0 - 100
AN(I)	-	NUMBER OF MOLECULES "A" IN CELL (I)
AT(I)	-	AN(I) * RN(I), MOVING POTENTIAL OF MOLECULE "A" IN CELL (I)
A(I)	-	INITIAL NUMBER OF "A" ADSORBED PER CELL, AT T=0
BB	-	BULK CONCENTRATION OF "B" IN EXTERIOR
LF	-	TOTAL NUMBER OF MOLECULES "A" AND "B" ALLOWED PER CELL
F	-	PROBABILITY OF MOVING POTENTIAL TRANSFER

5.3.1 PROGRAM STRATEGY

The basic program strategy assumes that the movement of the adsorbate/desorbate molecules within the zeolites pores is the rate determining step. The zeolite pore is modelled as an one-dimensional channel which is divided into 20 cells or interior compartments, (the number of cells can readily be expanded), Fig. 5.6. Each compartment may contain one or more molecular species: component A is referred to as the presorbed species which is therefore the desorbate molecule, whereas component B is the adsorbate molecule. The movement of any particular molecule from one cell to an adjacent cell is governed by a set of rules or constraints: First, in order to move, the molecule must possess a potential. The movement potential is defined as the product of the number of molecules of a species present in each cell times a randomly generated number between 0 and 100. In addition, this potential must be greater than some critical moving factor defined for each species separately. For example, consider molecule A in compartment (I); the potential for A to move from cell (I) exists if the following inequality is satisfied

$$AT(I) > CA$$

where

$AT(I) = AN(I) * R.N$

$AN(I)$ = Number of A in cell I

$R.N$ = Random Number between 0 and 100

and

CA = Critical Moving factor of A

A similar relationship holds for species B in the equation

$$BT(I) > CB$$

where $BT(I)$ is the potential of B in cell (I), and CB is the critical moving factor for B. Once a species has demonstrated that it has the potential to

move, then, the program examines as to whether or not there exists any physical limitations on movements and if not, in which direction and order movement will occur.

One restriction towards movement considers whether or not the adjacent cell is physically saturated with both A and B molecules: A loading factor, LF, is specified in the program which places a limit on the total number of molecules allowed in a given cell. If the number of molecules in a cell is equal to this loading factor, then, no molecule may move into this cell. Thus, prior to movement, the number of A and B molecules in adjacent compartments are compared to the loading factor to certify that room exists for movement into this cell.

A further limitation is imposed on the number of each individual species allowed in each compartment. An upper limit, AM and BM, sets the maximum number of A and B individually allowed in each cell. For example, if the number of species A in the adjacent compartment is equal to the maximum allowed, then, no movement of A into this compartment is permitted. This limitation could be used to establish the equilibrium saturation value of a particular component or to compensate for the size differences between different molecular species.

Another factor considered is the direction of movement. For a given time increment, if the species in cell (I) possesses the potential to move and if the previous limitations have not been violated, then, one molecule may move to each adjacent cell on the left- and right-hand side of cell (I). Thus, a total of two molecules may leave at a given time. If, however, the current cell contains only one molecule, then the decision as to which direction the movement will occur is based on which adjacent cell presently

has the lowest potential. Hence, the neighbouring potentials, AT(I-1) and AT(I+1), are compared and movement is made first towards the lower potential. After the first movement is made, the number of the remaining molecules is checked to determine whether movement may be made to the next cell also.

Another restriction on movement involves determining whether or not the potential of the cell under consideration is greater than the adjacent cells thus, movement of A to the left-hand cell is allowed only if

$$AT(I) > AT(I-1)$$

and for the right-hand side

$$AT(I) > AT(I+1)$$

The same conditions apply for the movement of B. Finally, the interaction between species A and B is accounted for by the transfer of moving potential from one component to another. For example, if cell(I) contains both A and B molecules, and the moving potential has been determined to be 500 for molecule A and 400 for molecule B, then, a portion of the moving potential is to be transferred from B to A. The amount transferred is calculated by multiplying the total potential of B with a potential transfer factor, F, between 0 and 1. If the value of F is 0.25, then, a potential of 100 is subtracted from the total potential of molecule B and adding on to molecule A. Thus, the new total potential in cell (I) will be 300 for molecule B and 600 for molecule A. This potential transfer can be related to the momentum transfer between the adsorbate/desorbate upon colliding with each other.

The total examination of the ability of a species to move is made for each component, A and B, for each cell, I = 1 to 22, at each time interval. Cells 2 to 21 are considered to be the internal compartments while cells 1

and 22 are modelled as being the exterior to the pore and thus are representative of the bulk phase. Additional restrictions are imposed by the boundary conditions set for cells 1 and 22. It is assumed that any A which leaves the pore would not diffuse back. This is achieved by setting the concentration of A in the exterior to zero. Results of the random walk model simulation are expressed as an approach to equilibrium, ZA and ZB, which are defined as

$$ZA = AL / (20 * AI)$$

and

$$ZB = (BL + BR) / (20 * BM)$$

where AL = Number of A having left the pore

AI = Initial number of A per cell

BL + BR = Total number of B having entered the pore

and BM = Maximum number of B allowed per cell.

The following analogies to program factors may be made: The length of the zeolite conducting channel can be related to the number of compartments considered. The critical moving factors, CA and CB, may be related to the activation barrier for diffusion. The loading factor may be related to the pore dimensions relative to the adsorbate/desorbate molecular sizes. The maximum individual species loading limits, AM and BM, can be related to the number of sites available for each species (i.e. a equilibrium adsorption factor) or to account for the difference in size between the various molecular species.

5.3.2 PROGRAM DESCRIPTION

A listing of the program is given in the Appendix A-4. The definition of the important parameters is given in Fig. 5.6. A simplified overall

FIG 5.7 MAIN PROGRAM, RANDOM WALK MODEL.

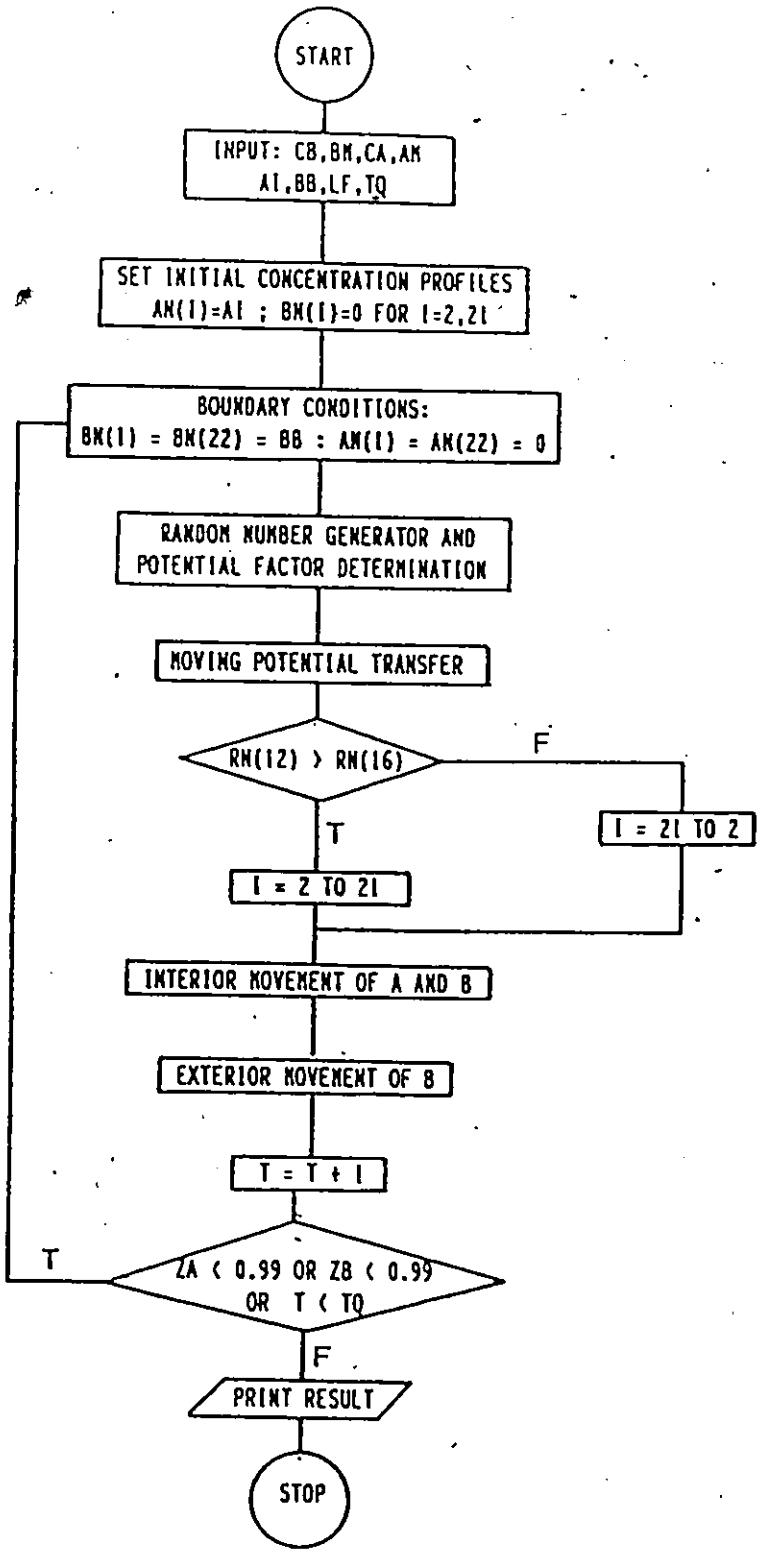

flowsheet of the program is shown in Fig. 5.7. The program initially reads in values of the various parameters such as the Critical Moving Factor, Loading Factors etc. Following this, the initial concentration profile is set. For this program, a uniform concentration profile of A and B is assumed although this may be readily adjusted to any desired form. The exterior boundary conditions are then specified. As mentioned earlier, the conditions are set to allow A to desorb and B to adsorb. The program then slips into an iterative scheme in which the following sequence of events are performed for each time interval; First, a random number for each species in each cell is generated and the subsequent potential of each component in each cell, AT(I) and BT(I), determined. Potential transfer from one component to another is then made providing the condition for such transfer exists. In the next step, the interior movement of A and B are considered one cell at a time. The order in which these cells are considered (i.e. left to right or right to left) are determined by comparing two randomly generated numbers. This is done to remove any bias introduced by systematically considering the cells in the same consistent fashion. Once movement of A and B are made in the interior, the exterior movement of B from the bulk is then considered. After all movements are made, calculation of the results in terms of the concentration profile and approach to equilibrium are performed. The time step is then incremented and unless one or both of the species have reached the equilibrium or the maximum number of iterations has been reached, the movement process is repeated by resetting the boundary conditions.

5.3.3 SIMULATION RESULTS

The adsorption/ desorption random walk simulation program was used in

several test cases. Cases studied involved the single component adsorption of molecule B and the desorption of molecule A. Also, the combined simultaneous adsorption and desorption of the respective B and A as well as the effects of the individual parameter on sorption rates were investigated.

In the first case, a single species B is diffusing into an initially empty pore. The results of this simulation experiment in terms of the concentration profile and the equilibrium uptake with time are shown in Fig. 5.8. As may be observed, the resulting concentration profiles are neither completely random nor perfectly symmetric. However, a general pattern is suggested with the concentration at the center cell being the lowest. As time progresses, the outer cells become increasingly saturated and the concentration at the center also increased. This conforms with the general trend expected.

In the second case, the desorption of the species A is studied. Here, the opposite trend is observed; Fig. 5.9 shows the concentration of A at the outer cells becomes very low while the center cell remained at a high level. As time progresses, more of the outer cells have their initial conentration significantly reduced while the inner cells only decreased slowly. Again, this is the approximate type of behaviour expected. The approach to equilibrium curves as a function of time are also shown in these two figures. Of particular interest was how well the simulated single component rate curves conformed to Fick's law. Crank [15] has suggested the solution for diffusion in slabs obeying Fick's law to be

$$Z = 1 - (8/\pi^2)\sum_{n=1}^{\infty}(2n+1)^{-2}\ \mathrm{EXP}\ (-(2n+1)^2\pi^2\tau/4)$$

$$Z = 2\,(\tau/\pi)^{1/2} \qquad (0 < Z < 0.45) \qquad 5.12$$

FIG 5.8 CONC. PROFILES AND UPTAKES OF SINGLE COMPONENT ADSORPTION

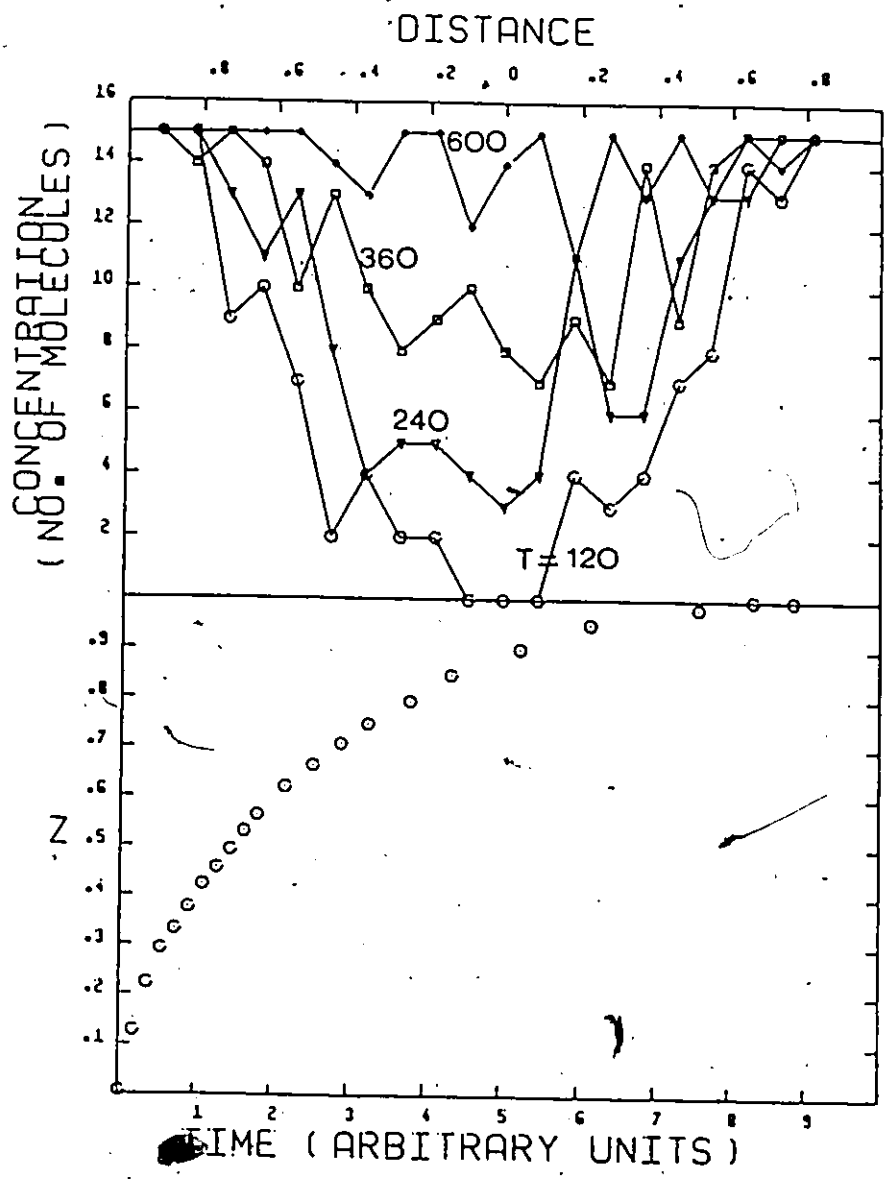

FIG 5.9 CONC. PROFILES AND UPTAKES OF SINGLE COMPONENT DESORPTION

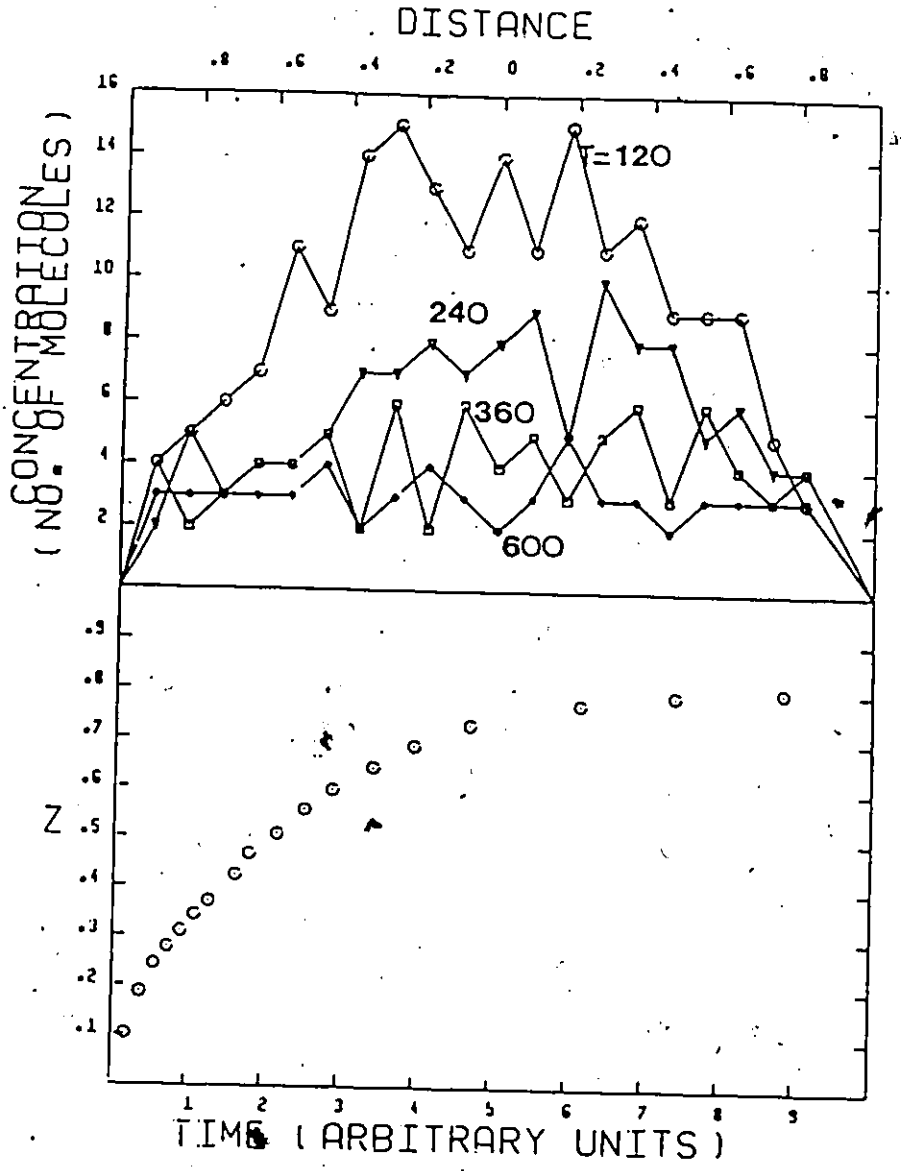

$$Z = 1 - (8/\pi^2)\ \mathrm{EXP}\ (-\pi^2 \tau/4) \qquad (\ 0.45 < Z < 1\ )$$

where $\tau = Dt/l^2$

A linear least squares fit was performed on the simulation rate data in the appropriate ranges of Z with Eqn. 5.12. In the adsorption case, the correlation coefficients for the short and long time intervals were calculated to be 0.986 and 0.976, whereas in the desorption case, the corresponding correlation coefficients were found to be 0.982 and 0.925, respectively. This suggests that the random walk model does approximate a Fick's law type of diffusion for the single component case.

The influence of the individual parameter on the sorption rate was investigated next. As mentioned earlier, the critical moving factor for adsorption/desorption, $CB/CA_{\tau=1}$ may be related to the activation barrier for diffusion; a high value of the critical moving factor represents a high barrier. Fig. 5.10 shows the effects of increasing the magnitude of CA; the concentration profiles were all determined at equal time, T=600. For CA = 300, it can be seen that most of the outer cells have already been saturated,, and the inner cells were also close to saturation. When CA is increased to 900, a much sharper profile resulted; the center cell is now completely devoid of any adsorbate molecules indicating the difficulty experienced by the inwardly migrating adsorbate molecules when the barrier is raised. Similar observations are made for the desorption case. As is shown in Fig. 5.11, at a low value of CB, CB= 300, most of the B molecules have already desorbed by T=600. But when CB is increased to 900, the majority of the presorbed molecules remained in the pore. The influences of this particular parameter on sorption rates can best be seen in the

FIG 5.10 SINGLE COMPONENT ADSORPTION, EFFECT OF THE CRITICAL MOVING FACTOR, CA

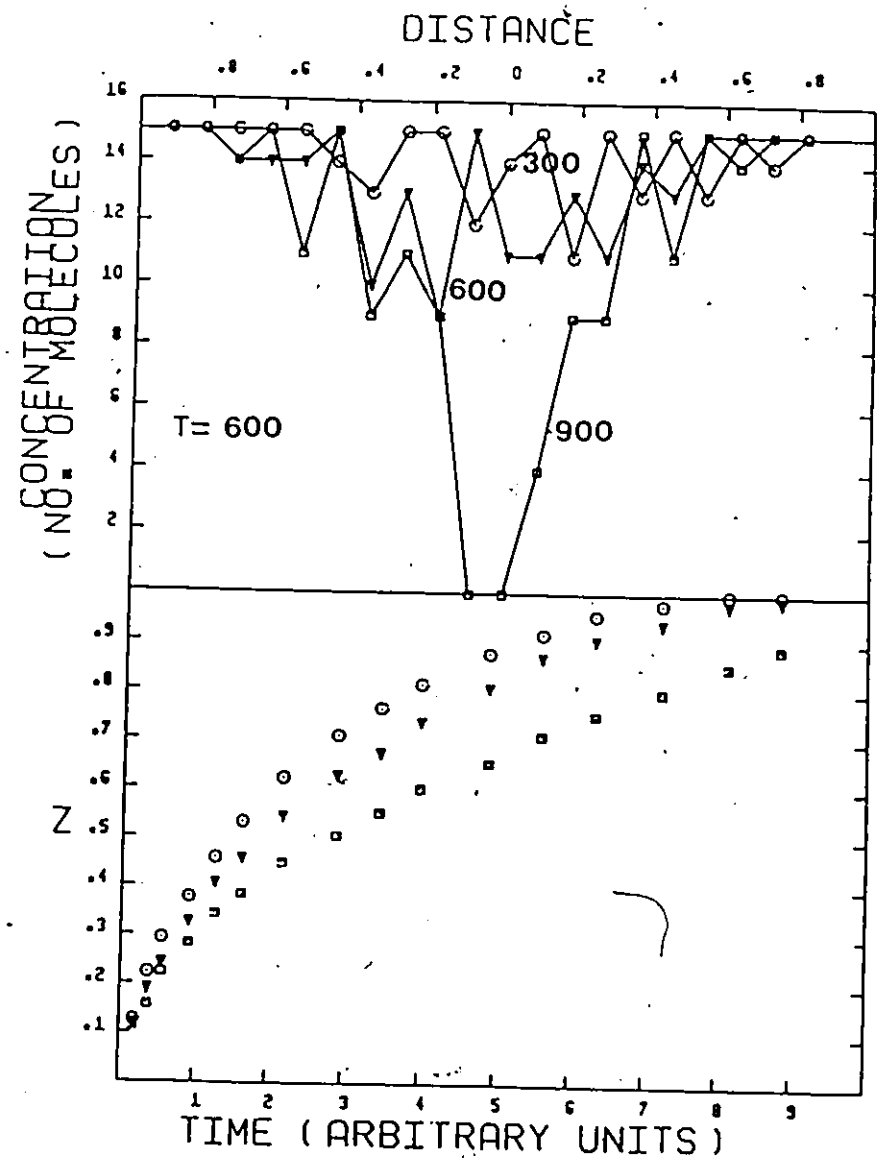

FIG 5.11 SINGLE COMPONENT DESORPTION, EFFECT OF THE CRITICAL MOVING FACTOR,- CB

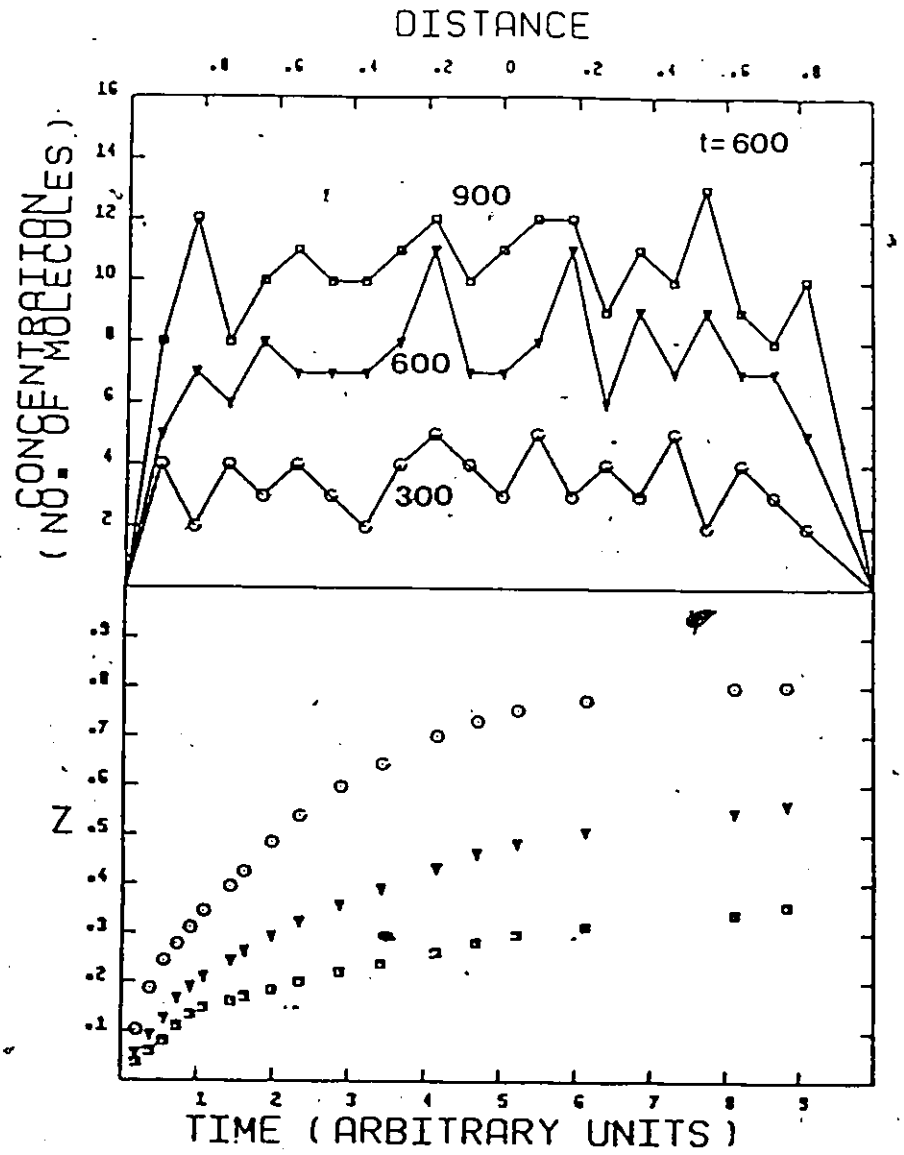

corresponding equilibrium uptake with time curves, Figs. 5.10 and 5.11; in both cases, increasing the value of the critical moving factor lowers the diffusion rate and causing a slower approach to equilibrium.

In most of the simulation experiments studied in this work, the conducting pore channel was divided into 20 equal segments, with each cell representing an individual zeolite cavity. The compartmental size, N, is therefore related to the length of the diffusion path or crystallite size. i.e., increasing the value of N corresponds to the lengthening of the diffusion path in which a particular molecule must travel. The influence of this parameter on sorption rates can be observed in Figs. 5.12 and 5.13: At equal time, T=600, the adsorption case shows that increasing N from 20 to 80 resulted in a much sharper profile with most of the interior cells empty. This is a direct consequence of not having sufficient time for the molecules to travel into the interior. Similar comments can be given to the desorption case, where at N=20, the concentration at the center can be observed to be reduced significantly from its initial level, whereas at N=80, most of the interior cells remained at a high concentration level. Increasing the values of N also has the beneficial result of smoothing out the profile curves; it removes the fluctuations typically encountered when N is small. In order to truly represent the random walk model to a real zeolite particle, however, the compartmental size N may have to be increased many more times; if fact, a real zeolite 4A particle with 1 micron size has a total of 3400 internal cavities. But the cost of running such computer program would become prohibitively expensive.

The simultaneous adsorption and desorption of molecules B and A was investigated next. In this case, the interior cells were first loaded to a

FIG 5.12 SINGLE COMPONENT ADSORPTION, EFFECT OF THE COMPARTMENTAL SIZE, N

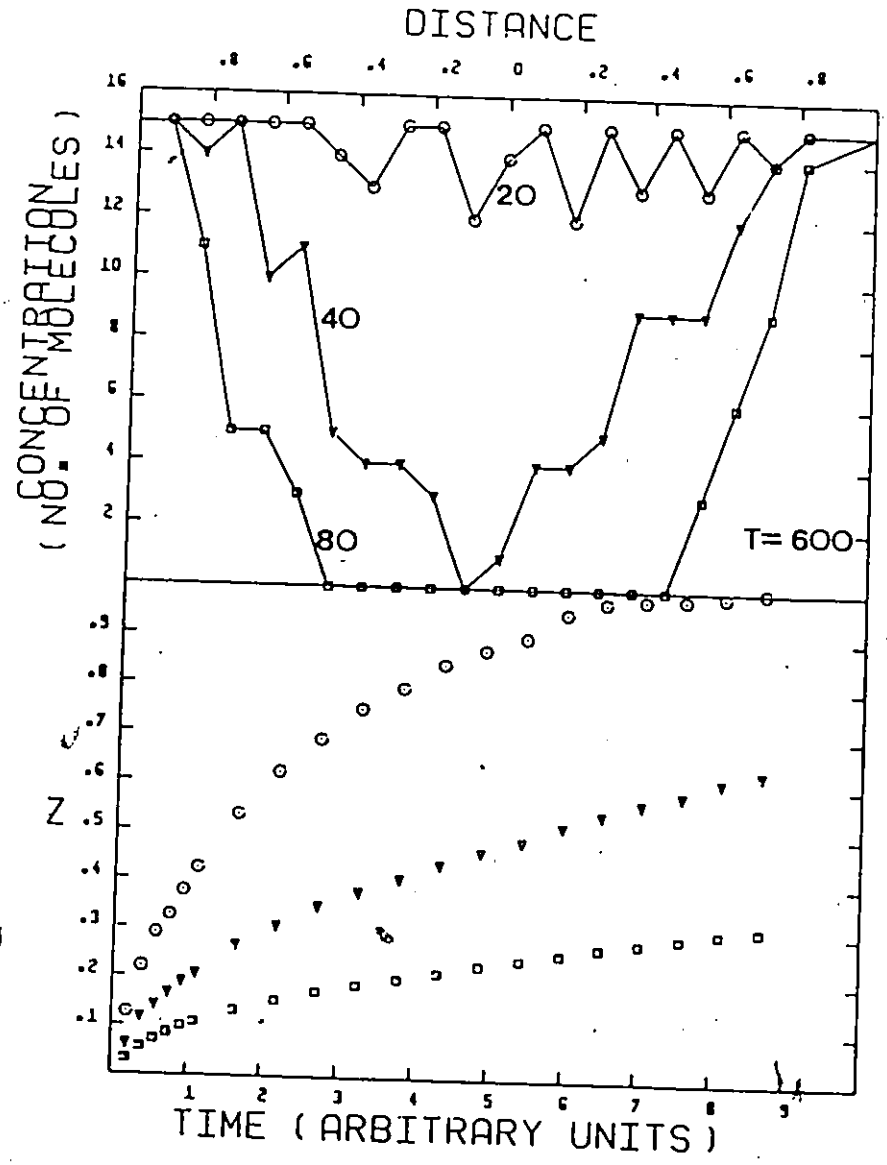

FIG 5.13 SINGLE COMPONENT DESORPTION, EFFECT OF THE COMPARTMENTAL SIZE, N

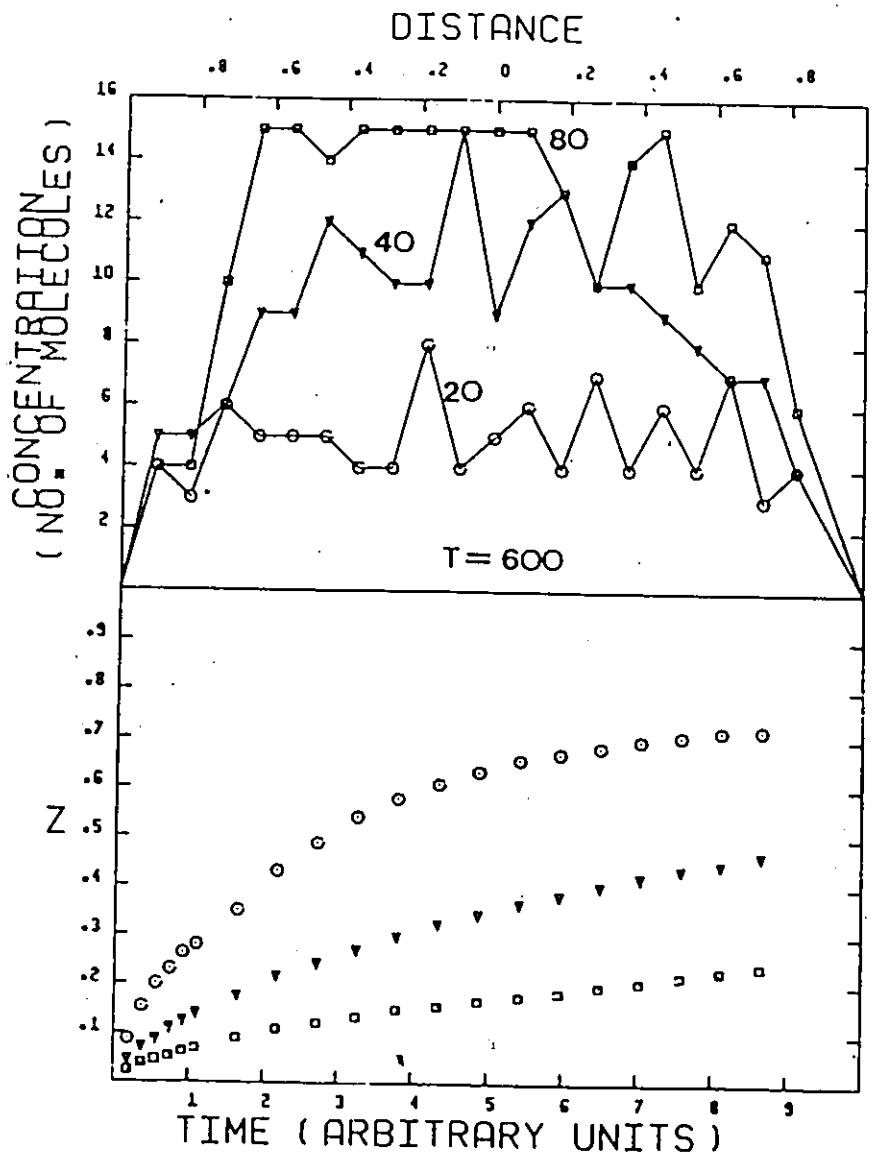

uniform coverage with species A. The exterior cells, cell (1) and cell(22), contained a fixed number of B molecules. Thus the desorption of A takes place concurrently with the adsorption of B. We designate molecule A as the counter desorbate and molecule B, the counter adsorbate. The major parameter of interest is the potential tranfer factor, F, which measures the degree of the moving potential transfer from one species to another, and thus accounts for the adsorbate/desorbate interaction.

The uptake rate curves for the counter adsorption and desorption are shown in Fig. 5.14, along with the single component rate curves for comparison. The counter adsorption rate curve lies consistently below the single component adsorption curve thus indicating a retardation of the adsorption rate of molecule B in the presence of molecule A. Conversely, the counter desorption rate curve lies consistently above the single component desorption curve and thus pointing to the enhancement of the desorption rate of molecule A by molecule B. The value of F is 0.2 in this particular case, which implies that whenever a molecule B encounters a molecule A, 20% of the moving potential is transferred from B to A.

In our binary component simulation stdies, we have also tried cases where the potential transfer factor was elliminated by setting its value to zero. The results show no significant divergence between the single and binary component retes in either the adsorption or desorption case. This suggests that the potential transfer is the major parameter in providing adsorbate/desorbate interaction.

Direct comparison of the adsorption/desorption rates of the single and binary system at different values of F were made by plotting the respective uptake curves against each other. First, from the adsorption

FIG 5.14 EQUILIBRIUM UPTAKES OF SORBATE MOLECULES IN SINGLE AND BINARY SYSTEMS.

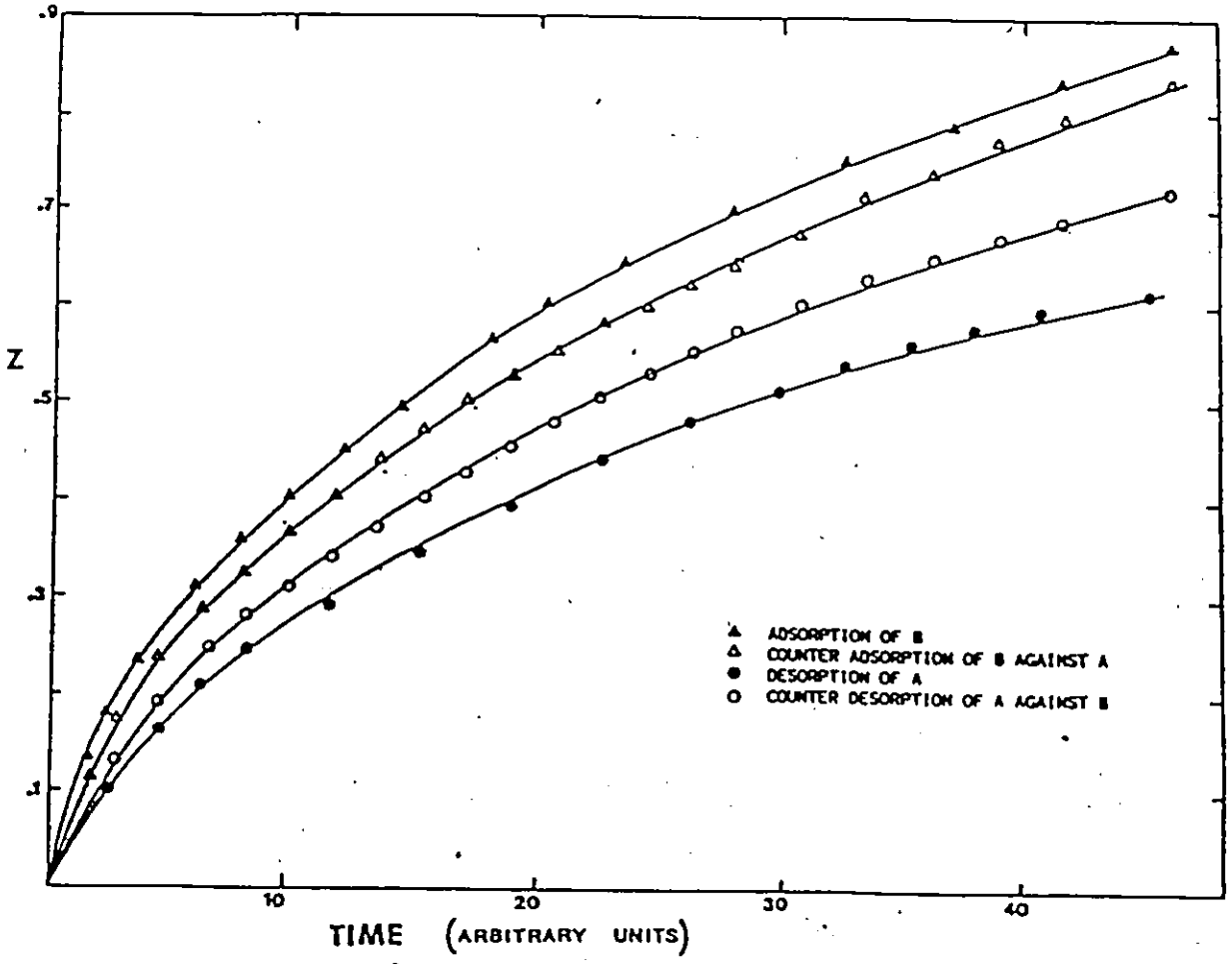

FIG 5.15 BINARY SORPTION SYSTEM, Z-ADSORPTION PLOT, EFFECT OF THE POTENTIAL TRANSFER FACTOR, F

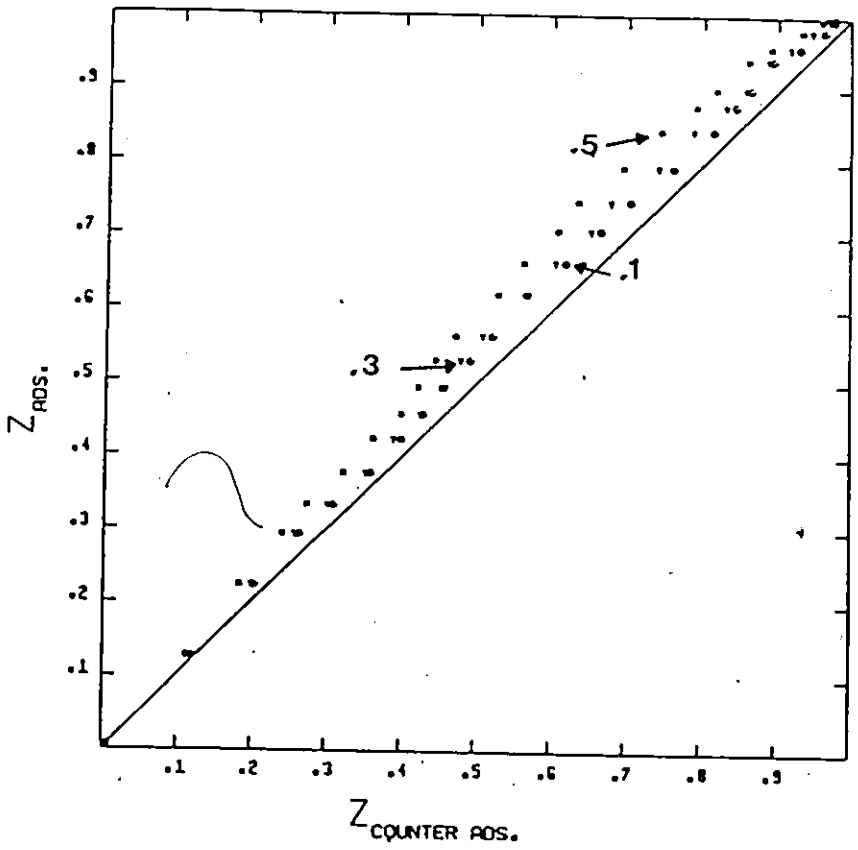

FIG 5.16 BINARY SORPTION SYSTEM, Z-DESORPTION PLOT, EFFECT OF THE POTENTIAL TRANSFER FACTOR, F

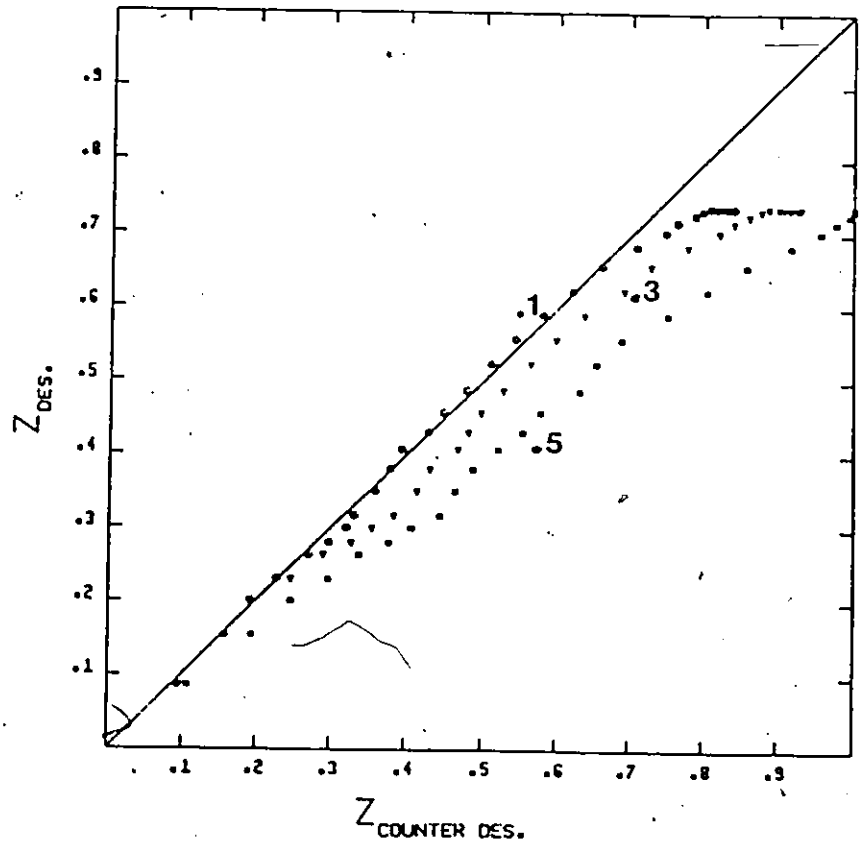

point of view, the effect of transferring the moving potential is shown to slow down the counter adsorbate rate causing in the Z-adsorption curve to lie above the diagonal reference line, Fig. 5.15. Increasing the value of F, i.e. increasing the probability or the percentage of potential transfer, resulted in the further slowing down of the adsorption rate shown by the greater distance away from the 45° line. From the desorption point of view, the opposite trend is observed, Fig. 5.16 shows the Z-desorption curve to deviate into the opposite direction and thus indicating the enhancement of the desorption rate. The degree of desorption rate enhancement increases further with increasing values of F. These results of the model simulation studies agree qualitatively to our experimental observations. Therefore, the random walk model indicates that the retardation and enhancement of the respective adsorption and desorption rates in the binary system may have been the consequences of the moving potential transfer, which lends support to the theory that in the narrow zeolite pore channels, molecular collisions between adsorbate/desorbate may occur, and the subsequent momentum transfer from one species to another may be responsible for the observed rate effects.

The last case studied investigates the influence of the overall loading factor, LF, on the binary system. The values of the other paramenter were kept the same as in the previous case except that LF was set to equal to the maximum loading factor for each individual species, i.e. LF=AM=BM=15. The lowering of LF in effect represents a narrowing of the pore size. Results of this simulation are shown in Fig 5.17. At T=120, it can be observed that the concentration of A at the exterior cells drops to zero quite rapidly, but the concentration in the interior cells remains at the initial

FIG 5.17 BINARY SORPTION SYSTEM, EFFECT OF TRAPPING

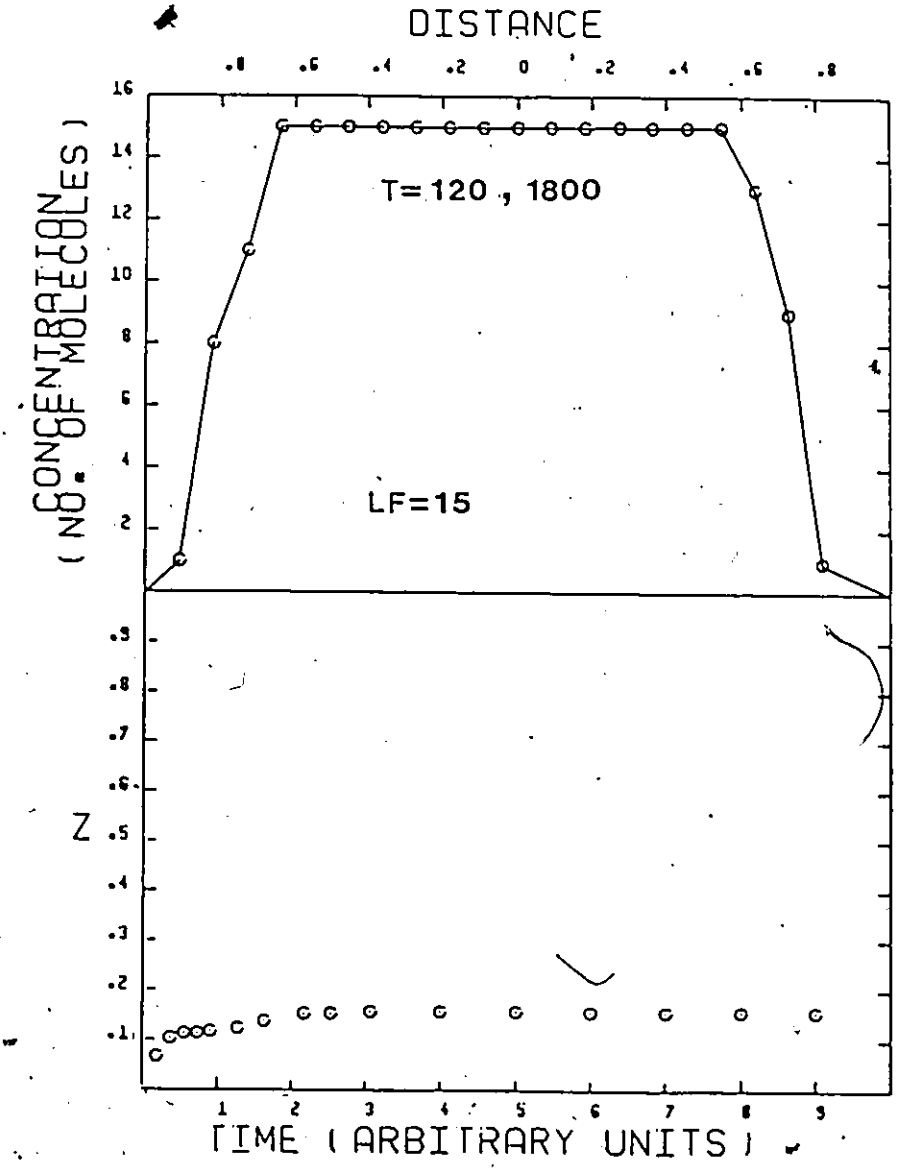

saturation level. This is caused by molecule B, diffusing inwardly, rapidly saturating the exterior cells and consequently, it becomes increasingly difficult for A to diffuse out since A is blocked from exiting by B. In fact, the concentration profile remained constant with progressive time increments; at T=1800, the same profile is observed, which indicates the trapping of molecule A. The phenomenon of trapping however can be removed by increasing the value of LF, for example, at LF=20, all of the presorbed molecules A desorbed.

In summary, the results of the simulation studies performed on the random walk model shows that the model has the capacity to produce many of the pertinent features observed in our experimental findings: In the single component sorption case, it can adequately represent a Fick's law type of diffusion. In the binary sorption system, it qualitatively indicates that the potential or momentum transfer may be reponsible for the observed rate effect. Also, the trapping of molecules in the binary system, could have been the result of the narrowness of the conducting pore size.

CHAPTER VI

CONCLUSION

The diffusion rates of sorbate molecules in zeolites depend on the physical and chemical nature of the sorbent as well as the sorbate molecules. Zeolitic diffusion rate has a high directional dependancy; adsorption usually has the larger rate while the desorption rate is much smaller. In small port zeolites, such as the 4A, the anionic framework plays an important role in determining the diffusion rates and molecules with a small cross-sectional area exhibit the highest rate. On the other hand, in large port zeolites, for example, mordenites, the physical properties become less of a factor and the chemical and electronic properties of the diffusant may gain increasing importance in determining the diffusion rate; molecules that are capable of strong interaction with the cations, such as CO_2 and C_2H_4 with the respective quadrupole moment and Π electrons, have a smaller rate.

For a given molecule, the diffusion rate increases with the increase in pore aperture size.

Diffusion rate of a given molecule differs considerably depending on whether it is involved in a single or binary system. Single component rate measurement can not be used to predict the kinetics of the binary system. Counter-adsorption rate of a molecular species is usually smaller than its corresponding single component adsorption rate into a pre-evacuated zeolite. Conversely, the counter-desorption rates are usually larger than the desorption rate in helium. The respective rate retardation and enhancement effect could have been the result of the molecular collision between adsorbate/desorbate and the subsequent momentum transfer from one

species to another.

In binary sorption systems, trapping of the preadsorbed molecule may occur if the pore aperture size relative to the sum total of the adsorbate/desorbate size becomes too small. Trapping, however, is not a permanent process and the amount can be recovered through desorption in inert helium.

The successful correlation between the two-dimensional virial equation and the experimental isotherms gives evidence that the physical state of the sorbed gas could be viewed as a two-dimensional gas. The first virial constant, ln K, confirms that molecules with 11 electrons and a quadrupole moment have strong interactions with the zeolitic electrostatic field. In terms of the sorbate-sorbate molecular interaction, the second virial constant shows it to be of a repulsive nature, which could result from the strong zeolite-sorbate interaction.

The novel random walk kinetic model developed for diffusion in zeolites shows promising signs for it produces many of the pertinent features observed in the experimental studies. Much work remains to be done to refine this model; in particular, the correlations between program factors and the real physical properties need to be established. Nonetheless, the model qualitatively suggests the observed binary rate effects to be the result of the moving potential transfer, which lends support to the momentum transfer theory. Also, it suggests the trapping of the preadsorbed molecules is the result of the narrowness of the conducting pores.

BIBLIOGRAPHY

1. Anderson, R.B., Kindl, B., and Eagan, J.D., AIChE. Sympos. Ser., 69, 39 (1973)

2. Argaver, R.J., and Landolt, G.R., US Patent 3,702,886 (1972)

3. Barrer, R.M., J. Soc. Chem. Ind., 04, 130 (1945)

4. Barrer, R.M., "Zeolite and Clay Minerals as Sorbents and Molecular Sieves", Academic Press, 1978

5. Barrer, R.M., Trans. Faraday. Soc., 40, 555 (1944)

6. Barrer, R.M., and Ibbitson, D., Trans. Faraday Soc., 40, 195 and 206 (1944)

7. Barrer, R.M., and Lee, J.A., Surface Sci., 12, 354 (1968)

8. Barrer, R.M., J. Colloid and Interface Sci., 21, 415 (1966)

9. Barrer, R.M., and Murphy, E.V.T., J. Chem. Soc. (A), 2506 (1970)

10. Brandt, W.W., and Rudloff, W., J. Phys. Chem. Solids, 26, 741 (1965)

11. Breck, D.W., J. Amer. Chem. Soc., 78, 5663 (1965)

12. Breck, D.W., "Zeolite Molecular Sieves", Wiley Inter-Science, (1974)

13. Carter, J.W., and Husain, H., Trans. Instr. Chem. Engrs., 50, 69 (1972)

14. Chan, Y.C., M.Eng. Thesis., McMaster University, Hamilton (1976)

15. Crank, J., "The Mathematics of Diffusion", Oxford (1954)

16. Damour, A., Ann. Mines., 17, 191 (1840)

17. Eagan, J.D., Ph.D. Thesis, McMaster University, Hamilton (1972)

18. Eagan, J.D., Kindl, B., and Anderson, R.B., Adv. Chem. Ser., 102, 164 (1971)

19. Eagan, J.D., and Anderson, R.B., J. Colloid and Interface Sci., 50, 419 (1975)

20. Eberley, P.E. Jr., Ind. Eng. Chem. Fundam., 8(1), 25 (1969)

21. Fuller, E.N., Schettler, P.D., and Giddings, J.C., Ind. Eng. Chem., 58, (5) 18; (8) 81 (1966)

22. Garg, D.R., and Ruthven, D.M., Chem. Eng. Sci., 27, 417 (1972)

23. Grandjean, F., Compt. Rendv., 149, 866 (1909)

24. Habgood, H.W., Can. J. Chem., 36, 1384 (1958)

25. Hedge, J.A., Adv. Chem. Ser., 102, 239 (1971)

26. Karger, J., and Bulow, M., Chem. Eng. Sci., 30, 893 (1975)

27. Karge, H.G., and Klose, K., Ber. Buns. Gesell., 78, 1263 (1974)

28. Kiselev, A.V., Adv. Chem. Ser., 102, 40 (1971)

29. Kondis, E.F., and Dranoff, J.S., Adv. Chem. Ser. 102, 181 (1971)

30. Kondis, E.F., and Dranoff, J.S., AIChE Sympos. Ser., 67, 25 (1972)

31. Kumar, J.D., Duncan, R.C., and Ruthven, D.M., Can. J. Chem. Eng., 60, 493 (1982)

32. Lee, H., Adv. Chem. Ser., 121, 314 (1973)

33. Loughlin, K.F., and Ruthven, D.M., Chem. Eng. Sci., 27, 1401 (1972)

34. Ma, Y.H., and Lee, T.Y., AIChE J., 22, 149 (1976)

35. Ma, Y.H., and Roux, A.J., AIChE J. 19, 1055 (1973)

36. Meier, W.M., Z. Kristallogr., 115, 439 (1961)

37. Minachev, K.M., and Isokov, Y.I., Adv. Chem. Ser., 121, 451 (1973)

38. Mobil Co., Netherland Patent 7,014,807 (1971)

39. Moore, R.M., and Katzer, J.R., AIChE J., 18, 816 (1972)

40. Nelson, E.T., and Walker, D.L., J. Appl. Chem., 11, 358 (1961)

41. Riekert, L., AIChE J., 17, 446 (1971)

42. Round, G.F., Habgood, H.W., and Newton, R., Separation Science., 1 (2 and 3), 219 (1966)

43. Ruthven, D.M., and Kumar, R., Can. J. Chem. Eng., 57, 342 (1979)

44. Ruthven, D.M., Lee, L.K., and Yucel, H., AIChE J., 26, 16 (1980)

45. Ruthven, D.M., Derrah, R.H., and Loughlin, K.F., Can. J. Chem., 51, 3514 (1973)

46. Sand, L.B., "Molecular Sieve", Soc. Chem. Ind., London, pp 71 (1968)

47. Satterfield, C.N., and Cheng, C.S., AIChE J., 18, 724 (1972)

48. Satterfield, C.N., Katzer, J.R., and Vieth, W.R., Ind. Eng. Chem. Fundam., 10, 478 (1971)

49. Satterfield, C.N., and Frabetti, A.J., AIChE J., 13, 731 (1967)

50. Satterfield, C.N., and Katzer, J.R., Adv. Chem. Ser., 102, 193 (1971)

51. Shah, D.B., and Ruthven, D.M., AIChE J., 23, 804 (1977)

52. Sheth, A.C., and Dranoff, J.S., AIChE Sympos. Ser., 69, 76 (1973)

53. Thomas, C.L., and Barmby, D.S., J. Catal., 12, 341, (1968)

54. Thompson, J.K., and Resing, H.A., J. Colloid and Interface Sci., 26 279 (1968)

55. Weigel, O., and Steinhoff., Z. Kristallogr., 61, 125 (1925)

56. Yucel, H., Ph.D. Thesis,Univ. New Brunswick, Fredricton (1979)

57. Yucel, H., and Ruthven, D.M., J. Colloid and Interface Sci., 74, 186 (1980)

APPENDIX A-1

GLASS VOLUME MEASUREMENTS IN VOLUMETRIC APPARATUS

Appendix A-1.1 Determination of Void Volume.

The void volume is the volume of the capillary tubing of the apparatus (referring to Fig.3.3) to the right of S_1, below S_2 and at the zero marks of the calibrated bulbs and mercury manometer. The glass bulbs were maintained at 32°C by circulating thermostatted water. Keeping S_1 closed, helium was admitted via S_2 which was then closed.

The total volume of He (V) is given by

$$V = V_V + V_B \tag{1}$$

where V_B = Volume of the calibrated bulbs at temp. T_B

V_V = Void volume at temp. T_R (Room temperature)

The number of moles of He present is

$$n_T = n_B + n_V$$

$$= \frac{PV_B}{RT_B} + \frac{PV_V}{RT_R}$$

$$= \frac{P}{R}\left(\frac{V_B}{T_B} + \frac{V_V}{T_R}\right) \tag{2}$$

Rearranging Eqn. (2) gives

$$PV_B = -P(T_B/T_R)V_V + n_T R T_B \tag{3}$$

Fig A-I.1 Helium Void Space Plot

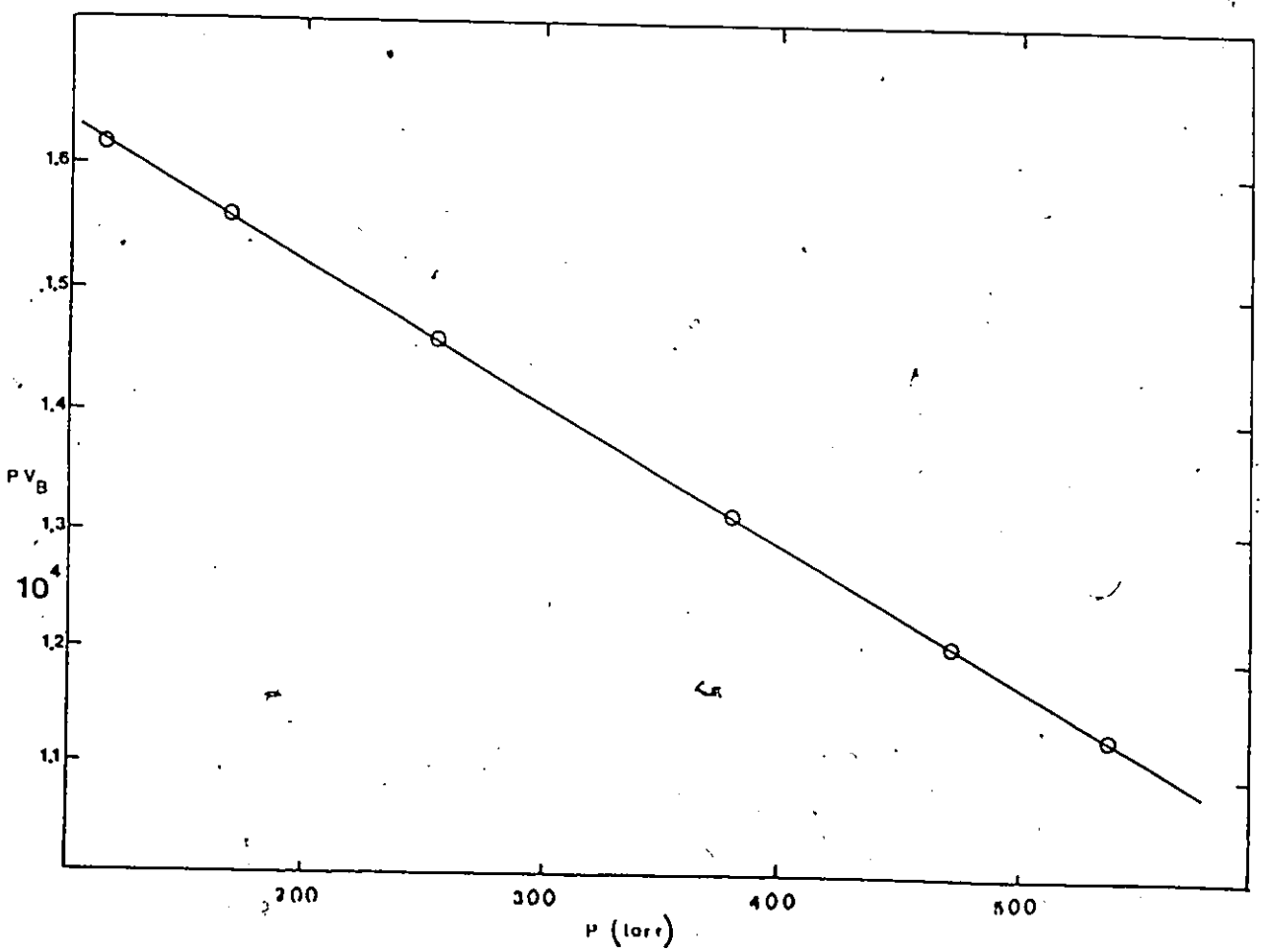

which is a straight line of the form

$$PV_B = -mp + b \qquad (4)$$

A series of P, V_B readings were recorded keeping S_2 closed. A plot of PV_B versus P is linear with a slope equal to $-(T_B/T_R)V_V$, Fig. A-1.1, where T_R is an average overall reading. The void volume, V_V = 11.565 cc, was used in calculating the volumetric data for all gases used.

Appendix A-1.2 Determination of Dead Space Factor

The Dead Space Factor (F) is defined as the volume of gas in cc (STP) per unit pressure to the left of S_1, but not adsorbed on the sample. The value of F is determined at a series of bath temperatures as follows:

(1) Keeping S_1 closed, He is admitted into the system via S_2. The inlet volume (V_I) in cc (STP) is

$$V_I = V_V + V_B \qquad (1)$$

where V_V = 11.565 cc converted to STP

V_B = Bulb volume (cc(STP)) at temperature T_B

(2) S_1 is then opened and a series of P, V_B readings are taken to calculate V_R, which is the volume remaining to the right of S_2. The Dead Space Factor is given by

$$F = (V_I - V_R)/P \qquad (2)$$

Re-arranging Eqn. (2) gives

$$V_R = V_I - FP \qquad (3)$$

A graph of V_R versus P is linear with the slope = -F.

Let V_1 be the volume to the left of S_1 at room temperature, and $V_2 = V_0 + aT$ be the volume at the bath temperature, where V_0 is a constant and a is the coefficient of thermal expansion of glass (assumed constant over the range of T studied), then

$$F = \frac{V_1(273)}{(760)T_R} + \frac{(V_0 + aT)(273)}{(760)\ T} \qquad (4)$$

or $$F = A + B/T \qquad (5)$$

Where $A = (273/760)(V_1/T_R + a)$ and $B = (273\ V_0)/760$, both are constants. Thus, plotting F against 1/T will give a straight line and the plots of F, determined at a series of sample bath temperatures, against 1/T, for zeolites 4A, Na-mordenite and H-mordenite, are shown in Fig. A-1.2.

Fig A-1.2 Temperature Dependence of Dead Space Factor

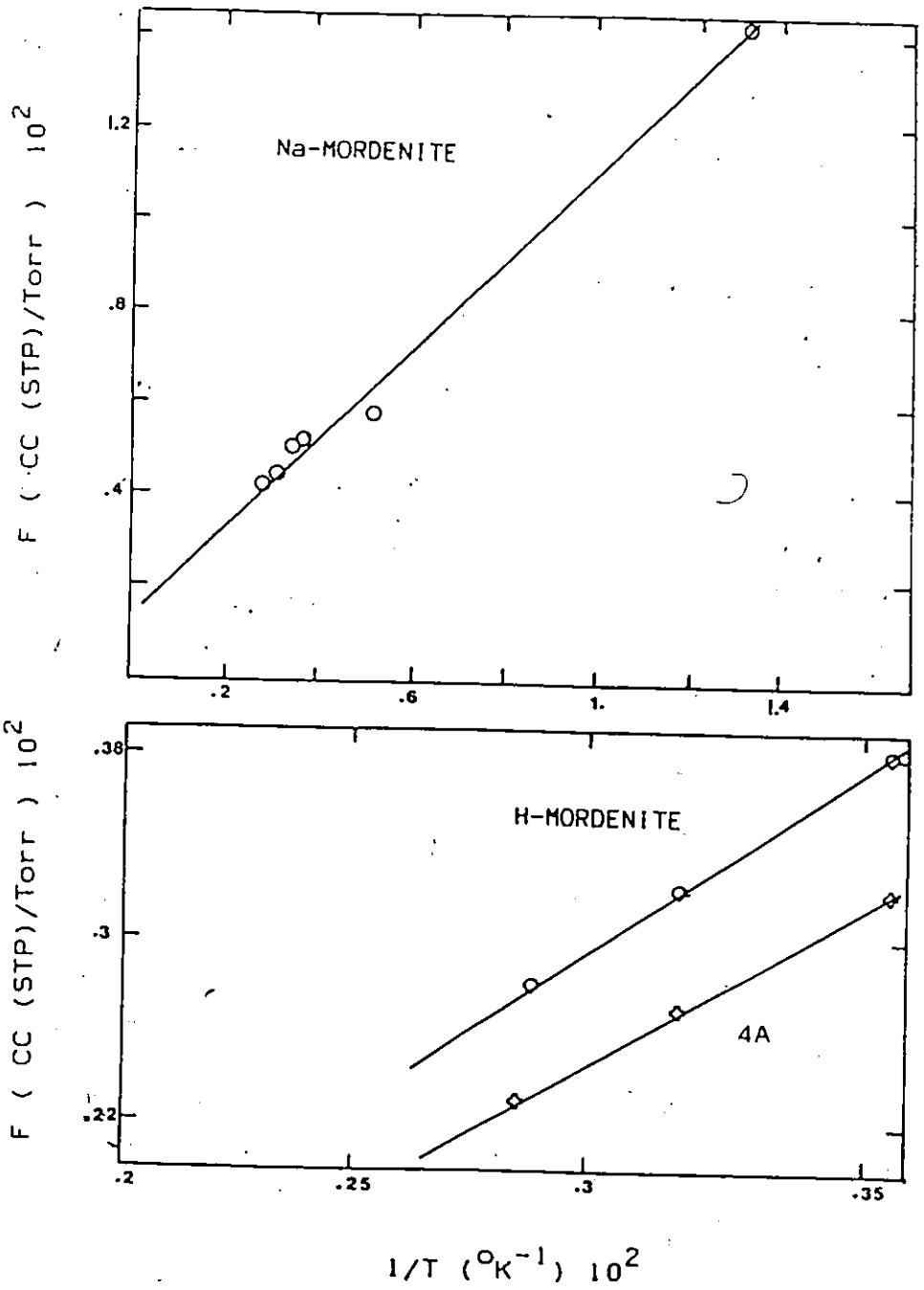

APPENDIX A-2

TWO-DIMENSIONAL VIRIAL EQUATION

Due to the narrow zeolite pore dimension, adsorbed molecules do not have the chance to pile up in more than one monolayer. Accordingly, conceptually, one can view the adsorbed phase to be a two-dimensional gas.

The two-dimensional form of the Virial equation for non-ideal gas is

$$\pi = RT \left(\frac{1}{A-\sigma} + \frac{\beta}{(A-\sigma)^2} + \frac{\gamma}{(A-\sigma)^3} + ...\right) \qquad (1)$$

where π is the spreading pressure, A is the surface area available to a molecule and, σ is the area per molecule in a close-packed arrangement.

At equilibrium the change in the free energy of the adsorbed two-dimensional gas is equal to the change in the free energy of the surrounding gas. Thus, the Gibbs equilibrium relationship should hold;

$$A\, d\pi = RT\, d\, \ell n\, P \qquad (2)$$

Differentiating Eqn.(1) and substituting into Eqn.(2) gives

$$(1/\theta)(1 + 2\beta(X/\sigma) + 3\gamma(X/\sigma)^2 + ...)\, dX = d\, \ell n\, P \qquad (3)$$

where $X = \theta/1-\theta$ with $\theta = \sigma/A$, the fractional coverage.

Re-arranging Eqn.(3) gives

$$((1+X)/X)\ (1+2\beta(X/\sigma) + 3\gamma(X/\sigma)^2 + \ldots)dX = d\ \ell n\ P \qquad (4)$$

Integrating Eqn.(4) gives

$$\ell n(P/X)-X = \ell n\ K + (\beta/\sigma)X\ (2+X) + (\gamma/\sigma^2)X^2\ (1.5+X)+ \ldots \qquad (5)$$

where $\ell n\ K$ is an integration constant, which is inversely proportional to the Henry's law constant since K approaches a limit of P/θ as θ approaches zero.

APPENDIX A-3

EQUATIONS FOR DESCRIBING DIFFUSION IN ZEOLITES

Appendix A-3.1 Fick's Law

Fick's second law of diffusion has often been used to interpret kinetic data for diffusion controlled processes. If the desorption of gas in zeolites is diffusion controlled, then Fick's law may be adequate to describe the sorption process.

Consider a spherical particle with radius "a". Assuming uniform initial concentration throughout the particle, and constant diffusivity "D". The solution of Fick's law of diffusion (15)

$$\frac{\partial c}{\partial t} = D \text{ div grad } c \qquad (1)$$

with boundary conditions,

$$c = c_\infty \text{ at } r = a \text{ for } t > 0$$

$$c = c_0 \text{ for } 0 \leq r < a \text{ at } t = 0$$

where r = distance from center of the sphere

c = concentration of sorbed phase.

Expressing in terms of fractional approach to equilibrium is

$$Z = 1 - \left(\frac{6}{\pi^2}\right) \sum_{n=1}^{\infty} \frac{1}{n^2} \exp\left(-\tau n^2 \pi^2\right) \qquad (2)$$

where n is an integer, and

$$Z = \frac{Q_t - Q_0}{Q_\infty - Q_0}$$

An alternative solution is

$$Z = 6(\tau)^{\frac{1}{2}} \left[\pi^{-\frac{1}{2}} + 2 \sum_{n=1}^{\infty} \text{ierf}\,(\frac{n}{\tau^{\frac{1}{2}}})\right] - 3\tau \qquad (3)$$

Eqn. (2) converges well for long time so that for $\tau > 0.16$, or $Z > 0.87$

$$Z = 1 - (\frac{6}{\pi^2}) \exp(-\pi^2\tau) \qquad (4)$$

Also, Eqn. (3) converges well for small time because for $\tau < 0.16$, the series $\sum_{n=1}^{\infty} \text{ierf}\,(n\tau^{-\frac{1}{2}})$ is zero. Thus, for $\tau < 0.16$ or $Z < 0.87$

$$Z = 6(\frac{\tau}{\pi})^{\frac{1}{2}} - 3\tau \qquad (5)$$

By completing the square, Eqn. (5) can be rearranged to give

$$(\pi\tau)^{\frac{1}{2}} = 1 \pm (1 - \pi Z/3)^{\frac{1}{2}} \qquad (6)$$

Similarly, the solution for infinite platelet (15) is

$$Z = 1 - \frac{8}{\pi^2} \sum_{n=1}^{\infty} (\frac{1}{(2n-1)^2}) \exp(-\frac{(2n-1)^2\pi^2\tau}{4}) \qquad (7)$$

$$Z = 2\,(\tau/\pi)^{\frac{1}{2}} \qquad 0 \leq Z < 0.45 \qquad (8)$$

$$Z = 1 - (\frac{8}{\pi^2}) \exp(-\frac{\pi^2\tau}{4}) \qquad 0.45 \leq Z < 1.0 \qquad (9)$$

The solution for a cube is obtained from the corresponding platelet solution using the relation

$$(1 - Z_{\text{cube}}) = (1 - Z_{\text{platelet}})^3$$

This result is based on treatment of an analogous heat conduction prob-

lem in which the solution in three dimensions is obtained from the product of three solutions in one dimension.

Therefore, the solution for a cube is

$$Z = 1 - \frac{512}{\pi^6}\left[\sum_{n=1}^{\infty}\left(\frac{1}{(2n-1)^2}\right)\exp\left(-\frac{(2n-1)\pi^2\tau}{4}\right)\right] \qquad (10)$$

$$Z = \left(\frac{6}{\pi^{1/2}}\right)\tau^{1/2} - \left(\frac{12}{\pi}\right)\tau + \left(\left(\frac{2}{\pi^{1/2}}\right)\tau^{1/2}\right)^3 \qquad 0 \leq Z < 0.83 \qquad (11)$$

$$Z = 1 - \left(\frac{512}{\pi^6}\right)\exp\left(-\frac{3\pi^2\tau}{4}\right) \qquad 0.83 \leq Z < 1.0 \qquad (12)$$

In equations (2) through (12) $\tau = Dt/a^2$

where "D" is the apparent diffusivity, "t" is the time, and "a" is the radius, half-thickness and half edge of the respective sphere, platelet and cube.

Appendix A-3.2. Particle Size Distribution

The solutions of Fick's law all showed dependence on "a". Hence, the application of these equations is only legitimate if all zeolite particles are of the same size in any given batch of sample. In reality, crystal size variation is often considerable and its effect on the rate curve can be dramatic. Therefore, the measurement of the particle size distribution is important.

Mathematically, we can incorporate the size distribution into the rate expression in the following way. The average approach to

equilibrium can be expressed as

$$\bar{Z} = f(D,t) = \int_{-\infty}^{+\infty} f(a)\, Z(D,t)\, d\, \ell n\, a \qquad (13)$$

where $f(a)$ = probability distribution function in terms of weight of the particle size. For small particles, $f(a)$ would be a log-normal distribution function, i.e.

$$f(a) = \frac{1}{\sqrt{2\pi}\, \ell n\, \sigma} \exp\left(-\left(\frac{\ell n(\frac{a}{\bar{a}})}{\sqrt{2}\, \ell n\, \sigma}\right)^2\right) \qquad (14)$$

$f(a)\, d\, (\ell n\, a)$ = wt. fraction of particles with sizes between a and a exp $(d\, \ell n\, a)$, and

$\bar{a}$ = wt. average particle size.

σ = $\dfrac{\text{size below which 50 wt.\% of particles lie}}{\text{size below which 15.87 wt.\% of particles lie}}$

Hence, the larger the value of σ, the broader the size distribution and more markedly does a composite rate curve deviate from that for single particles (Fig. 4,5). Now let

$$x = \frac{\ell n\, (\frac{a}{\bar{a}})}{\sqrt{2}\, \ell n\, \sigma}$$

and $$dx = d\, \ell n\, a / \sqrt{2}\, \ell n\, \sigma\ .$$

Substituting x and dx into equation (14) we have

$$\bar{Z}\,(D,t) = \frac{1}{\sqrt{\pi}} \int_{-\infty}^{\infty} \exp(-x^2) \cdot Z(x,D,t)\, dx \qquad (14)$$

where $Z(x,D,t)$ is a function of the particle size via the definition of x, and its value is determined by the rate equation used.

The integration in equation (14) can be simplified by using the Gauss Hermite integration techniques, i.e.

$$\bar{Z}(D,t) = \frac{1}{\sqrt{\pi}} \sum_{i=1}^{N} P_i \, Z(x_i, D, t) \tag{15}$$

P_i's are tabulated weighting factors and the x_i's are roots of the Hermite polynomial of order N.

APPENDIX A-4 Computer Program Listing of Random Walk Model

```
      PROGRAM TST

C     THIS PROGRAM USES RANDOM NUMBER GENERATOR TO SIMULATE SORPTION
C     KINETICS IN ZEOLITES.

      DIMENSION AN(1001),BN(100)
      DIMENSION ZA(5000),ZB(5000)
      DIMENSION AT(1001),BT(100)

C     THE OBJECTIVE OF THIS SORPTION SIMULATION IS TO INVESTIGATE
C     THE EFFECT OF CRITICAL MOVING FACTOR FOR DESORBATE,A
C     ON THE CONCENTRATION PROFILE AND ALSO
C     THE APPROACH TO EQUILIBRIUM.

C     THIS IS THE CASE FOR BINARY SORPTION

C     TO EVALUATE THE EFFECT OF TRAPPING BY VARYING LF
C     TO EVALUATE THE EFFECT OF POTENTIAL TRANSFER, FACTOR

      INTEGER T
      INTEGER TQ
      INTEGER TP
      REAL LF
      INTEGER NR
      REAL R(2300)
      DOUBLE PRECISION CSEED
      OPEN(UNIT=5,FILE='INPUT')
      OPEN(UNIT=6,FILE='OUTPUT')

C     INITIALIZE ALL INTERIOR POINTS.
C     NUMBER OF PRE-SORBED SORBATES ARE IN AN.
C     INITIAL NUMBER OF SORBATES IS AI.
C     ADSORBATES ARE IN BN.
      IOPT=1

C     N IS THE TOTAL NUMBER OF NODAL POINTS INCLUDING THE
C     EXTERIOR POINTS OF BOTH SIDES EG FOR 20 COMPARTMENTS OR
C     CAVITIES.

      N=22


C     LF:LOADING FACTOR, WHICH IS THE MAXIMUM
C     NUMBER OF SORBATE PERMITTED IN A GIVEN COMPARTMENT
      LF=15.0

C     CRITICAL MOVING FACTOR FOR A,CA

      CA=200.0

C     CRITICAL MOVING FACTOR FOR B,CB

      CB=200.0

C     MAXIMUM NUMBER OF DESORBATE PER COMPARTMENT AM

      AM=15.0

C     MAXIMUM NUMBER OF ADSORBATE PER COMPARTMENT, BM.

      BM=15
      DO 300 KL=1,6
      READ(5,*) AI
      BB=100.0

C     FACTOR IS THE PROBABILITY OF POTENTIAL TRANSFER

      FACTOR=0.2
      BK=BL=AL=0.0
      T=0

C     TP IS THE PRINT OUT TIME.

      TP=60

C     MAXIMUM TIME ITERATION TO

      TQ=1900

      CSEED=123457.00
      NR=200
      DO 10 I=2,N-1
      AN(I)=AI
      BN(I)=0.0
   10 CONTINUE

C     BOUNDARY CONDITIONS
   25 AN(1)=AN(N)=0.0
      BN(1)=BN(N)=BB

C     FINDING RANDOM NUMBERS

      CALL GGUBFS(CSEED,NR,IOPT,R)
      DO 30 I=1,N
      AT(I)=AN(I)*R(I)+1.0
      BT(I)=BN(I)*R(I+100)*100.0
   30 CONTINUE

C     EVALUATE POTENTIAL TRANSFER

      DO 32 I=2,N-1
      AT(I)=AT(I)+FACTOR*BT(I)
      BT(I)=BT(I)-FACTOR*BT(I)
   32 CONTINUE

C     CHOOSE THE DIRECTION OF THE SEQUENCE

      START=2
      STOP=N-1
      INC=1
      IF(R(12).GT.R(16)) GO TO 40
      START=N-1
      STOP=2
      INC=-1
   40 DO 50 I=START,STOP,INC

C     COMPARING THE POTENTIAL OF ADSORBATES AND DESORBATES IN A
C     GIVEN COMPARTMENT.

      IF(BT(I).GT.AT(I)) GO TO 142

C     DECIDE WHETHER A CAN MOVE AGAINST THE CRITICAL
C     MOVING FACTOR CA.

      IF(AT(I).GT.CA) CALL A400(AN,AT,AM,BN,LF,I,N)

C     DECIDE WHETHER B CAN MOVE AGAINST THE CRITICAL MOVING FACTOR CB.

      IF(BT(I).GT.CB) CALL B500(BN,BT,BM,AN,LF,I,N)

      GO TO 50

C     B MOVES FIRST OWING TO A-HIGHER POTENTIAL
C     DECIDE WHETHER B CAN MOVE AGAINST CRITICAL MOVING CRITICAL
C     MOVING FACTOR CB

  142 IF(BT(I).GT.CB) CALL B500(BN,BT,BM,AN,LF,I,N)

C     DECIDE WHETHER A CAN MOVE AGAINST CRITICAL MOVING FACTOR CA

      IF(AT(I).GT.CA) CALL A400(AN,AT,AM,BN,LF,I,N)
   50 CONTINUE

C     AFTER MOVING ALL THE INTERIOR POINTS,CONSIDER
C     NOW THE BOUNDARIES.

      IF(BT(1).LT.CB) GO TO 160
      IF(BN(2)+AN(2).GE.LF.OR.BN(2).GE.BM) GO TO 150
      IF(BT(1).GT.BT(2)) THEN
      BN(2)=BN(2)+1.0
      BR=BR+1.0
      ENDIF
  160 IF(BT(N).LT.CB) GO TO 170
      IF(BN(N-1)+AN(N-1).GE.LF.OR.BN(N-1).GE.BM) GO TO 170
      IF(BT(N).GT.BT(N-1)) THEN
      BN(N-1)=BN(N-1)+1.0
      BL=BL+2.0
      ENDIF
  170 T=T+1

C     TOTAL UP THE NUMBER OF DESORBATE DESORBED

      AL=AL+AN(1)+AN(N)

C     CALCULATE THE APPROACH TO EQUILIBRIUM OF BOTH
C     DESORBATE A AND ADSORBATE B.
C     THERE ARE N-2 COMPARTMENTS.

      ZA(T)=AL*100.0/(FLOAT(N-2)*AI)
      ZB(T)=(BL+BR)*100.0/(FLOAT(N-2)*BM)

C     DATA PRESENTATION

      IF(ZA(T).GE.99.0.AND.ZB(T).GE.99.0) GO TO 90
```

```
      IF(NCOUT.TP).EQ.0.0) GO TO 730
      IOPT=0
      GO TO 25
C
C     PRINT OUT  THE CONCENTRATION PROFILE.
C
  700 PRINT*,'T=',T
      IF(N.LE.12) GO TO 82
      IF(N.EQ.22) GO TO 83
      IF(N.LE.34) GO TO 84
      IF(N.LE.46) GO TO 92
      IF(N.EQ.48) GO TO 94
   82 WRITE(6,85) (AN(I),I=1,N)
      WRITE(6,85) (BN(I),I=1,N)
   85 FORMAT(10X,22F5.2,3X)
      GO TO 89
   83 WRITE(6,86) (AN(I),I=1,N)
      WRITE(6,86) (BN(I),I=1,N)
   86 FORMAT(10X,22F5.2,3X)
      GO TO 89
   84 WRITE(6,87) (AN(I),I=1,N-1,2)
      WRITE(6,87) (BN(I),I=1,N-1,2)
   87 FORMAT(10X,21F5.2,3X)
      GO TO 89
   92 WRITE(6,93) (AN(I),I=1,N,2)
      WRITE(6,93) (BN(I),I=1,N,2)
      GO TO 89
   94 WRITE(6,93) (AN(I),I=2,N,4)
      WRITE(6,93) (BN(I),I=2,N,4)
   93 FORMAT(10X,21F5.2,3X)
   89 IF(T.GE.TO) GO TO 90
      IOPT=0
      GO TO 25
   90 WRITE(6,101)
      DO 95 J=1,TO/.05
      TAU=(CA/(AM*100))*FLOAT(J)
      WRITE(6,102) J,TAU,ZA(J),ZB(J)
   95 CONTINUE
  101 FORMAT(21X,34H ITP      TAU        ZA         ZB    /)
  102 FORMAT(20X,I4,3F10.4,/)
      PRINT*,'NUMBER OF TOTAL ZEOLITIC COMPARTMENT  N=',N
      PRINT*,'MAXIMUM TOTAL LOADING FACTOR FOR A GIVEN COMPARTMENT'
      PRINT*,'LF=',LF
      PRINT*,'MAXIMUM DESORBATE LOADING FACTOR   AM=',AM
      PRINT*,'MAXIMUM ADSORBATE LOADING FACTOR   BM=',BM


      PRINT*,'INITIAL DESORBATE CONCENTRATION AI=',AI
      PRINT*,'BOUNDARY CONDITION FOR ADSORBATE  B0=',B0
      PRINT*,'CRITICAL MOVING FACTOR FOR DESORBATE CA=',CA
      PRINT*,'CRITICAL MOVING FACTOR FOR ADSORBATE CB=',CB
      PRINT*,'PERCENTAGE OF POTENTIAL TRANSFER FACTOR=',FACTOR
  800 CONTINUE
      STOP
      END
```

```
      SUBROUTINE ADSORB(AN,AT,AM,BM,LF,I,N)
      DIMENSION AN(*),AT(*),BN(*)
      REAL LF
      INTEGER N
C
C     A MOVES CONSIDER WHETHER THERE IS ANY SORBATE TO BE MOVED.
C
      IF(AN(I).EQ.0.0) GO TO 499
      IF(I.EQ.2) THEN
      TL=0.0
      TR=AN(I+1)+BN(I+1)
      GO TO 407
      ENDIF
      IF(I.EQ.N-1) THEN
      TL=AN(I-1)+BN(I-1)
      TR=0.0
      GO TO 407
      ENDIF
C
C     SAFETY MARKER
C
      IF(I.EQ.1.OR.I.EQ.N) GO TO 499
C
C     ADDING UP ALL THE SORBATES IN A GIVEN COMPARTMENT ON
C     EITHER SIDE FOR BOTH A AND B.
C
      TL=AN(I-1)+BN(I-1)
      TR=AN(I+1)+BN(I+1)
C
C     LF IS THE UPPER LOADING FACTOR PER COMPARTMENT
C     CHECK IF THE ADJACENT COMPARTMENT HAS ROOM
C     FOR ACCEPTING SORBATE.
C
      IF(TL.GE.LF.AND.TR.GE.LF) GO TO 499
C
C     CHECK THE POTENTIAL ON EITHER SIDE AND DECID  WHICH
C     DIRECTION THE SORBATE MOVES FIRST.
C
  407 IF(AT(I-1).LT.AT(I+1)) GO TO 450
C
C     MOVE TO THE RIGHT FIRST AND CHECK CONDITIONS
C     WHETHER THAT MOVE IS POSSIBLE.
C
      IF(TR.GE.LF.OR.AN(I+1).GE.AM) GO TO 450
C
C     CHECK TO SEE IF THERE IS ANY SORBATE TO BE MOVED.
C
      IF(AN(I).EQ.0.0) GO TO 499
C
C     CHECK TO SEE IF THE COMPARTMENT HAS THE POTENTIAL TO MOVE.
C
      IF(AT(I).GT.AT(I+1)) THEN
      AN(I)=AN(I)-1.0
      AN(I+1)=AN(I+1)+1.0
      ENDIF
C
C     CONSIDER MOVE TO THE LEFT
C
      IF(TL.GE.LF.OR.AN(I-1).GE.AM) GO TO 499
C
C     CHECK TO SEE IF THERE IS ANY SORBATE TO BE MOVED.
C
      IF(AN(I).EQ.0.0) GO TO 499
C
C     CHECK POTENTIAL TO SEE IF IT IS POSSIBLE TO MOVE.
C
      IF(AT(I).GT.AT(I-1)) THEN
      AN(I)=AN(I)-1.0
      AN(I-1)=AN(I-1)+1.0
      GO TO 499
      ENDIF
  450 IF(TL.GE.LF.OR.AN(I-1).GE.AM) GO TO 460
      IF(AN(I).EQ.0.0) GO TO 499
      IF(AT(I).GT.AT(I-1)) THEN
      AN(I)=AN(I)-1.0
      AN(I-1)=AN(I-1)+1.0
      ENDIF
C
C     MOVE TO RIGHT
C
  460 IF(AN(I).EQ.0.0.OR.TR.GE.LF) GO TO 499
      IF(AN(I+1).GE.AM) GO TO 499
      IF(AT(I).GT.AT(I+1)) THEN
      AN(I)=AN(I)-1.0
      AN(I+1)=AN(I+1)+1.0
      ENDIF
  499 RETURN
      END
```

```
      SUBROUTINE MSOUT(DN,BT,BX,AN,LF,I,NI
      DIMENSION DN(*),AN(*),BT(*)
      REAL LF
      INTEGER N
C
C     A MOVES.CHICK TO SEE IF THERE IS MOLECULE IN
C     COMPARTMENT TO MOVE.
C
      IF(DN(I).LE.0.01) GO TO 599
C
C     NO NEED TO CONSIDER THE BOUNDARY CONDITION.
C
      TL=AN(I-1)+DN(I-1)
      TR=AN(I+1)+DN(I+1)
      IF(TL.GE.LF.AND.TR.GE.LF) GO TO 599
C
C     CONSIDER WHICH DIRECTION A MOVES FIRST
C
      IF(BT(I-1).LT.BT(I+1)) GO TO 550
C
C     MOVES TO THE RIGHT, IF POSSIBLE
C
      IF(TR.GE.LF.OR.DN(I+1).GE.BM) GO TO 550
      IF(BT(I).GT.BT(I+1)) THEN
      DN(I)=DN(I)-1.0
      DN(I+1)=DN(I+1)+1.0
      ENDIF
C
C     CONSIDER MOVES TO THE LEFT
C
      IF(TL.GE.LF.OR.DN(I-1).GE.BM) GO TO 599
C
C     ANY A SURFACE LEFT
C
      IF(DN(I).EQ.0.0) GO TO 599
C
C     POTENTIAL TO MOVE
C
      IF(BT(I).GT.BT(I-1)) THEN
      DN(I)=DN(I)-1.0
      DN(I-1)=DN(I-1)+1.0
      ENDIF
      GO TO 599
C
C
C     MOVE TO THE LEFT
C
  550 IF(TL.GE.LF.OR.DN(I-1).GE.BM) GO TO 560
      IF(BT(I).GT.BT(I-1)) THEN
      DN(I)=DN(I)-1.0
      DN(I-1)=DN(I-1)+1.0
      ENDIF
  560 IF(DN(I).LE.0.0.OR.TR.GE.LF) GO TO 599
      IF(DN(I+1).GE.BM) GO TO 599
      IF(BT(I).GT.BT(I+1)) THEN
      DN(I)=DN(I)-1.0
      DN(I+1)=DN(I+1)+1.0
      ENDIF
  599 RETURN
      END
```

APPENDIX A-5\ RATE DATA

(Note; Data entries under the temperature columns are values of Z, the approach to equilibrium)

Notations: ADS. - Adsorption, DES. - Desorption
C.ADS. - Counter Adsorption, C.DES. - Counter Desorption

1. ZEOLITE - 4A
SORBATE MOLECULE - CO_2
(Adsorption into Pre-evacuated Zeolite and Desorption in He)

Temp.	0°C		20°C			40°C		
Time (min)	ADS.	DES.	TIME (min)	ADS.	DES.	TIME (min)	ADS.	DES.
2.00	0.100	0.053	2.00	0.076	0.077	2.00	0.082	0.079
4.0	0.199	0.094	4.0	0.152	0.134	4.0	0.163	0.141
6.0	0.300	0.122	6.0	0.228	0.176	6.0	0.245	0.191
8.0	0.397	0.143	8.0	0.304	0.207	8.0	0.327	0.229
10.0	0.497	0.160	10.0	0.380	0.235	10.0	0.409	0.265
12.0	0.591	0.174	12.0	0.456	0.257	12.0	0.491	0.294
14.0	0.679	0.186	15.0	0.569	0.288	14.0	0.613	0.334
16.0	0.759	0.196	18.0	0.683	0.315	18.0	0.733	0.369
18.0	0.833	0.205	21.0	0.795	0.338	21.0	0.843	0.399
[illegible]	0.898	0.213	24.0	0.896	0.359	24.0	0.937	0.427
[illegible].0	0.955	0.221	27.0	0.981	0.379	27.0	1.00	0.452

2. ZEOLITE - 4A
SORBATE MOLECULE - CO_2
(Counter-adsorption against C_2H_4 [a], and C_2H_6 [b])

Temp.	0°C		20°C			40°C	
TIME (min)	C.ADS [b]	TIME	C.ADS. [a]	C.ADS. [b]	TIME	C.ADS. [a]	
2.0	0.075	2.0	0.085	0.077	2.0	0.085	
4.0	0.151	4.0	0.166	0.150	4.0	0.163	
6.0	0.226	6.0	0.241	0.224	6.0	0.243	
8.0	0.301	8.0	0.294	0.298	8.0	0.321	
10.0	0.377	10.0	0.347	0.373	10.0	0.388	
12.0	0.452	12.0	0.378	0.446	12.0	0.447	
14.0	0.528	15.0	0.411	0.562	15.0	0.509	
16.0	0.603	18.0	0.438	0.673	18.0	0.553	
18.0	0.679	21.0	0.459	0.781	21.0	0.587	
20.0	0.741	24.0	0.476	0.865	24.0	0.617	
22.0	0.804	27.0	0.492	0.925	27.0	0.641	
24.0	0.837						

3. ZEOLITE - 4A
SORBATE MOLECULE - CO_2
(Counter-desorption against C2H4 [a], and C2H6 [b])

TEMP.	0°C			20.0°C	
TIME (min)	C.DES. [a]	C.DES [b]	TIME (min)	C.DES. [a]	C.DES [b]
2.0	0.070	0.062	1.43	0.048	0.055
6.00	0.156	0.138	2.78	0.085	0.089
10.0	0.210	0.178	5.49	0.154	0.152
14.0	0.251	0.205	8.18	0.209	0.191
20.0	0.299	0.235	12.216	0.271	0.239

27.0	0.343	0.262	16.35	0.321	0.276
38.0	0.399	0.295	23.93	0.398	0.331
52.0	0.456	0.328	31.38	0.460	0.374
68.0	0.509	0.359	42.67	0.537	0.427
83.0	0.550	0.384	57.69	0.618	0.484
106.0	0.603	0.417	72.68	0.683	0.530
136.0	0.659	0.453	91.39	0.748	0.579
166.0	0.705	0.485	110.18	0.801	0.620
205.0	0.752	0.520	136.4	0.858	0.668
			170.18	0.911	0.721
			215.19	0.959	0.771
			263.98	0.989	0.817
			346.41	1.00	0.875
			429.54	1.00	0.918
			519.59	1.00	0.959

4. ZEOLITE - 4A
SORBATE MOLECULE - C_2H_4
(Single Component Adsorption and Desorption in Helium)

TEMP.	0°C			20.0°C			40.0°C	
TIME (min)	ADS.	DES.	TIME (min)	ADS.	DES.	TIME (min)	ADS.	DES.
4.0	0.118	0.029	1.64	0.077	0.028	1.43	0.073	0.045
6.04	0.178	0.036	3.23	0.151	0.050	2.87	0.146	0.083
10.02	0.264	0.050	4.85	0.226	0.069	4.34	0.220	0.115
16.03	0.341	0.067	6.52	0.301	0.086	5.75	0.289	0.143
22.86	0.403	0.077	8.19	0.371	0.102	7.23	0.359	0.173
30.34	0.455	0.093	9.84	0.434	0.117	8.70	0.426	0.199
41.45	0.515	0.114	13.10	0.530	0.144	10.33	0.496	0.225
52.87	0.563	0.134	16.32	0.598	0.169	11.74	0.553	0.247
63.96	0.602	0.151	19.81	0.655	0.195	13.23	0.607	0.268
82.88	0.654	0.179	23.56	0.705	0.219	14.64	0.653	0.288
105.37	0.701	0.207	29.08	0.763	0.251	17.46	0.729	0.325
139.00	0.753	0.245	34.82	0.811	0.283	20.44	0.790	0.360
182.69	0.799	0.288	42.32	0.860	0.321	24.20	0.850	0.402
257.72	0.850	0.351	51.52	0.906	0.365	29.97	0.915	0.459
407.74	0.902	0.447	64.83	0.954	0.418	35.46	0.958	0.508
632.79	0.941	0.549	81.53	0.994	0.480	42.94	0.999	0.567

5. ZEOLITE - 4A
SORBATE MOLECULE - C_2H_4
(Counter-adsorption against CO_2)

TEMP.	0°C		20.0°C		40.0°C	
TIME (min)	C.ADS.	TIME (min)	C.ADS.	TIME (min)	C.ADS.
4.00	0.032	1.64	0.053	1.43	0.046
6.04	0.045	3.23	0.076	2.87	0.082
10.02	0.070	4.85	0.099	4.34	0.120
16.03	0.104	6.52	0.121	5.75	0.153
22.86	0.139	8.19	0.143	7.23	0.186
30.34	0.173	9.84	0.162	8.70	0.217

41.45	0.218	13.10	0.199	10.33	0.250
52.87	0.258	16.32	0.231	11.74	0.277
63.96	0.294	19.81	0.263	13.23	0.303
82.88	0.347	23.56	0.296	14.64	0.328
105.37	0.400	29.08	0.339	17.46	0.374
139.0	0.467	34.82	0.381	20.44	0.420
182.69	0.537	42.32	0.429	24.20	0.469
257.72	0.625	51.52	0.485	29.97	0.543
407.74	0.728	64.83	0.550	35.46	0.600
632.79	0.804	81.53	0.620	42.94	0.669

6. ZEOLITE - 4A
SORBATE MOLECULE - C_2H_4
(Counter-desorption against CO_2)

TEMP.	20°C		40°C
TIME	C.DES.	TIME	C.DES.
2.19	0.035	1.41	0.049
4.45	0.064	4.22	0.136
6.65	0.087	7.02	0.216
8.82	0.108	9.82	0.293
13.31	0.146	12.63	0.357
20.01	0.194	17.59	0.446
26.57	0.236	21.34	0.497
37.52	0.297	26.81	0.557
64.05	0.415	30.55	0.591
82.58	0.481	38.07	0.650
101.51	0.541	45.55	0.697
131.52	0.620	56.82	0.753
165.08	0.693	64.34	0.784
210.08	0.772	75.57	0.824
263.90	0.847	86.84	0.857
343.91	0.932	101.80	0.893
		116.85	0.922
		131.81	0.946
		146.85	0.970

7. ZEOLETE - 4A
SORBATE MOLECULE - C_2H_6
(Single Component Adsorption and Desorption)

TEMP.	0°C			20°C	
TIME (min)	ADS.	DES.	TIME (min)	ADS.	DES.
1.62	0.049	0.032	1.65	0.060	0.052
4.88	0.106	0.069	3.37	0.104	0.089
9.11	0.150	0.098	6.70	0.156	0.132
16.59	0.203	0.134	10.02	0.194	0.168
25.88	0.251	0.171	17.57	0.259	0.228
39.12	0.303	0.211	25.06	0.308	0.271
57.86	0.358	0.254	32.58	0.348	0.300
76.60	0.400	0.289	47.58	0.412	0.364
110.37	0.458	0.341	58.85	0.452	0.398
144.11	0.501	0.382	77.6	0.507	0.446

196.61	0.550	0.433	100.09	0.560	0.498
282.87	0.603	0.503	122.62	0.606	0.532
422.50	0.636	0.578	148.89	0.650	0.572
			186.35	0.707	0.617
			223.93	0.754	0.654
			277.68	0.814	0.697
			318.98	0.853	0.735
			386.49	0.904	0.770
			481.53	0.956	0.801

8. ZEOLITE - 4A
SORBATE MOLECULE - C_2H_6
(Counter-adsorption against CO_2)

TEMP.	0°C		20°C
TIME (min)	C.ADS.	TIME (min)	C.ADS.
1.62	0.001	1.65	0.005
4.88	0.004	3.37	0.008
9.11	0.0009	6.70	0.014
16.59	0.017	10.02	0.021
25.88	0.030	17.57	0.037
39.12	0.048	25.06	0.053
57.86	0.070	32.58	0.070
76.60	0.093	47.58	0.098
110.37	0.135	58.85	0.119
144.11	0.180	77.60	0.152
196.61	0.240	100.09	0.188
282.87	0.320	122.62	0.220
422.50	0.424	148.89	0.259
		186.35	0.306
		223.93	0.340
		277.68	0.390
		318.98	0.438
		386.49	0.480
		481.83	0.530

9. ZEOLITE -4A
SORBATE MOLECULE - C_2H_6
(Counter-desorption against CO_2)

TEMP.	0°C		20°C
TIME (min)	C.DES.	TIME (min)	C.DES.
2.99	0.058	1.77	0.094
11.16	0.110	5.22	0.144
22.38	0.127	8.61	0.173
35.61	0.127	14.68	0.203
56.16	0.127	21.18	0.218
86.18	0.127	32.39	0.225
119.93	0.127	43.86	0.230
164.94	0.127	58.85	0.235
224.97	0.127	84.87	0.244
284.99	0.127	107.41	0.252

385.82	0.127	137.42	0.261
475.86	0.127	174.90	0.272
648.45	0.127	220.97	0.285
		287.35	0.300
		369.88	0.320
		489.82	0.320
		617.35	0.320

10. ZEOLITE - NaMORDENITE
SORBATE MOLECULE - CO_2
(Single Component Adsorption and Desorption)

TEMP.	20°C			40°C			60°C	
TIME (min)	ADS.	DES.	TIME (min)	ADS.	DES.	TIME (min)	ADS.	DES.
2.00	0.108	0.100	2.00	0.114	0.107	2.00	0.152	0.129
4.00	0.216	0.170	4.00	0.229	0.186	4.00	0.305	0.225
6.00	0.324	0.220	6.00	0.343	0.243	6.00	0.457	0.306
8.00	0.432	0.258	8.00	0.457	0.288	8.00	0.609	0.358
10.00	0.540	0.288	10.00	0.572	0.320	10.00	0.761	0.407
12.00	0.648	0.312	12.00	0.686	0.350	10.16	0.773	0.409
14.00	0.756	0.334	13.00	0.743	0.363	11.44	0.870	0.432
16.00	0.864	0.353	13.88	0.794	0.372	12.63	0.955	0.452
17.00	0.917	0.361	15.08	0.862	0.386	16.56	1.00	0.509
17.46	0.942	0.365	16.20	0.923	0.397	22.05	1.00	0.568
18.57	1.00	0.375	17.27	0.974	0.408	27.82	1.00	0.616
23.71	1.00	0.410	22.84	1.00	0.453	31.57	1.00	0.641
33.21	1.00	0.459	32.33	1.00	0.509	40.84	1.00	0.693
46.20	1.00	0.509	41.63	1.00	0.549	55.84	1.00	0.754
61.20	1.00	0.553	60.37	1.00	0.607	74.92	1.00	0.808
83.73	1.00	0.601	86.66	1.00	0.663	100.97	1.00	0.861
117.44	1.00	0.654	120.04	1.00	0.713	142.04	1.00	0.916
168.77	1.00	0.712	169.09	1.00	0.761	187.09	1.00	0.957
215.14	1.00	0.752	229.12	1.00	0.803	254.6	1.00	0.998
305.22	1.00	0.806	319.13	1.00	0.845			
395.27	1.00	0.852						

11. ZEOLITE - NaMORDENITE
SORBATE MOLECULE - CO_2
(Counter-adsorption against C_2H_4 [a], and C_2H_6 [b])

TEMP.	20°C			40°C			60°C	
TIME (min)	C.ADS. [a]	C.ADS. [b]	TIME (min)	C.ADS. [a]	C.ADS. [b]	TIME (min)	C.ADS. [a]	C.ADS. [b]
2.00	0.108	0.108	2.00	0.120	0.119	2.00	0.152	0.154
4.00	0.219	0.223	4.00	0.239	0.237	4.00	0.305	0.308
6.00	0.330	0.338	6.00	0.359	0.363	6.00	0.459	0.461
8.00	0.440	0.453	8.00	0.478	0.488	8.00	0.612	0.615
10.00	0.551	0.569	10.00	0.590	0.610	10.00	0.762	0.769
12.00	0.663	0.686	12.00	0.690	0.707	10.16	0.773	0.781
14.00	0.771	0.794	13.00	0.777	0.820	11.44	0.868	0.879
16.00	0.876	0.873	13.88	0.820	0.845	12.63	0.938	0.965
17.00	0.917	0.897	15.08	0.875	0.907	16.56	0.980	1.00
17.46	0.935	0.935	16.20	0.923	0.967			

18.57	0.980	0.970	17.27	0.94	1.00

12. ZEOLITE - NaMORDENITE
SORBATE MOLECULE - CO_2
(Counter-desorption against C_2H_4 [a], C_2H_6 [b])

TEMP.	20°C			40°C			60°C	
TIME (min)	C.DES. [a]	C.DES. [b]	TIME (min)	C.DES. [a]	C.DES. [b]	TIME (min)	C.DES. [a]	C.DES. [b]
1.61	0.108	0.087	2.02	0.143	0.135	2.34	0.199	0.169
3.23	0.227	0.169	3.98	0.285	0.239	4.59	0.389	0.292
4.81	0.329	0.225	5.73	0.372	0.306	6.60	0.493	0.375
7.91	0.477	0.305	7.38	0.444	0.352	8.68	0.581	0.428
12.44	0.595	0.383	9.05	0.497	0.396	10.82	0.646	0.483
16.19	0.655	0.428	11.61	0.549	0.443	14.60	0.726	0.542
23.71	0.729	0.498	17.34	0.636	0.522	22.05	0.815	0.625
32.21	0.789	0.558	22.84	0.681	0.576	27.82	0.862	0.676
46.20	0.840	0.615	32.33	0.738	0.645	31.57	0.890	0.702
61.20	0.880	0.662	41.63	0.777	0.688	40.84	0.939	0.751
83.73	0.926	0.710	60.37	0.831	0.752	55.84	0.990	0.807
117.44	0.974	0.758	86.66	0.880	0.808	74.92	1.00	0.857
168.77	1.00	0.800	120.40	0.925	0.855	100.97	1.00	0.901
215.14	1.00	0.836	169.09	0.962	0.901	142.04	1.00	0.957
305.22	1.00	0.876	229.12	1.00	0.941	187.09	1.00	0.990
395.27	1.00	0.911	319.13	1.00	0.995	254.60	1.00	1.00

13. ZEOLITE - NaMORDENITE
SORBATE MOLECULE - C_2H_4
(Single Component Adsorption and Desorption)

TEMP.	20°C			40°C			60°C	
TIME (min)	ADS.	DES.	TIME (min)	ADS.	DES.	TIME (min)	ADS.	DES.
1.77	0.155	0.136	1.50	0.150	0.121	2.00	0.242	0.175
3.28	0.291	0.216	3.00	0.299	0.203	3.50	0.423	0.285
5.32	0.475	0.242	4.50	0.449	0.271	5.00	0.604	0.369
8.91	0.794	0.376	5.90	0.588	0.311	5.14	0.621	0.374
11.06	0.939	0.415	7.66	0.755	0.362	7.05	0.835	0.444
13.13	0.995	0.446	9.34	0.872	0.392	8.88	0.973	0.498
18.99	1.00	0.515	11.06	0.924	0.424	12.64	1.00	0.580
26.49	1.00	0.578	19.50	0.955	0.518	16.37	1.00	0.639
34.00	1.00	0.625	27.01	0.961	0.575	24.60	1.00	0.729
45.28	1.00	0.678	37.83	1.00	0.632	34.02	1.00	0.797
94.03	1.00	0.811	52.83	1.00	0.688	45.94	1.00	0.856
137.30	1.00	0.876	67.84	1.00	0.729	68.45	1.00	0.924
184.37	1.00	0.925	94.11	1.00	0.780	98.48	1.00	0.981
259.38	1.00	0.979	115.42	1.00	0.809			
			214.26	1.00	0.887			

14. ZEOLITE - NaMORDENITE
SORBATE MOLECULE - C_2H_4

(Counter-adsorption against CO_2)

TEMP.	20°C		40°C		60°C	
TIME (min)	C.ADS.	TIME (min)	C.ADS.	TIME (min)	C.ADS.	
1.77	0.151	1.50	0.139	2.00	0.228	
3.28	0.265	3.00	0.291	3.50	0.378	
5.32	0.385	4.50	0.365	5.00	0.509	
8.91	0.537	5.90	0.426	7.05	0.609	
11.06	0.594	7.66	0.501	8.88	0.676	
13.13	0.632	9.34	0.539	11.21	0.733	
18.68	0.703	11.06	0.575	16.70	0.807	
27.93	0.766	19.50	0.667	24.16	0.859	
46.65	0.833	27.22	0.711	42.98	0.923	
69.21	0.877	43.95	0.765	95.50	0.989	
108.70	0.922	70.18	0.812			
193.00	0.972	126.49	0.855			

15. ZEOLITE - NaMORDENITE
SORBATE MOLECULE - C_2H_4
(Counter-desorption against CO_2)

TEMP.	20°C		40°C		60°C	
TIME (min)	C.DES.	TIME (min)	C.DES.	TIME (min)	C.DES.	
1.63	0.118	1.66	0.134	1.77	0.193	
3.24	0.220	3.31	0.238	3.60	0.342	
4.87	0.308	4.97	0.326	5.39	0.458	
6.49	0.395	6.68	0.440	7.24	0.565	
8.12	0.480	8.34	0.490	9.03	0.664	
11.35	0.652	10.00	0.572	10.85	0.762	
18.99	1.00	11.70	0.658	12.65	0.850	
		13.76	0.742	14.47	0.920	
		15.00	0.816	16.29	0.963	
		16.73	0.874	18.15	0.991	
		21.89	0.953	24.60	1.00	
		28.13	0.988			
		37.83	1.00			

16. ZEOLITE - NaMORDENITE
SORBATE MOLECULE - C_2H_6
(Single Component Adsorption and Desorption)

TEMP.	20°C			40°C			60°C	
TIME (min)	ADS.	DES.	TIME (min)	ADS.	DES.	TIME (min)	ADS.	DES.
1.79	0.327	0.220	1.34	0.310	0.264	1.00	0.294	0.275
3.53	0.627	0.356	1.95	0.447	0.319	1.50	0.433	0.373
5.32	0.849	0.449	2.34	0.530	0.354	2.00	0.560	0.459
7.13	0.951	0.523	3.34	0.715	0.444	2.50	0.668	0.527
8.93	0.998	0.580	3.90	0.795	0.494	2.00	0.756	0.589
10.95	1.00	0.634	4.34	0.847	0.521	3.50	0.824	0.637

14.74	1.00	0.712	5.34	0.929	0.577	4.00	0.874	0.682
20.41	1.00	0.795	5.95	0.958	0.612	4.50	0.911	0.718
27.82	1.00	0.868	6.34	0.972	0.634	5.00	0.938	0.752
42.24	1.00	0.951	7.97	1.00	0.691	6.00	0.973	0.808
			9.96	1.00	0.750	7.60	1.00	0.871
			13.95	1.00	0.830	9.60	1.00	0.928
			18.10	1.00	0.884	12.51	1.00	0.981
			24.10	1.00	0.932			
			35.53	1.00	0.981			

17. ZEOLITE - NaMORDENITE
SORBATE MOLECULE - C_2H_6
(Counter-adsorption against CO_2)

TEMP. 20°C		40°C		60°C	
TIME (min)	C.ADS.	TIME (min)	C.ADS.	TIME (min)	C.ADS.
1.79	0.174	1.34	0.266	1.00	0.372
3.53	0.260	1.95	0.299	1.50	0.400
5.32	0.321	2.34	0.321	2.00	0.427
7.13	0.379	3.34	0.375	2.50	0.455
8.93	0.423	3.90	0.405	3.00	0.483
12.95	0.506	4.34	0.429	3.50	0.510
17.90	0.583	5.34	0.470	4.00	0.538
23.71	0.651	5.95	0.490	4.50	0.566
31.23	0.715	6.34	0.503	5.00	0.593
53.72	0.832	7.99	0.559	6.00	0.627
74.79	0.890	9.94	0.613	7.30	0.675
97.00	0.929	11.93	0.662	9.73	0.738
		15.84	0.739	12.15	0.784
		19.78	0.802	14.68	0.822
		24.46	0.861	20.32	0.886
		32.00	0.934	34.21	0.976
		39.50	0.980		

18. ZEOLITE - NaMORDENITE
SORBATE MOLECULE - C_2H_6
(Counter-desorption against CO_2)

TEMP. 20°C		40°C		60°C	
TIME (min)	C.DES.	TIME (min)	C.DES.	TIME (min)	C.DES.
1.78	0.214	1.94	0.297	1.00	0.354
3.64	0.380	4.02	0.493	1.50	0.409
5.47	0.489	6.03	0.622	2.00	0.463
7.30	0.595	8.06	0.725	2.50	0.518
9.09	0.683	10.04	0.807	3.00	0.573
12.82	0.857	11.95	0.875	3.50	0.628

14.74	0.936	13.91	0.934	4.00	0.683
20.41	1.00	15.84	0.979	4.50	0.738
27.82	1.00	18.10	1.00	5.00	0.793
42.24	1.00	24.10	1.00	6.00	0.843
53.26	1.00	35.53	1.00	7.60	0.939
				9.60	1.00
				12.51	1.00

19. ZEOLITE - H-MORDENITE
SORBATE MOLECULE - CO_2
(Single Component Adsorption and Desorption)

TEMP.	0°C			20°C			40°C	
TIME (min)	ADS.	DES.	TIME (min)	ADS.	DES.	TIME (min)	ADS.	DES.
3.80	0.110	0.107	2.00	0.111	0.082	1.10	0.100	0.082
6.00	0.220	0.203	4.00	0.222	0.165	2.28	0.206	0.169
9.00	0.330	0.281	6.00	0.333	0.245	3.40	0.308	0.247
12.00	0.440	0.348	8.00	0.445	0.317	5.50	0.498	0.383
15.00	0.550	0.401	10.00	0.556	0.378	6.91	0.624	0.450
18.00	0.660	0.447	11.00	0.611	0.406	8.07	0.723	0.506
20.00	0.734	0.474	12.19	0.677	0.437	10.35	0.889	0.592
20.89	0.766	0.486	13.23	0.732	0.461	11.46	0.950	0.626
21.94	0.803	0.499	14.20	0.782	0.483	12.56	0.997	0.659
24.13	0.873	0.523	16.18	0.872	0.522	15.20	1.00	0.721
26.43	0.933	0.546	18.17	0.943	0.559	18.21	1.00	0.777
28.69	0.978	0.568	20.11	0.993	0.590	22.85	1.00	0.841
38.50	1.00	0.642	24.56	1.00	0.652	30.30	1.00	0.908
55.27	1.00	0.729	32.07	1.00	0.730	49.08	1.00	0.987
77.80	1.00	0.804	41.56	1.00	0.800			
115.26	1.00	0.879	49.07	1.00	0.841			
190.22	1.00	0.955	69.53	1.00	0.916			
257.60	1.00	0.989	107.11	1.00	0.988			

20. ZEOLITE - H-MORDENITE
SORBATE MOLECULE - CO_2
(Counter-adsorption against C_2H_6)

TEMP.	0°C		20°C		40°C	
TIME (min)	C.ADS.	TIME (min)	C.ADS.	TIME (min)	C.ADS.	
1.94	0.063	2.00	0.081	1.96	0.146	
3.81	0.124	4.00	0.187	3.95	0.294	
5.75	0.187	6.00	0.294	5.93	0.442	
7.82	0.255	8.00	0.401	7.94	0.591	
9.50	0.309	10.00	0.508	10.03	0.733	
11.43	0.372	11.00	0.561	11.99	0.843	
13.33	0.434	12.19	0.624	14.00	0.924	
15.39	0.502	13.23	0.678	15.95	0.975	
17.27	0.563	14.20	0.727			

19.26	0.628	16.18	0.820
21.20	0.690	18.17	0.894
23.20	0.752	20.11	0.950
25.11	0.805	21.89	0.894
28.86	0.887		
32.84	0.939		
42.47	0.971		

21. ZEOLITE - H-MORDENITE
SORBATE MOLECULE - CO_2
(Counter-desorption against C_2H_6)

TEMP.	0°C		20°C		40°C	
TIME (min)	C.DES.	TIME (min)	C.DES.	TIME (min)	C.DES.	
2.38	0.083	1.14	0.043	1.91	0.144	
4.72	0.169	3.51	0.175	3.84	0.287	
7.24	0.264	5.27	0.273	5.77	0.419	
9.66	0.348	7.02	0.363	7.70	0.526	
12.05	0.421	8.79	0.442	9.67	0.612	
16.95	0.526	10.52	0.506	11.53	0.676	
21.52	0.597	12.50	0.567	13.45	0.730	
29.00	0.678	14.23	0.612	15.36	0.773	
38.50	0.747	18.02	0.688	19.19	0.839	
55.27	0.824	21.75	0.745	23.06	0.886	
77.80	0.884	27.51	0.809	28.98	0.936	
115.26	0.941	33.01	0.845	36.99	0.978	
190.22	1.00	44.24	0.916	49.08	1.00	
257.6	1.00	55.51	0.956			
		66.76	0.984			
		80.82	1.00			

22. ZEOLITE - H-MORDENITE
SORBATE MOLECULE - C_2H_6
(Single Component Adsorption and Desorption)

TEMP.	0°C			20°C			40°C	
TIME (min)	ADS.	DES.	TIME (min)	ADS.	DES.	TIME (min)	ADS.	DES.
2.50	0.186	0.165	1.77	0.220	0.167	1.93	0.340	0.345
5.00	0.371	0.323	3.47	0.429	0.363	3.80	0.644	0.610
5.74	0.426	0.365	5.24	0.634	0.520	3.98	0.665	0.636
7.72	0.570	0.457	7.02	0.803	0.644	5.79	0.876	0.796
9.57	0.697	0.529	8.85	0.919	0.732	6.02	0.903	0.817
11.54	0.814	0.591	10.62	0.988	0.801	8.10	1.00	0.923
13.49	0.899	0.645	14.36	1.00	0.893	10.11	1.00	0.982
15.36	0.953	0.687	18.24	1.00	0.948			
17.33	0.985	0.727	23.51	1.00	0.986			
22.69	1.00	0.808						
29.88	1.00	0.880						

44.87	1.00	0.957
59.88	1.00	0.987

23. ZEOLITE -- H-MORDENITE
SORBATE MOLECULE - C_2H_6
(Counter-adsorption against CO_2)

TEMP. 0°C		20°C		40°C	
TIME (min)	C.ADS.	TIME (min)	C.ADS.	TIME (min)	C.ADS.
2.50	0.181	1.77	0.171	1.93	0.349
5.00	0.359	3.47	0.372	3.80	0.636
5.74	0.402	5.24	0.549	5.79	0.830
7.72	0.517	7.02	0.670	7.74	0.925
9.57	0.592	8.85	0.750	9.67	0.972
11.54	0.658	10.62	0.799	11.53	0.997
13.49	0.703	14.23	0.863		
15.36	0.739	20.01	0.912		
17.33	0.767	31.25	0.955		
20.83	0.807	59.25	0.989		
28.06	0.853				
50.57	0.922				
125.62	0.958				

24. ZEOLITE - H-MORDENITE
SORBATE MOLECULE - C_2H_6
(Counter-desorption against CO_2)

TEMP. 0°C		20°C		40°C	
TIME (min)	C.DES.	TIME (min)	C.DES.	TIME (min)	C.DES.
1.94	0.119	1.81	0.154	1.93	0.383
3.81	0.243	3.65	0.349	3.80	0.651
5.75	0.355	5.44	0.502	3.98	0.677
7.82	0.456	7.22	0.620	5.79	0.850
9.50	0.525	9.00	0.710	6.02	0.863
11.43	0.594	10.85	0.783	8.10	0.980
13.33	0.654	12.66	0.837	10.11	1.00
15.39	0.710	14.48	0.878		
17.27	0.755	16.29	0.909		
19.26	0.798	21.89	0.960		
23.20	0.870	25.62	0.972		
28.86	0.945				
34.73	0.989				

APPENDIX A - 6

KINETIC DATA TREATMENT

Experimental sorption sequence of a typical counter-diffusion experiment is as follows;

For simplicity, let molecule A be the counter-adsorbate and molecule B, the counter-desorbate.

1. Zeolite powder was activated at 450 °C under vacuum for 24 hours.
2. Adsorption of molecule B was initiated by passing gas mixture B (B plus helium) over activated zeolite. (Note, this establishes the single component adsorption kinetics of molecule B)
3. The sorption tube was isolated and the remaining system purged with gas mixture A (A plus helium).
4. The adsorption of molecule A was initiated by allowing A to contact with zeolite containing molecule B.

Since molecule B desorbs, therefore, the counter-adsorption of molecule A takes place simultaneously with the counter-desorption of molecule B.

For single component desorption, the system was first purged with helium, and then, helium was passed over the zeolite containing molecule B.

For a particular set of single component sorption experiments, the adsorption rate of gas mixture A in helium at time, t, is determined by component mass balance, i.e.

Component A:

$$\text{Rate of disappearence due to adsorption} = \text{Input rate} - \text{Output rate}$$

or

$$r_a = F_0X_0 - F_1X_1 \qquad 1$$

where

r_a is the adsorption rate of molecule A in (cc STP/gm min)

F_0, F_1 are the respective inlet and outlet total flow rates (helium + A) in (cc STP/gm min)

X_0, X_1 are the respective inlet and outlet mole fractions of A. (Note; for ideal gas, the mole and volume fractions are equivalent)

The relationship between F_0 and F_1 is established with component mass balance on helium, i,e,

$$0 = F_0(1-X_0) - F_1(1-X_1) \qquad 2$$

hence

$$F_1 = F_0(1-X_0) / (1-X_1) \qquad 3$$

Substituting Eqn. 3 into Eqn. 1, we have

$$r_a = F_0X_0 - \frac{F_0(1-X_0)\,X_1}{(1-X_1)} \qquad 4$$

Algebraic manipulation of Eqn. 4 gives

$$r_a = F_0(1-X_0)\left[\frac{X_0}{(1-X_0)} - \frac{X_1}{(1-X_1)}\right] \qquad 5$$

In the actual experiment, F_0 is measured by the flowmeter whereas the mole fractions X_0 and X_1 are determined directly with gas chromatography.

For single component desorption, the rate of desorption r_d is evaluated in a similar fashion; through component mass balance, i.e.

$$-r_d = F_0(1-X_0)\left[\frac{X_0}{(1-X_0)} - \frac{X_1}{(1-X_1)}\right] \quad 6$$

However, since the inlet is pure helium, X_0 is therefore zero, and F_0 is simply the total flowrate of helium. This yields a simplified expression for the desorption rates;

$$r_d = F_0X_1 \,/\, (1-X_1) \quad 7$$

In the binary counter-diffusion experiments, the method of evaluating adsorption and desorption rates is again through component balances. For simplicity, let molecule A be the adsorbate while molecule B, the desorbate. Also, the adsorption of molecule A takes place simultaneously with the desorption of molecule B.

Component A:

$$r_{a,A} = F_0X_{0,A} - F_1X_{1,A} \quad 8$$

helium:

$$0 = F_0(1-X_{0,A}) - F_1(1-X_{1,A}-X_{1,B}) \quad 9$$

hence

$$F_1 = F_0(1-X_{0,A}) \,/\, (1-X_{1,A}-X_{1,B}) \quad 10$$

Substituting Eqn. 10 into Eqn. 8 and with algebraic manipulation, we have

$$r_{a,A} = F_0(1-X_{0,A})\left[\frac{X_{0,A}}{(1-X_{0,A})} - \frac{X_{1,A}}{(1-X_{1,A}-X_{1,B})}\right] \quad 11$$

Component B:

$$-r_{d,B} = F_0 X_{0,B} - F_1 X_{1,B} \qquad 12$$

But $X_{0,B} = 0$, and substituting Eqn. 10 into Eqn. 12, it yields

$$r_{d,B} = F_0(1-X_{0,A}) \left[\frac{X_{1,B}}{(1-X_{1,A}-X_{1,B})}\right] \qquad 13$$

Where F_0 is again the total inlet flowrate or $F_0(1-X_{0,A})$ is the helium flow rate. $X_{0,A}$, $X_{0,B}$ and $X_{1,A}$, $X_{1,B}$ are the respective inlet and outlet mole fractions for component A and B.

The direct result of the kinetic experiments is therefore the sorption rates (r_a,r_d). One typical example is shown in Fig. A-6-1, where the instantaneous adsorption rate of ethane on zeolite 4A at 0 °C is plotted against time.

The time history of the sorption rates can then be integrated to give the amount adsorbed (Q_t) at time t. In this work, the integration is done by a numerical technique, trapezoidal rule. The resultant Q_t against t is shown in Fig. A-6-2.

The dimensionless variable Z, known as the approach to equilibrium is defined as

$$Z = (Q_t - Q_0) / (Q_\infty - Q_0) \qquad 14$$

where Q_t is the total amount adsorbed at time t,
Q_0 is the initial amount adsorbed, and
Q_∞ is the saturation amount adsorbed.

In this work, the saturation amount adsorbed (Q_∞) of the various sorbates studied were obtained from equilibrium isotherms at the appropriate temperature and pressure level that corresponds to the partial pressure of the component of interest in the gas

mixture. The accuracy of the kinetic measurements can be seen from the comparison of the equilibrium uptakes between the kinetic and static systems. This is shown in Table 4-9, where the equilibrium uptakes of ethane from the two systems are compared. As indicated, the differences are less than 5%.

The equilibrium uptakes or the approach to equilibrium, Z, can now be plotted against time, t. This is shown in Fig. A-6-3. The values of Z versus t of a repeated run is also shown in this figure to demonstrate the reproducibility of results. In this work, the values of Z against t were non-linear least square fitted to the Fick's law solution (Appendix A-3) to yield values of diffusivity, D. In general, the calculated diffusivities from repeated runs varied between 5 and 15%.

FIGURE A-6-1 INSTANTANEOUS ADSORPTION RATE VERSUS TIME

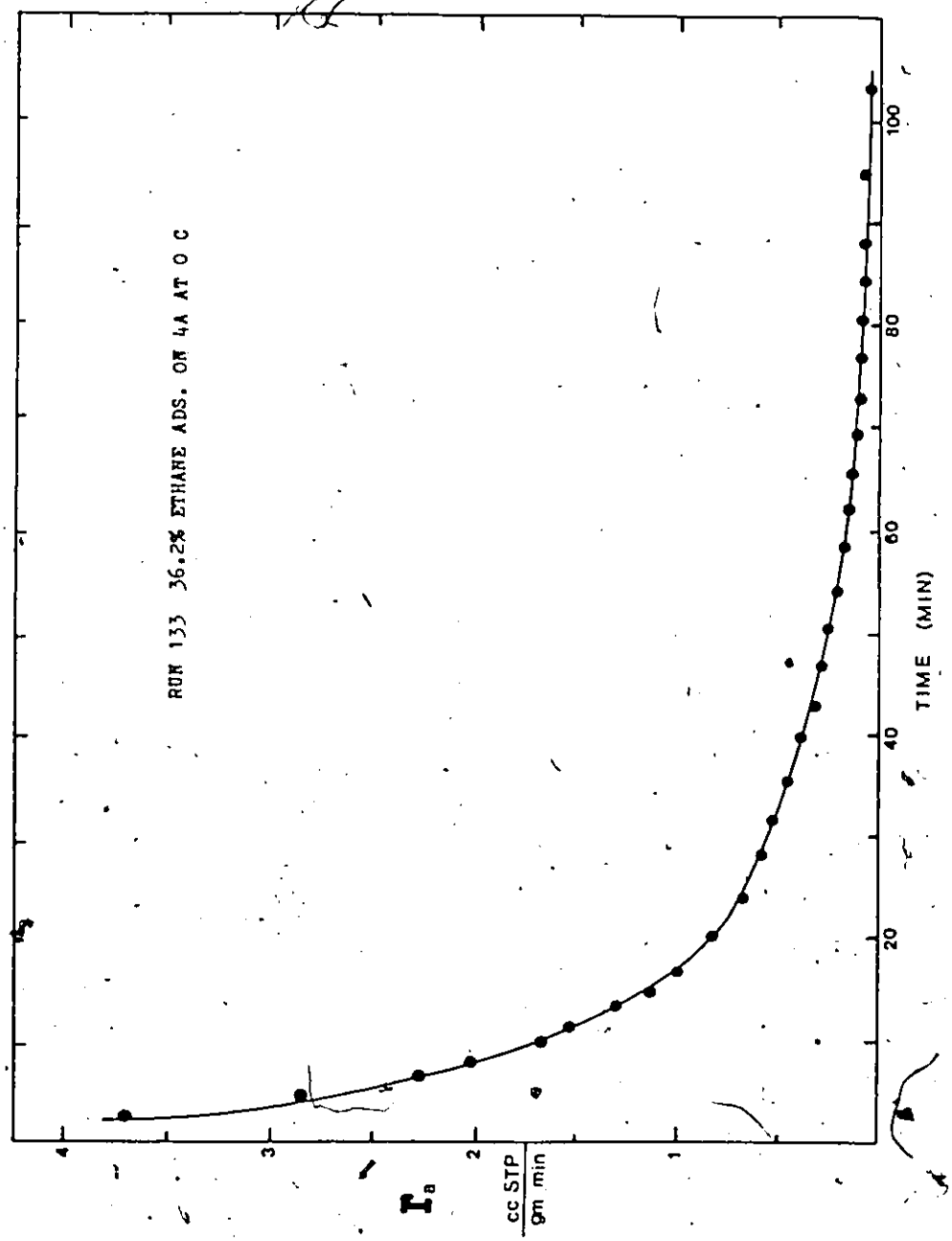

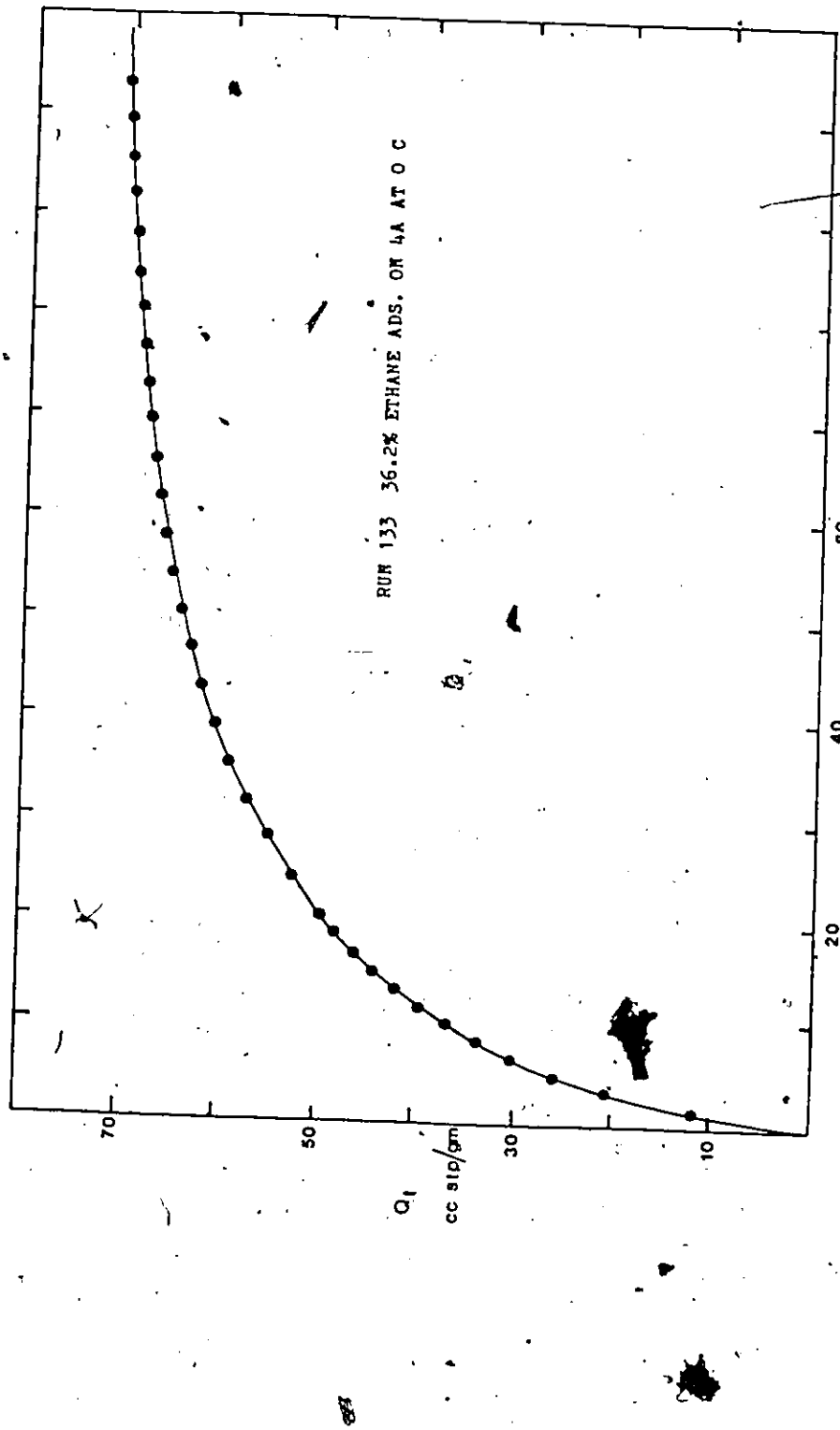

FIGURE A-6-2 AMOUNT ADSORBED VERSUS TIME

FIGURE A-6.3 APPROACH TO EQUILIBRIUM, Z, VERSUS TIME

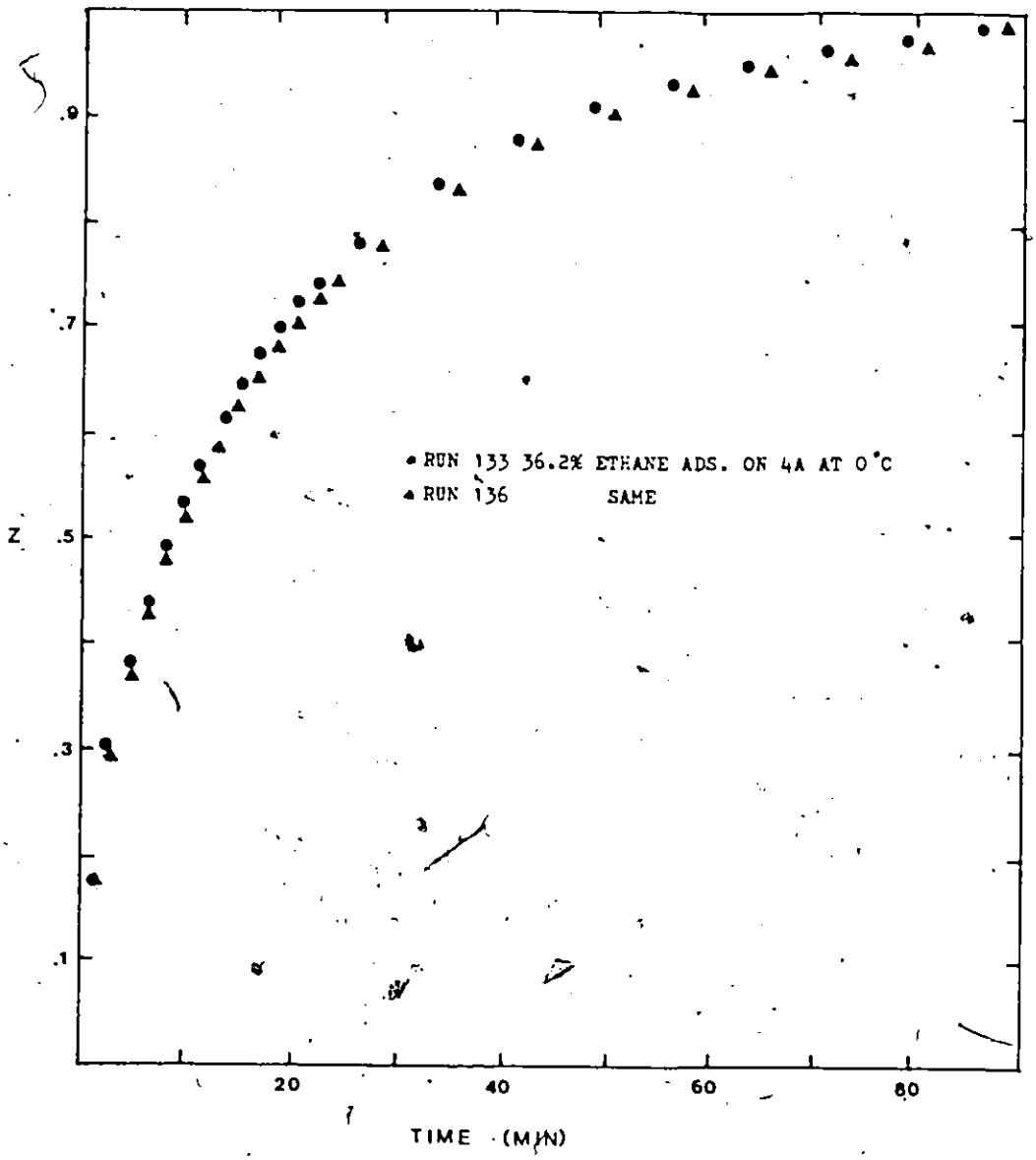

APPENDIX A-7

NOTATION

a	Radius of sphere, cm
A	Angstrom
b	Langmuir constant, $torr^{-1}$
c	Concentration of sorbed phase, $mole/cm^3$ (crystal)
D	Diffusivity of sorbed phase, cm^2/sec
D_O	Limiting diffusivity, cm^2/sec
D_k	Knudsen diffusivity, cm^2/sec
E	Activation energy, KJ/mole
J	Diffusive flux of sorbed species, $mole/cm^2$ sec
M	Molecular weight, gm
p	Partial pressure, torr
P	Pressure, atm
q_{st}	Isosteric heat, KJ/mole
Q	Amount adsorbed, cc STP/gm
r	Radial position variable, cm
R	Gas constant
t	Time variable, sec
T	Temperature, °K
U	Velocity of sorbed species, cm/sec
x	Distance in X-direction, cm
X	Mole fraction
Z	Fractional approach to equilibrium, dimensionless, $= (Q_t-Q_0) / (Q_\infty-Q_0)$

SUBSCRIPTS

1,2,i,A,B	Refer to component 1,2,i,A,B
m, s	Saturation concentration, mole/cm^3

GREEK LETTERS

ν	Special diffusion volume, cm^3
μ	Chemical potential, energy/mole
θ	Dimensionless concentration, or coverage
τ	Dimensionless time variable, = Dt/a^2
π	Spreading Pressure

SYMBOLS RELATED TO RANDOM WALK MODEL

A(I)	Initial number of molecule A adsorbed per cell
BB	Bulk concentration of molecule B at exterior cell
AM, BM	Maximum number of molecule A or B allowed per cell
AN(I), BN(I)	Number of molecule A or B in cell(I)
AT(I), BT(I)	Moving potential of molecule A or B in cell(I)
CA, CB	Critical moving values for molecule A or B
CF	Total number of molecule A and B allowed per cell
RN	Random number generated between 0-100
T	Time (arbitrary units, corresponds to 1 computer iteration step)